111-32
27685
P-65

NASA Contractor Report 194983

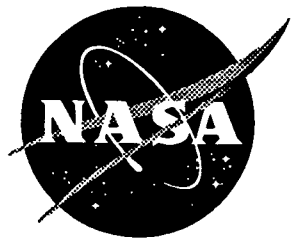

# Experimental Evaluation of Shape Memory Alloy Actuation Technique in Adaptive Antenna Design Concepts

W. Neill Kefauver and Bernie F. Carpenter
*Martin Marietta Astronautics Division, Denver, Colorado*

(NASA-CR-194983) EXPERIMENTAL EVALUATION OF SHAPE MEMORY ALLOY ACTUATION TECHNIQUE IN ADAPTIVE ANTENNA DESIGN CONCEPTS Final Report (Martin Marietta Corp.) 65 p

N95-12896

Unclas

G3/32 0027685

Contract NAS1-18455
September 1994

National Aeronautics and
Space Administration
Langley Research Center
Hampton, Virginia 23681-0001

Table of Contents

List of Figures

Research Support Task for Large Scale Antenna Pattern Measurements in a Near Field Facility - Contract No. NAS1-18455

ORIGINAL CONTAINS
COLOR ILLUSTRATIONS

## Abstract

Creation of an antenna system that could autonomously adapt contours of reflecting surfaces to compensate for structural loads induced by a variable environment would maximize performance of space-based communication systems. Design of such a system requires the comprehensive development and integration of advanced actuator, sensor and control technologies. As an initial step in this process, a test has been performed to assess the use of a shape memory alloy as a potential actuation technique. For this test, an existing, offset, cassegrain antenna system was retrofit with a subreflector equipped with shape memory alloy actuators for surface contour control. The impacts that the actuators had on both the subreflector contour and the antenna system patterns were measured; the measured data is presented herein. The results of this study indicate the potential for using shape memory alloy actuation techniques to adaptively control antenna performance; both variations in gain and beam steering capabilities were demonstrated. Future development effort is required to evolve this potential into a useful technology for satellite applications.

## Introduction

Space-based communication antennas are fabricated with state-of-the-art composite materials to meet stringent dimensional tolerance and weight specifications. Optimization of antenna system performance requires on orbit structural control of these reflector surfaces. Variations in thermal loads throughout an orbit can produce distortions in antenna structures, resulting in cyclic gain disturbances and the potential need for periodic recalibration. One proposed approach to mitigate the impacts of such disturbances is to develop an adaptive antenna system that provides for active control of reflector surfaces. Creation of such a system will require the comprehensive development and integration of advanced actuator, sensor and control technologies. As a first step in this process, a demonstration of using shape memory alloy actuators to attain antenna surface control has been undertaken. The principle thrust of this effort concerns the measurement of reflector deformations and the associated changes in the field patterns that can be attained in a representative adaptive antenna system.

## Technical Approach

The cassegrain antenna, developed by TRW for the NASA Advanced Communications Technology Satellite (ACTS) program, was selected as the baseline system for this study. This antenna consists of a 106.8 inch diameter primary reflector that is offset fed by a pair of subreflectors and a cluster of feed horns. For this study, the baseline design was modified to use a single subreflector and a single feed horn; this test configuration is shown in Figure 1. The test subreflector was designed to be dimensionally equivalent to one of the baseline subreflectors. A system of shape memory alloy actuators were incorporated into the test subreflector design to allow for alteration of the reflecting surface contour, thus providing a means to vary the response of the antenna system. Measurements of both dimensional changes that occur at the subreflector contour and the impacts that such changes have on the near- and far-field patterns produced by the antenna system were taken for various actuation schemes. The resultant data set,

presented herein, provides an initial basis for evaluating the relative merits of using shape memory alloy actuation techniques in adaptive antenna design concepts.

The adaptive subreflector, shown in Figure 2, consists of a hyperbolically contoured, honeycomb panel with a series of hubs located on the back (non-reflecting) side of the panel and sets of shape memory alloy wires suspended between adjacent hub pairs. Each wire set, referred to as a string, consists of 20, 0.020 inch diameter, NiTiNOL wires aligned in a plane parallel to the panel; the ends of the wires are locked into the respective hubs. The wire sets are electrically coupled to a power supply such that current flow in each string can be individually controlled. Strain gauges are attached to the back side of the panel, located essentially at the mid points of the wire sets; one gauge per string. These strain gauges are wired into feedback circuitry that limits the current flow in the strings to yield desired levels of localized strain in the panel. The desired strain levels are set by the relative positions of slide potentiometers; each string has a dedicated control potentiometer. When zero current flows through a string, the wires apply no load to the panel and the original (baseline) contour is maintained. Application of current heats the wires, resulting in a contraction force that pulls the hubs together, locally strains the panel and alters the contour. Subsequent removal of current flow permits the wires to cool, relaxing the applied force and allowing the panel to spring back to the original contour.

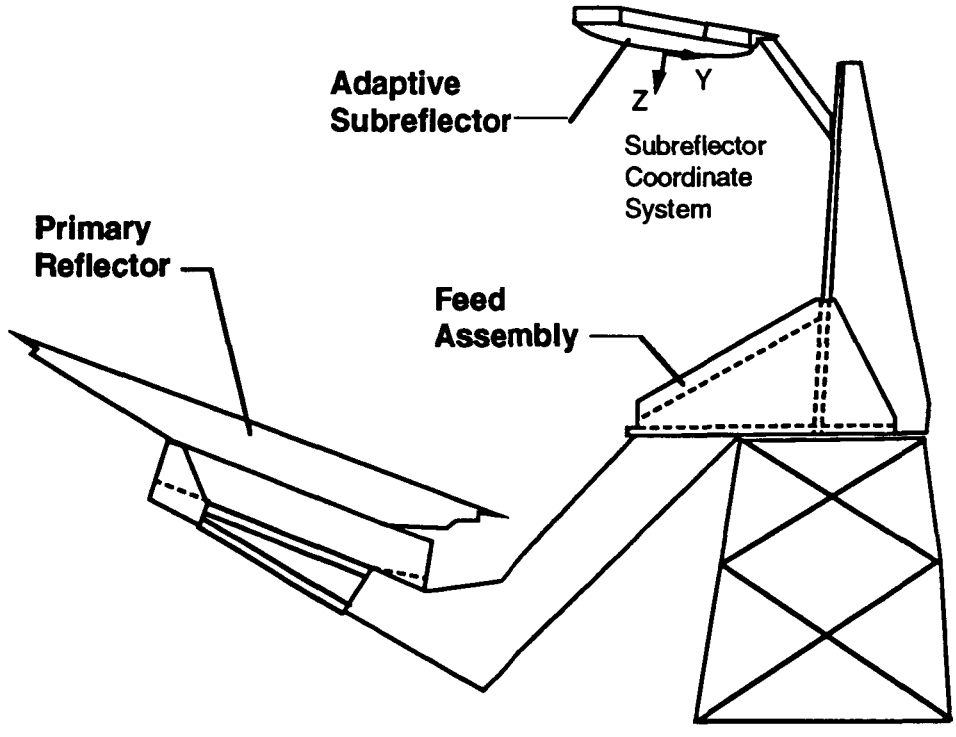


Figure 1. Antenna System Test Configuration

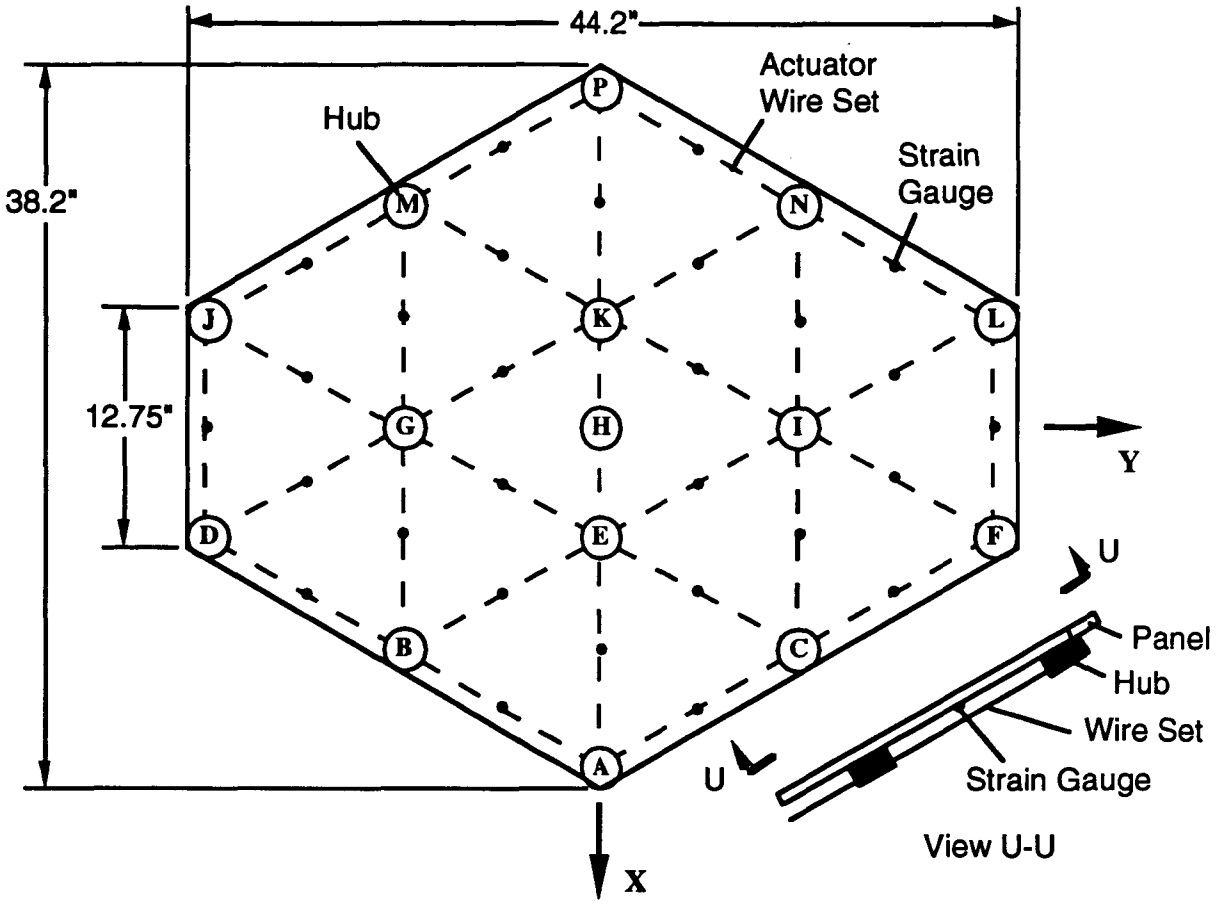


Subreflector as viewed looking at reflective (convex, front) surface; hubs, actuator wire sets & strain gauges are located on back, viewed as if panel is transparent. Note, the subreflector contour is that of an offset hyperbolic surface, +Y points toward the vertex; therefore, the +Y half has move curvature than the -Y half.

Figure 2. Adaptive Subreflector

Two series of tests were performed in this study: the first involved the use of a theodolite system to measure subreflector contour deformations caused by the actuator strings; in the second, antenna patterns were measured for various subreflector actuation schemes. Both of these test series are discussed in detail below. The primary intent of these tests was to provide a data set sufficient to allow future structural modeling of the adaptive subreflector (use deformation data) and to make a preliminary assessment of the adaptive antenna concept (use antenna pattern data).

## Theodolite Tests

The adaptive antenna subreflector was exercised to confirm the operation of and to measure the deflection and strain caused by the various shape memory alloy actuators mounted on the back of the unit. Deflections and strains were measured for: (1) the actuation of each individual string, (2) the combined actuation of all strings and (3) the combined actuation of the perimeter strings. During these tests, each string actuation was set to roughly 20% of the maximum possible strain capability. The results, consisting of deflection and strain measurements, are presented in Appendix A. These results indicate that all strings are functional and provide a base set of data necessary for future structural analysis of the this adaptive subreflector design.

### Objectives

The primary objective for exercising the adaptive antenna subreflector was to confirm that all strings are functional and have the ability to deform the reflecting surface. A secondary objective was to gather quantitative data regarding the relative motion and strain imparted to the subreflector by the various strings.

### Approach, Setup & Operations

The basic approach used to perform the operational tests was to mount the subreflector on a rigid support structure and then measure the positions of select points on the subreflector surface both before and during actuation of the various strings. Strains at select points on the back side of the subreflector were also measured both before and during each actuation. Measurements were taken for each string actuated individually and then two composites were taken: one where all strings were actuated simultaneously and one where only the perimeter strings were actuated. A theodolite system was used to measure subreflector deflections; the strain gauges used in the feedback control loops for the shape memory alloy actuator strings measured strains.

The upper half of the antenna support structure, to which the subreflector normally is mounted when the antenna is fully assembled, was used to hold the subreflector for the theodolite tests. This structure was laid over backwards so as to allow positioning of the subreflector in a nearly vertical orientation (see Figure 3), thus simplifying both the mounting process and the taking of data. Since the antenna support structure was used, in this test, simply to support the subreflector in an opportune orientation for the measurement system, no attempt was made to place the subreflector in the proper orientation required for antenna alignment. (In fact, the subreflector was rotated 180 degrees about the Z-axis from the "proper antenna alignment orientation"; refer to Figures 1 & 3.) The subreflector was supported off the center hub ("H", see Figure 2) which was connected to the support structure using four bolts equally spaced around the hub.

Fifteen theodolite targets were placed on the front (reflecting) surface of the subreflector; these targets were located at the approximate projected centers of the hubs (note that the hubs are on the back of the subreflector) and were assigned letter designators that matched their corresponding hub designators (refer to Figure 2). The contour of the subreflector surface was mapped by measuring the locations of these fifteen target points using the dual telescope, theodolite system. The twenty-eight strain gauges that provide feedback to the string control electronics were monitored during the actuation tests to obtain strain data. Note that there is one anomaly in the shape memory alloy wire layout between hub pairs that needs mention; refer Figure 2 to follow this discussion. The center hub (H) is unique in that no wires are attached to this hub. Instead, a cutout has been provided that allows the wire set spanning between hubs E and K to pass through H.

Due to the location of H between E and K, no strain gauge is located under this E-K string. Since the E-K string has no strain gauge available for feedback control, this string was never actuated during any of the tests. References made herein to all strings imply all but string E-K.

The baseline approach for measuring subreflector deflection was to first map the subreflector front surface prior to string actuation; map the surface after string actuation and surface stabilization (which required just a few seconds); then deactuate, allow the surface to restabilize (which required roughly 15 minutes) and remap. The remap provides the initial map for the next string actuation. This baseline approach was followed throughout the first day of testing during which the individual actuations of four different strings (i.e., A-C, A-E, B-D & B-E) were tested. The results of this first day of testing indicated that the subreflector nominally returns to original shape once a given string is deactuated; therefore, the remapping exercise was deemed to be unnecessary and deleted from the procedure. Thereafter, a baseline map was taken at the beginning of each day and assumed valid throughout that day of testing; a minimum of 15 minutes was allowed between string deactuation for one test and string actuation for the next to allow the subreflector to return to the baseline state.

Due to a lack of available equipment during the first three days of testing, only 20 (of 28) strain gauges could be monitored at a given time; therefore, only this subset of strain gauge data was taken during the tests where each string was actuated individually. This subset of data was adjusted as required to always include the strain gauge of interest (i.e., that one located below the string being actuated). During the final day of testing, the required equipment was available so that all 28 strain gauges could be monitored; therefore, a complete set of strain gauge data was taken when the two combined actuation tests (i.e., all strings and just perimeter strings) were performed.

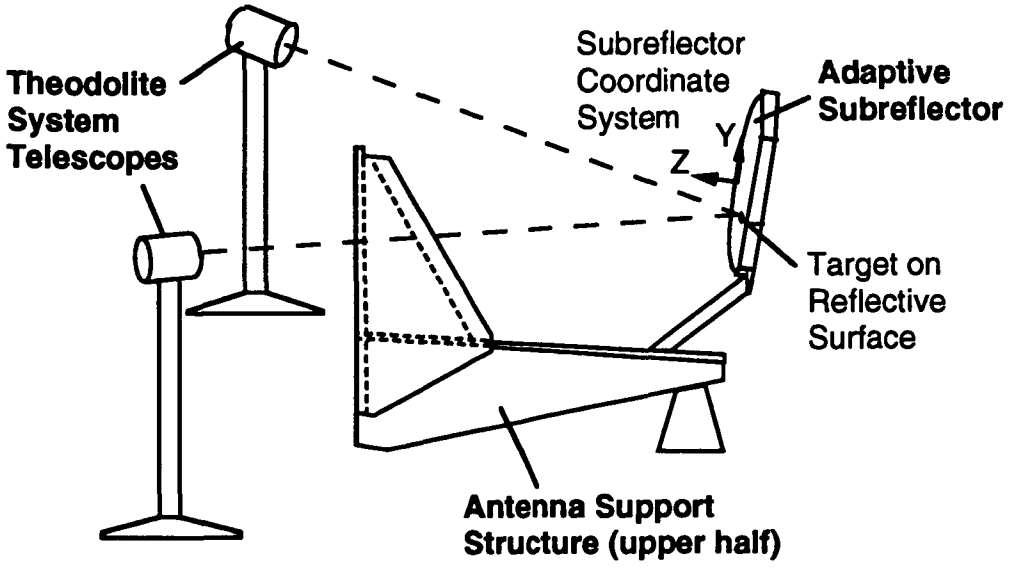


Figure 3. Theodolite Test Configuration

For all theodolite tests, string actuation was limited to yield roughly 20% of the maximum producible strain. This limit was achieved by mounting stop bars on the control box to restrict the allowable motion of the slide potentiometers (used to set strain levels) to roughly 20% of their total available motion. Actuation of a given string was accomplished by simply sliding the potentiometer control lever up against the stop bar. This limitation was imposed to preclude damaging the subreflector.

Results & Observations

Data collected during the subreflector actuation tests is presented in Appendix A; one data sheet is provided per test. Each data sheet contains: (1) a diagram of the subreflector which indicates the actuated string(s); (2) a listing of the relative power levels (% of total capability) at which all strings were set during actuation; (3) the strain data measured once the surface stabilized following actuation; (4) the measured positions, both before (baseline) and after actuation, of the 15 theodolite targets mounted on the subreflector surface; and (5) the computed relative motion of the 15 targets. This data provides deformation and strain information necessary to support future modeling and analysis efforts required to better understand the extent of contour control provided by the actuation system developed for this particular adaptive subreflector design.

The original plan for exercising the strings was to test each string individually and then run one additional test with all strings actuated; this plan was followed. Results of the individual string actuation tests verified all strings to be operational. Evaluation of the deformation data from these tests (see Figures A-1 through A-28, Appendix A) reveals an asymmetry in the structural characteristics of the subreflector that appears to be most evident in the -X+Y quadrant. This conclusion is drawn by simply comparing the location of maximum deformation caused by a given string in a given quadrant to that of a symmetric string in another quadrant. Such comparisons indicate that 4 of 6 strings per quadrant yield symmetric responses for the following quadrant pairs: +X+Y/+X-Y (symmetry about X-axis), +X-Y/-X-Y (symmetry about Y-axis) and +X+Y/-X-Y (diagonal symmetry). However, only 2 of 6 strings yield symmetric responses when comparing the -X+Y quadrant with +X+Y or +X-Y and only 1 symmetric response is noted when compared with -X-Y.

During the "all strings actuated" test, the perimeter strings were noted to be slack. The lack of tension in the perimeter strings implied that only the inner set of strings were actually deforming the subreflector and that the resultant strains induced at the perimeter by the actuation of this inner set of strings was greater than the strains produced by the perimeter strings when actuated at the same power level as the inner set. To test this hypothesis, an additional test was conducted where only the perimeter strings were actuated. The strains measured around the perimeter during the "all strings actuated" test were found to be, on average, 3.5 times greater than those measured during the "perimeter only" test (refer to Figures A-29 & A-30, Appendix A).

## Near-Field Tests

A series of tests were performed at the Near-Field Measurement Laboratory on the adaptive antenna system to determine the impact of the shape-actuated subreflector on system performance. These tests were conducted following an initial boresighting operation during which the subreflector was aligned within the antenna system and baseline performance was measured with no subreflector actuation. The subreflector actuation schemes considered in this test series include symmetric actuation of all strings, asymmetric actuation across subreflector axes and selective actuation of strings to attain a desired deformations. The results obtained from these tests reveal the relative efficacy of using shape memory actuation technology to attain adaptive antenna control.

### Objectives

The primary objective for performing the near-field tests was to measure the extent of gain change and beam steering that can be attained by flexure of the adaptive subreflector using various actuation schemes. A secondary objective was to use microwave holography to map the changes in the subreflector surface caused by the actuations. Results of these measurements provide a basis for assessing the feasibility of the adaptive antenna concept.

### Boresighting Operations & Evaluation

To dramatically demonstrate the effects of surface distortion, the decision was made to test the system at 26 GHz. To do this testing required a precision alignment of the antenna system; however, the alignment geometry was not clearly known because the original subreflector and feed were not included in the system when delivered. Therefore, the system was aligned using data collected from the near-field scanner starting at a lower frequency. After several iterations to determine the proper gain of the feed and approximate location of the subreflector for optimum system performance at 6 GHz, the frequency was increased to 18 GHz and then 26 GHz.

The boresighting of this antenna was complicated greatly by the lack of meaningful mechanical reference points. With a center fed reflector, approximate lateral alignment is known by merely finding the center of the reflector; axial alignments of the feed and subreflector are then roughed in by measuring distances from the center or vertex to each of these pieces of hardware. With a large offset reflector, conventional crude methods are not very useful. Without an obvious lateral position marked, positioning of the subreflector could only be guessed at based upon the remaining mounting hardware. This initial guess turned out to be over 8 inches off. This error was determined through the near-field measurements indicating that the feed needed to be located directly over the main reflector to achieve a beam peak on boresight. After making this correction to the subreflector, the feed position could be finely tuned both axially and laterally. The resultant system response at 6 GHz is shown in Figure 4. The pattern is nearly ideal at this frequency, with surface errors resulting in only 0.018 dB loss. The focusing of the antenna is clearly near optimal because of the symmetry of the first sidelobes and the depth of the null between the main beam and first sidelobe.

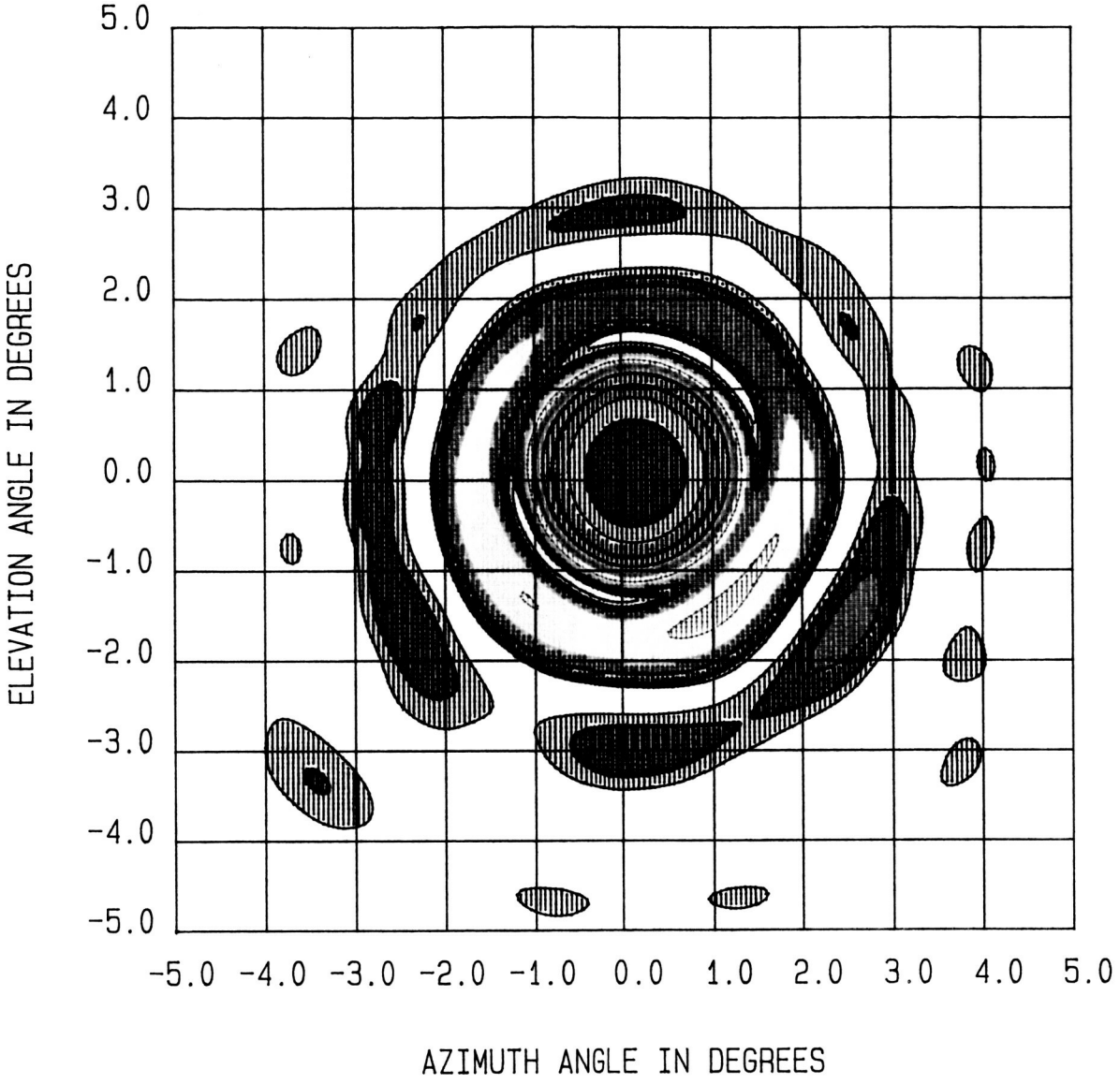


Color Scale (dB):

| | | | | | | | |
|---|---|---|---|---|---|---|---|
| 0 | > | Red | > -3 | -15 | > | Lime | > -18 |
| -3 | > | Black | > -6 | -18 | > | Yellow | > -21 |
| -6 | > | Purple | > -9 | -21 | > | Orange | > -24 |
| -9 | > | Blue | > -12 | -24 | > | Red | > -27 |
| -12 | > | Green | > -15 | -27 | > | Black | > -30 |

Figure 4: 6 GHz Far-Field Data After Alignment

Next, the alignment process was repeated at 18.6 GHz. After verifying reasonable performance at 18.6 GHz, the frequency was increased to 26 GHz. Initially the SA standard gain horn from 18 to 26 GHz was used as the feed for this measurement; however, the gain of this horn was too high so the SA standard gain horn from 26 to 40 GHz was used instead. This horn change reduced the feed gain from 24.9 to 23.2 dB, broadening the beam width from 13° to 15.9°, much closer to the 17.2° beamwidth desired to achieve a 10 dB edge taper. The actual edge taper is shown in Figure 5, a contour plot of aperture amplitude. The aperture amplitude was obtained by taking the data collected over the near-field and performing a mathematical transformation to regenerate the data as it would appear in a plane level with the center of the reflector surface. Figure 6 shows the amplitude data that was collected in the near-field 110 inches above the reflector. In the near-field data the amplitude is significantly distorted, this distortion is caused by the propagation of surface errors interfering with the desired plane wave. At the aperture plane this effect is greatly reduced even though it is primarily caused by the subreflector, the reduction in the effect on amplitude arises from the fields only having traveled a third of the distance they travel to reach the near-field scan plan. Figure 7 shows the far-field performance of the nominal antenna system. Although, this pattern has obviously been degraded by surface errors, it is still a reasonable pattern for some applications. For this research effort the important effect to measure is the change from nominal, this change can be directly evaluated by the methods described above of aperture back projection followed by one intuitive step described below.

To clarify the effects of flexing the subreflector, the decision was made to plot the patterns resulting from ratioing aperture phase before and after subreflector actuation. This approach dramatically reduces the effects of surface position errors in the nominal case as can be seen in Figure 8, a plot of the far-field resulting from ratioing the nominal aperture fields on successive days. As the plot shows for this idealized case there is a slight asymmetry between the E and H-planes of data, with the H-plane of the data running from the top to bottom of the page. The lower sidelobes of the E-plane are due to the narrower beamwidth of the E-plane of the horn increasing the edge taper of the aperture by 5 dB (see Figure 5).

At 26 GHz, with the proper horn alignment and horn gain, two drivers on system performance became readily apparent. First, the surface of one of the reflectors was not very good for this frequency band. Good surfaces for most applications are considered to have surface roughness not exceeding 0.01 wavelengths RMS (root mean squared) or loss due to surface errors of 0.017 dB. At 26 GHz, the 0.005 wavelength roughness would correspond to 0.0023", the observed system surface RMS at nominal was much higher -- almost 0.01" or approximately 0.022 wavelengths. This amount of surface error results in a gain loss of approximately 0.34 dB. Because the main reflector, a graphite honeycomb construction, should not have deformed significantly since original baselining, the RMS of the main reflector was assumed to be 0.0055", based upon a 1984 report. This leaves a residual RMS for the subreflector of 0.0083". The second driver on system performance was the relatively small, usable area of the subreflector, as shown in Figure 9. This active region corresponded to the 22.6" diameter beam aperture image having an area of 401 square inches; the total area of the subreflector was 1126 square inches. Within this usable area, the subreflector has only 4 actuator strings available for tensioning. In addition, there was an extra node (hub H, see Figure 9) in this region making it stiffer than the remaining subreflector. Deformation data gathered during theodolite testing (see Appendix A, Figure A-29) confirms the relative stiffness within this active region.

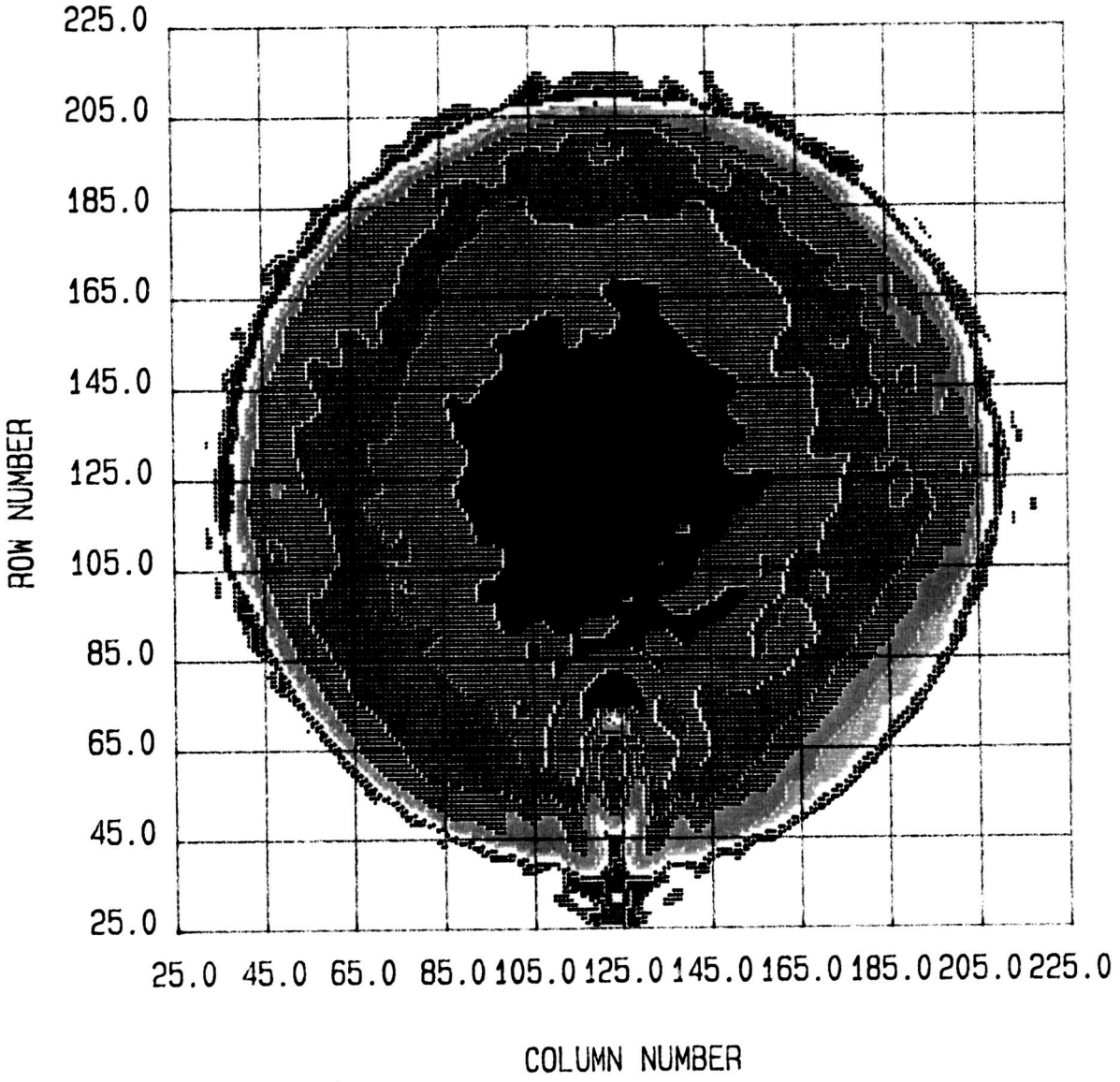


Color Scale (dB):

| | | | | | | | |
|---|---|---|---|---|---|---|---|
| 0 | > Red | > -3 | | -15 | > Lime | > -18 |
| -3 | > Black | > -6 | | -18 | > Yellow | > -21 |
| -6 | > Purple | > -9 | | -21 | > Orange | > -24 |
| -9 | > Blue | > -12 | | -24 | > Red | > -27 |
| -12 | > Green | > -15 | | -27 | > Black | > -30 |

Figure 5: Aperture Field Amplitude Plot

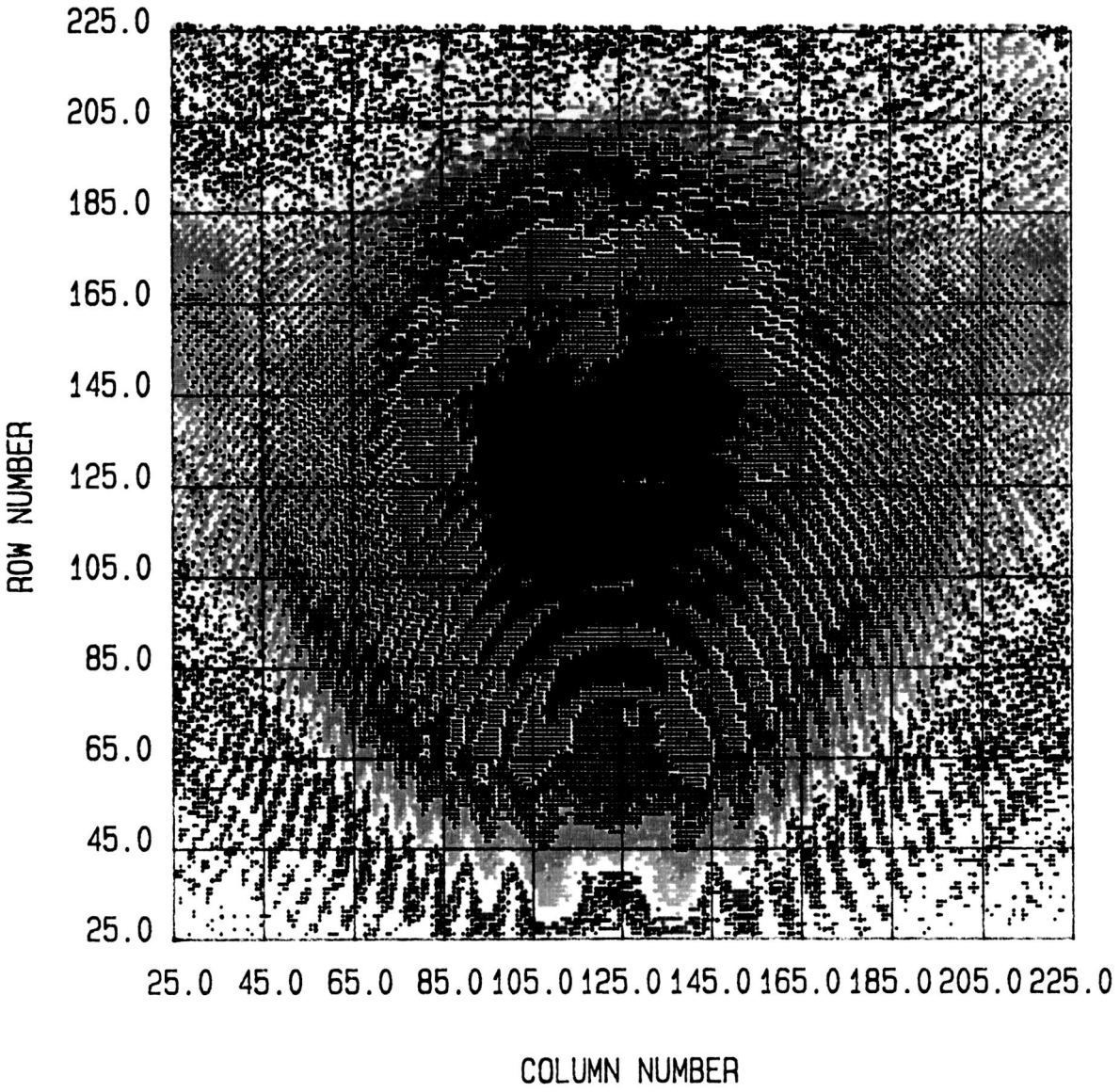


Color Scale (dB):

| | | | | | | | |
|---|---|---|---|---|---|---|---|
| 0 | > | Red | > -3 | -15 | > | Lime | > -18 |
| -3 | > | Black | > -6 | -18 | > | Yellow | > -21 |
| -6 | > | Purple | > -9 | -21 | > | Orange | > -24 |
| -9 | > | Blue | > -12 | -24 | > | Red | > -27 |
| -12 | > | Green | > -15 | -27 | > | Black | > -30 |

Figure 6: Near-Field Amplitude Plot

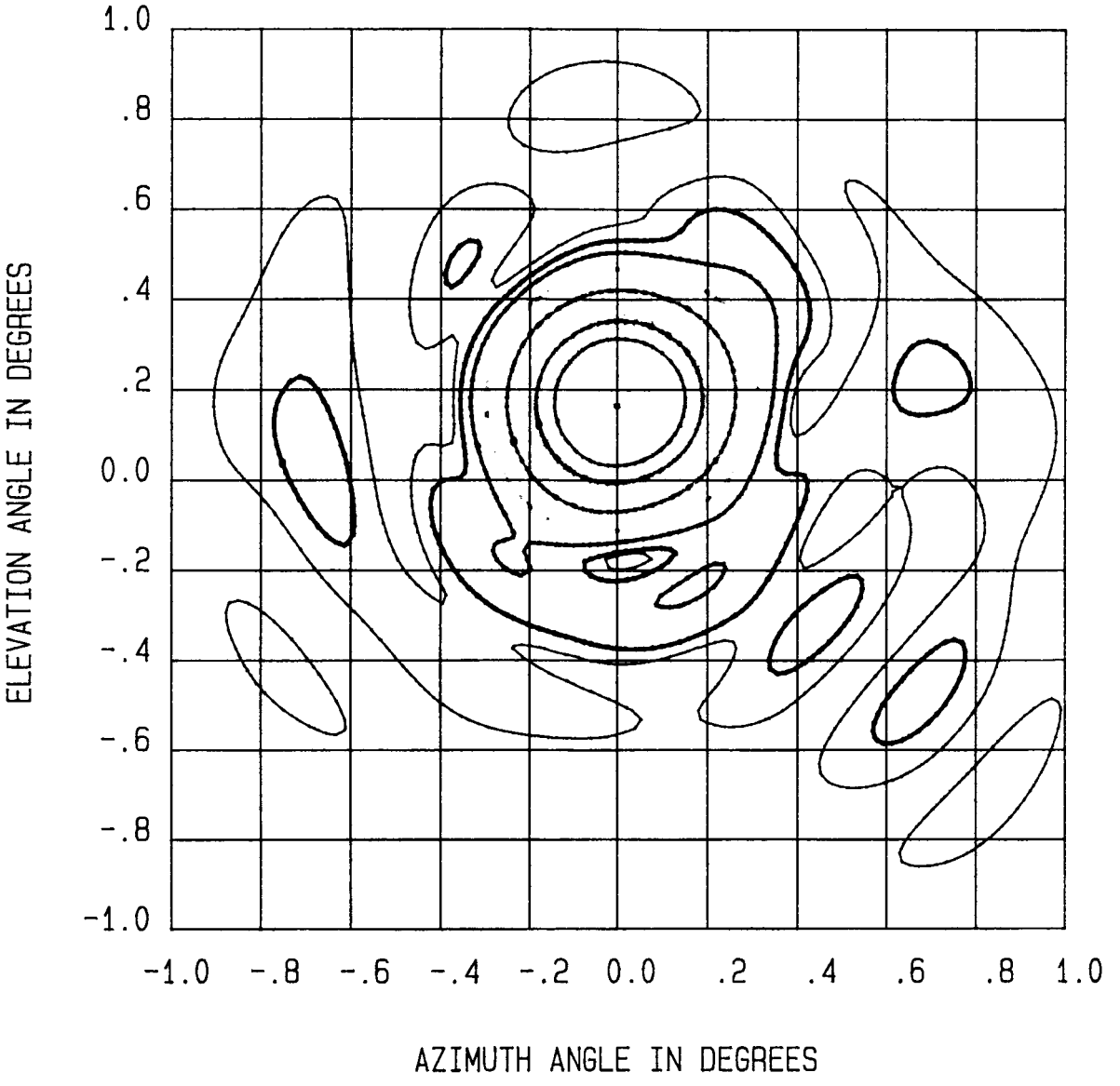


Color Scale (dB):

| | | | | | |
|---|---|---|---|---|---|
| Purple | = | -0.0001 | Yellow | = | -15 |
| Blue | = | -3 | Orange | = | -20 |
| Green | = | -5 | Red | = | -25 |
| Lime | = | -10 | Black | = | -30 |

Figure 7: Reference Baseline Far-Field with Surface Errors

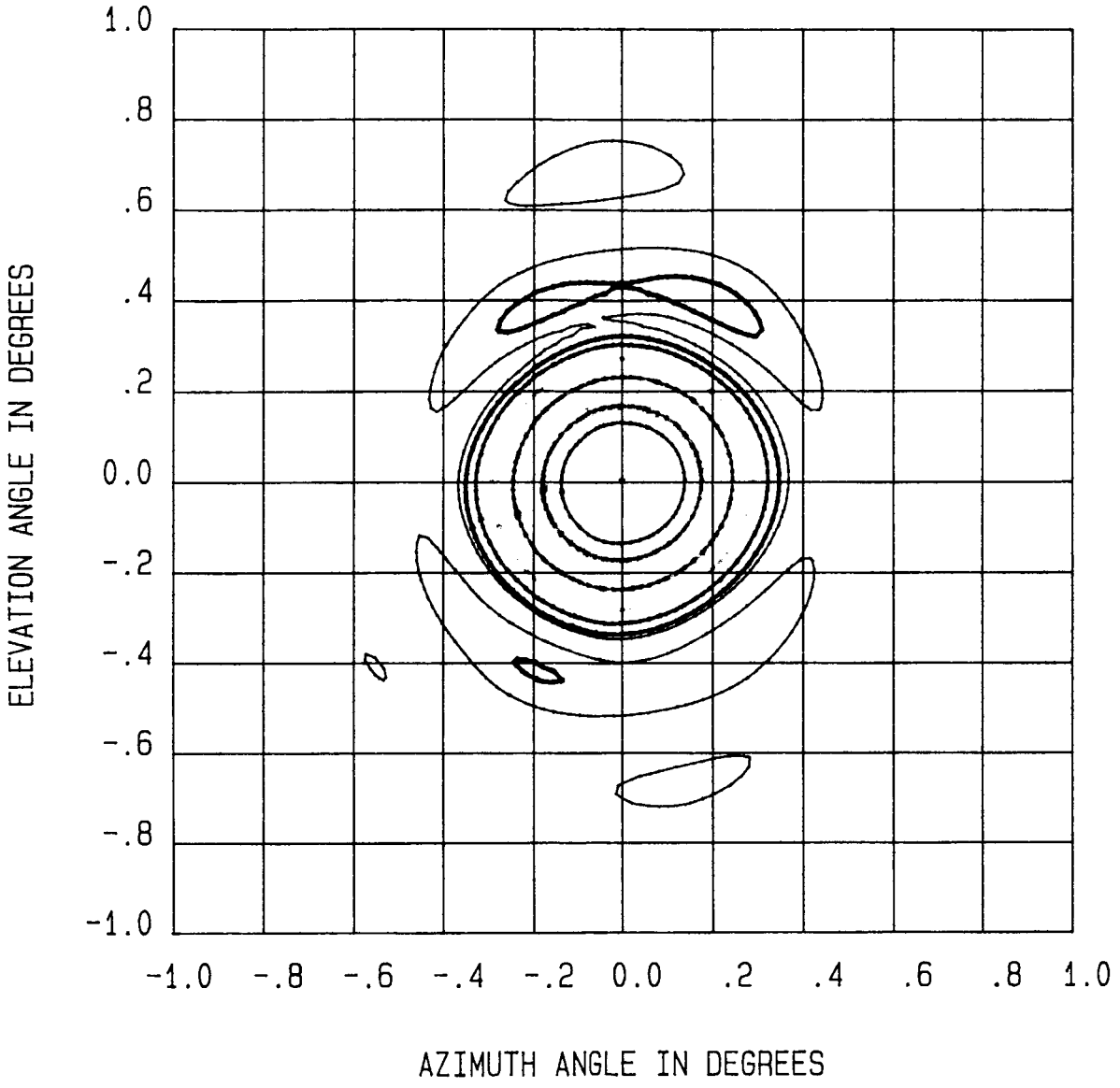


Color Scale (dB):

| | | | | | |
|---|---|---|---|---|---|
| Purple | = | -0.0001 | Yellow | = | -15 |
| Blue | = | -3 | Orange | = | -20 |
| Green | = | -5 | Red | = | -25 |
| Lime | = | -10 | Black | = | -30 |

Figure 8: Reference Baseline Far-Field with Ideal (Ratioed) Surface

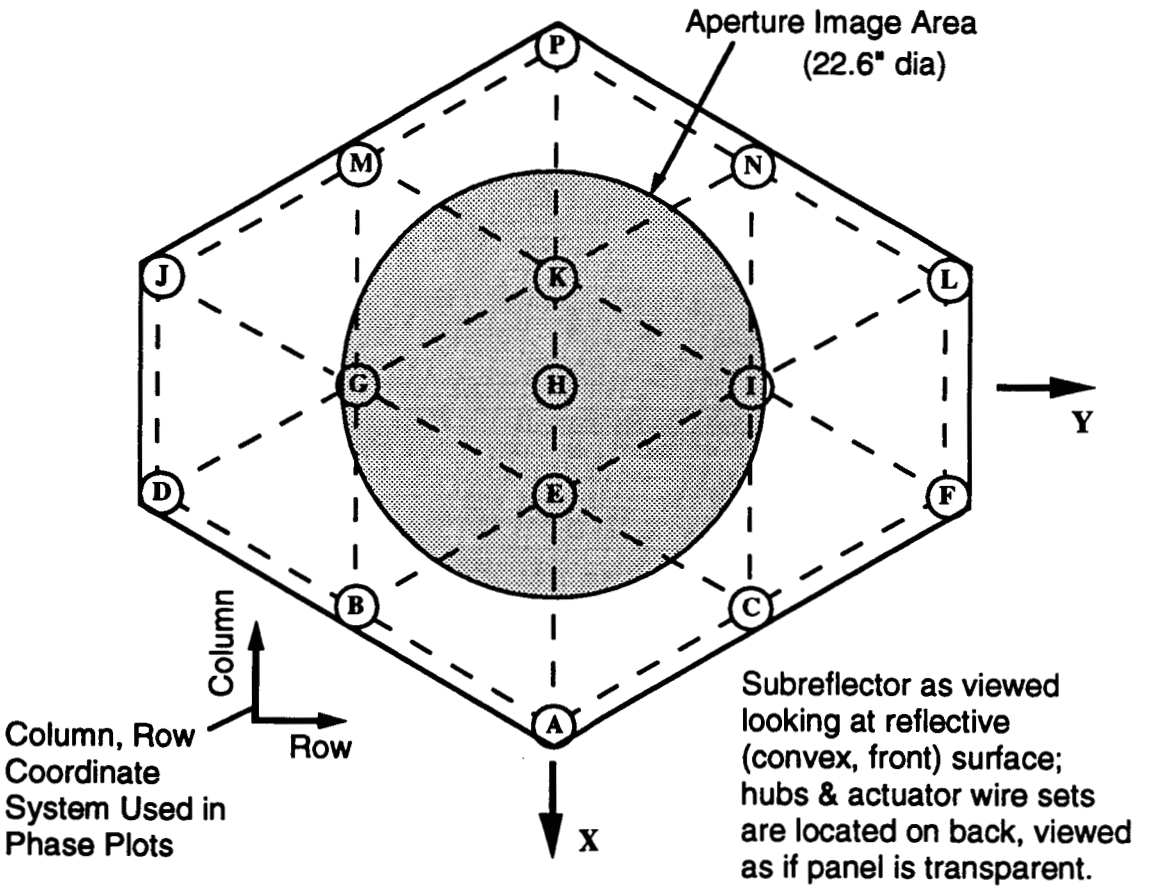


Figure 9. Antenna Subreflector Layout with Aperture Image Overlay

Test Descriptions, Results & Observations

The first three tests performed with the subreflector actuated consisted of symmetric actuation schemes. In Test 1, all strings were actuated simultaneously at the 20% level; for Test 2, all but the ten perimeter strings were actuated at 20%; and for Test 3, only the ten perimeter strings were actuated, again at 20%. The actuation schemes used in Tests 1 & 3 are identical to those used in the last two theodolite tests (see Appendix A, Figures A-29 & A-30) and were selected as points of cross reference. Test 2 was run to determine if the perimeter strings, when actuated at the same level as the interior strings, have any impact on the antenna pattern; results of the theodolite tests indicated that these perimeter strings should have no affect. The perturbation on aperture phase caused by actuating all strings at 20% (Test 1) is shown in Figure 10. The difference in aperture phase for Tests 1 and 2 is shown in Figure 11 and an overlay of the far-field antenna responses for these two tests is presented in Figure 12; the differences shown by these comparisons are minor implying that the two cases are essentially identical, as expected. Aperture phase results and far field data for Test 3 are presented in Figures 13 and 14, respectively.

The results of these first three tests indicate that the placement of the perimeter actuators has made them relatively useless to effect significant changes in the performance of the antenna system, whereas, the interior set of actuators can easily change the system performance. In addition, beam steering and gain change, desired goals of this test effort, have been achieved. The gain change attained in Test 1, clearly seen in the broadening of the main beam of the pattern (compare Figures 8 & 12), was -0.62 dB. This gain loss was caused by the increased curvature of the subreflector defocusing the antenna and thus broadening the beam. The odd result of the actuation in Test 1 was the asymmetric distortion of the reflector in the offset plane. As shown in Figure 10, the one side of the aperture (row numbers <125) has remained almost fixed in position relative to baseline while the remaining area has pivoted about it. This was expected to happen based on the subreflector design with the center point (node H) as a fixed position. However, what is surprising is that this fixed region on the reflector is apparently shifted off-center in the +Y direction (compare row/column coordinates in Figures 9 & 10) approximately 5 inches. The assumption is that a stiff region must exist, caused by a varying end-to-end rigidity in the subreflector, rather than a simple hard point at the mounting node because a 5 inch misalignment should have been readily perceived by visual inspection. All subsequent testing continued to show the apparent existence of this rigid region in the subreflector. Note that since the curvature of the subreflector is greater in the +Y half than in the -Y half (refer to note in Figure 2), a greater stiffness in the +Y half is not unexpected.

The next four tests (4 through 7) performed on the antenna involved the use of asymmetric actuation schemes where only strings on a given half of the subreflector were actuated; all actuations were at the 20% level. For Test 4, all strings on the -Y half were actuated (i.e., strings A-B, A-E, B-D, B-E, B-G, D-G, D-J, E-G, G-J, G-K, G-M, J-M, K-M, K-P, M-P). In Test 5, all strings on the +Y half were actuated (i.e., strings A-C, A-E, C-E, C-F, C-I, E-I, F-I, F-L, I-K, I-L, I-N, K-N, K-P, L-N, N-P). The perturbations of the aperture phase for Test 4 and Test 5 are shown in Figures 15 and 16, respectively. The far-field perturbations of Tests 4 and 5 are overlaid in Figure 17. The noticeable effect of the stiff region under this condition was to reduce steering in the elevation direction for Test 5. Test 4 steered the reflector more because the actuated strings are located in the softer (-Y) region of the subreflector.

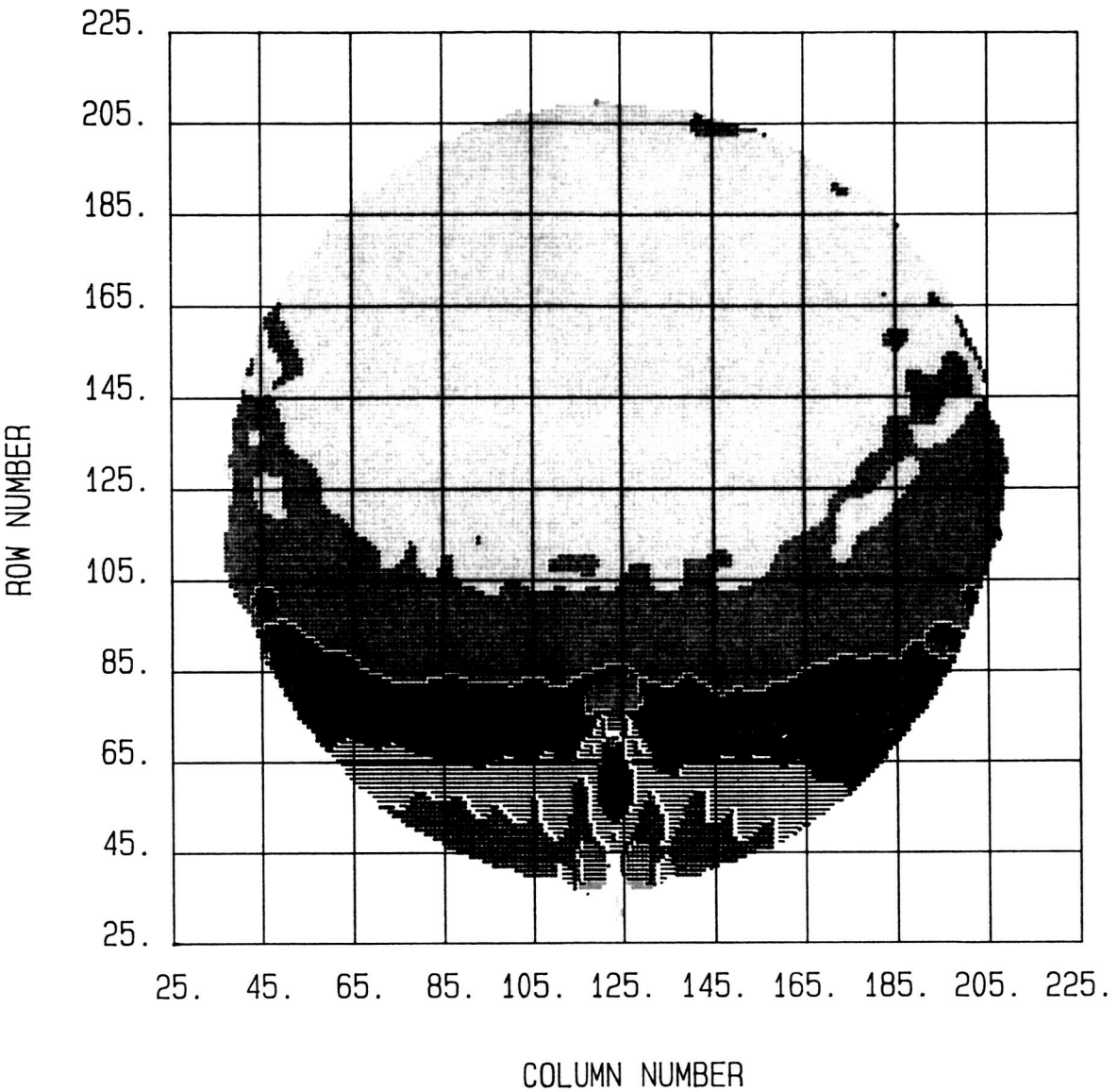


Color Scale:

| | | | | | | | | |
|---|---|---|---|---|---|---|---|---|
| -180° | < | Black | < | -135° | 0° | < | Lime | < 45° |
| -135° | < | Red | < | -90° | 45° | < | Green | < 90° |
| -90° | < | Orange | < | -45° | 90° | < | Blue | < 135° |
| -45° | < | Yellow | < | 0° | 135° | < | Purple | < 180° |

Figure 10: Aperture Phase Change with All Actuators at 20% (Test 1)

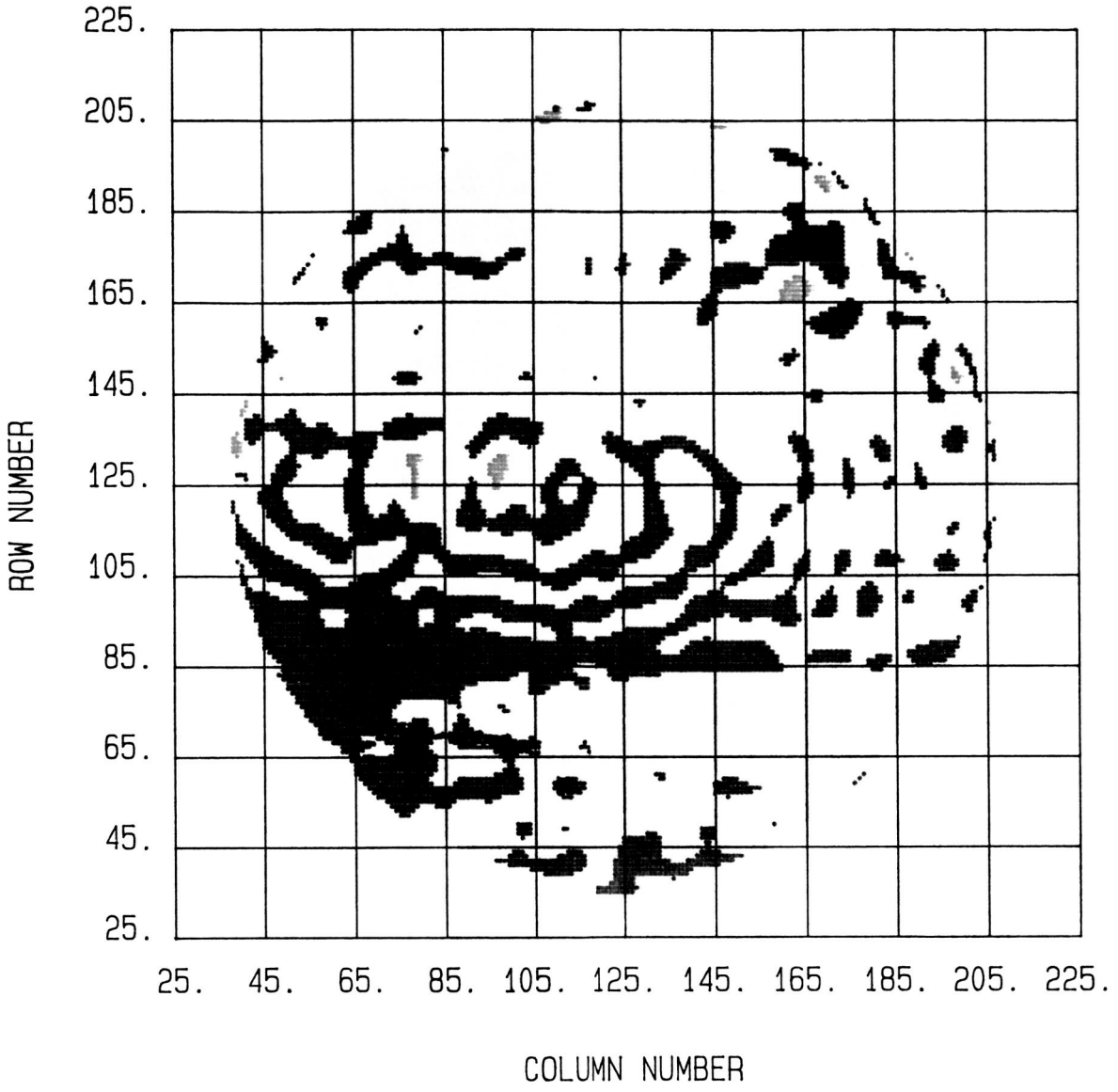


Color Scale:

| | | | | | | | | |
|---|---|---|---|---|---|---|---|---|
| -28° | < | Black | < | -20° | 4° | < | Lime | < 12° |
| -20° | < | Red | < | -12° | 12° | < | Green | < 20° |
| -12° | < | Orange | < | -4° | 20° | < | Blue | < 28° |
| -4° | < | Yellow | < | 4° | 28° | < | Purple | < 36° |

Figure 11: Aperture Phase of Test 1 and Test 2 Ratioed

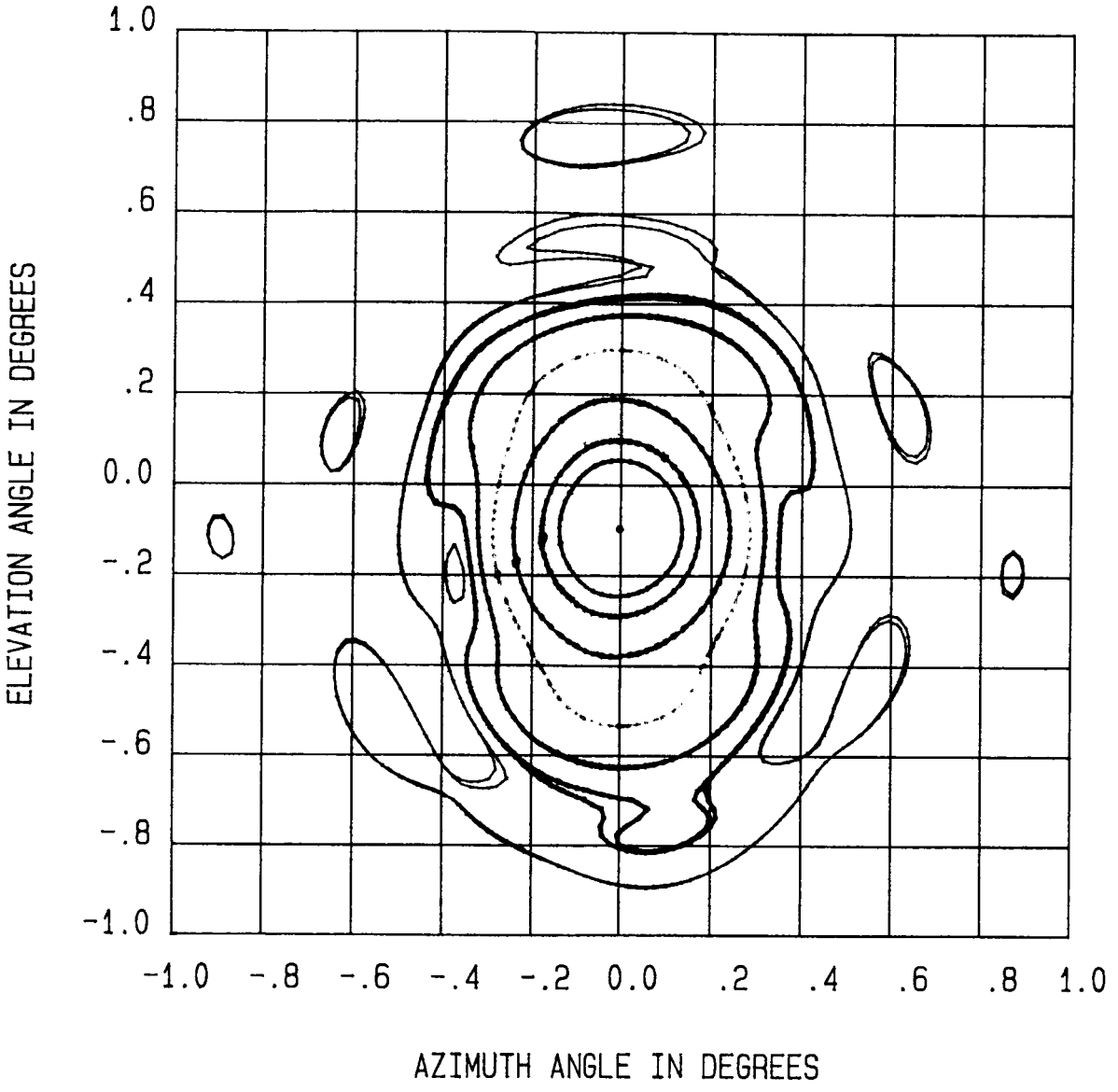


Color Scale (dB):

| | | | | | |
|---|---|---|---|---|---|
| Purple | = | -0.0001 | Yellow | = | -15 |
| Blue | = | -3 | Orange | = | -20 |
| Green | = | -5 | Red | = | -25 |
| Lime | = | -10 | Black | = | -30 |

Figure 12: Overlay of Far-Field Perturbations of Test 1 and Test 2

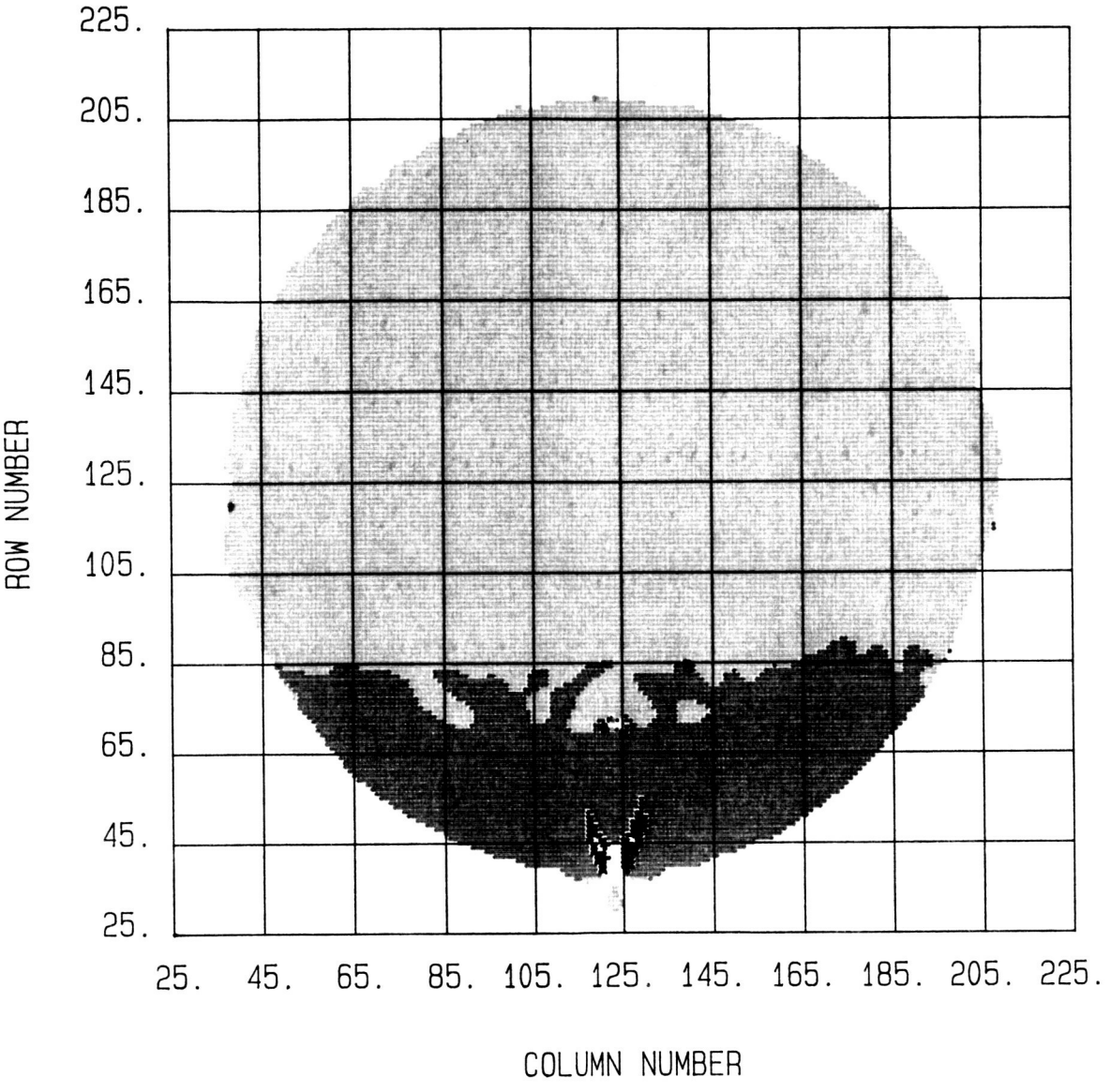


Color Scale:

| | | | | | | | | |
|---|---|---|---|---|---|---|---|---|
| -180° | < | Black | < | -135° | 0° | < | Lime | < 45° |
| -135° | < | Red | < | -90° | 45° | < | Green | < 90° |
| -90° | < | Orange | < | -45° | 90° | < | Blue | < 135° |
| -45° | < | Yellow | < | 0° | 135° | < | Purple | < 180° |

Figure 13: Aperture Phase Change of Test 3

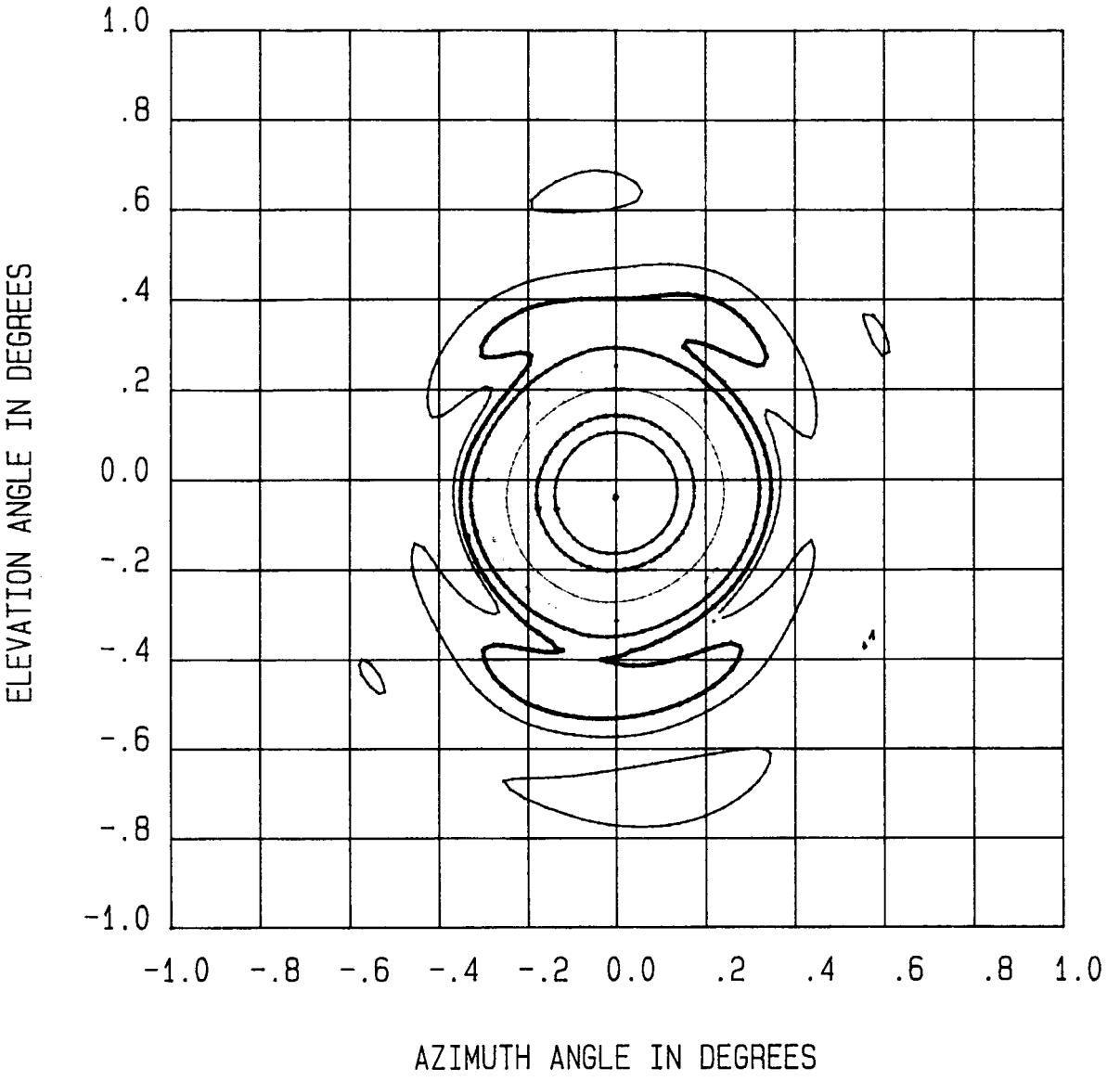


Color Scale (dB):

| | | | | | |
|---|---|---|---|---|---|
| Purple | = | -0.0001 | Yellow | = | -15 |
| Blue | = | -3 | Orange | = | -20 |
| Green | = | -5 | Red | = | -25 |
| Lime | = | -10 | Black | = | -30 |

Figure 14: Far-Field Perturbation of Test 3

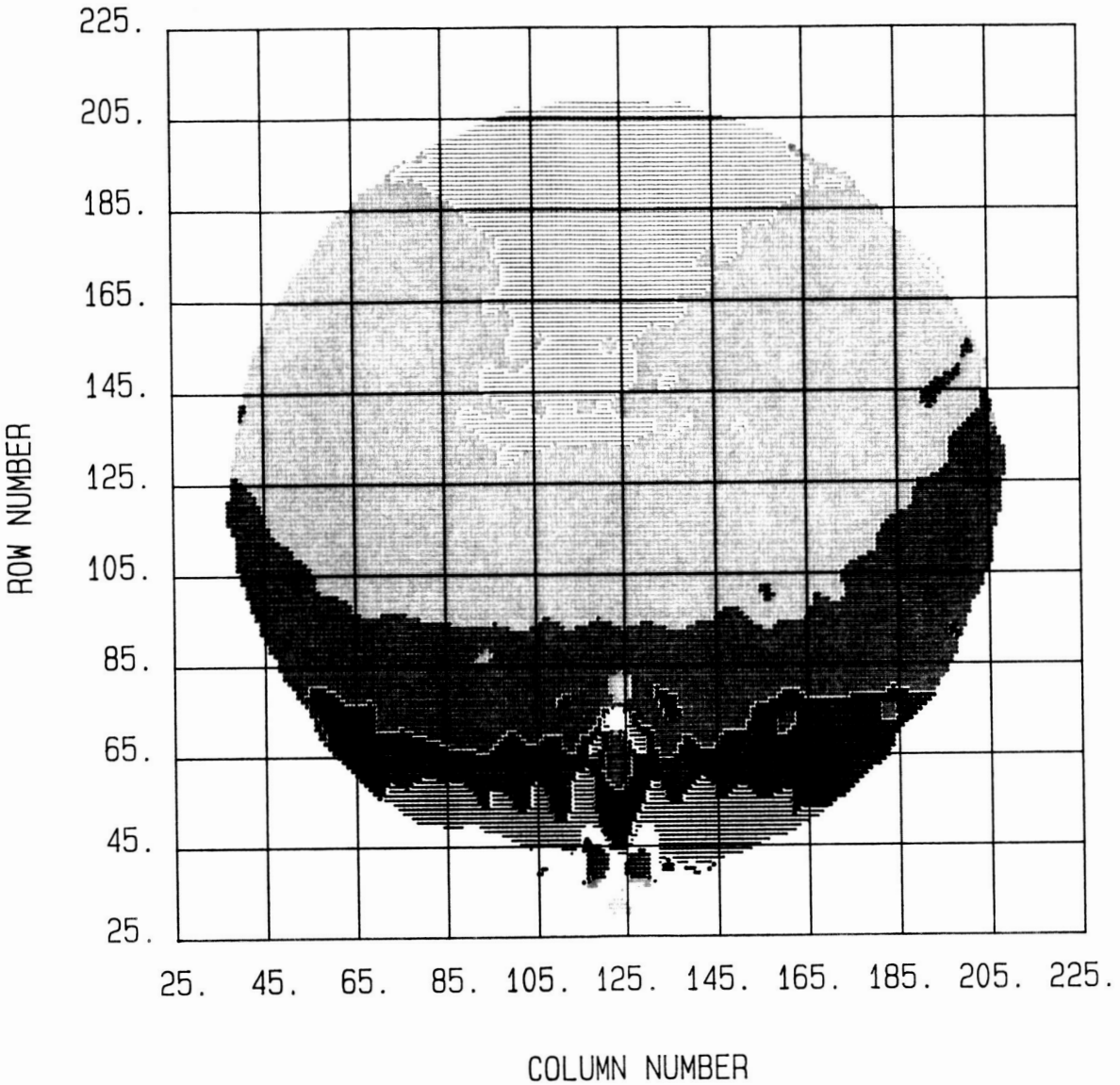


Color Scale:

| | | | | | | | | |
|---|---|---|---|---|---|---|---|---|
| -180° | < | Black | < | -135° | 0° | < | Lime | < 45° |
| -135° | < | Red | < | -90° | 45° | < | Green | < 90° |
| -90° | < | Orange | < | -45° | 90° | < | Blue | < 135° |
| -45° | < | Yellow | < | 0° | 135° | < | Purple | < 180° |

Figure 15: Aperture Phase Change of -Y Half Actuation (Test 4)

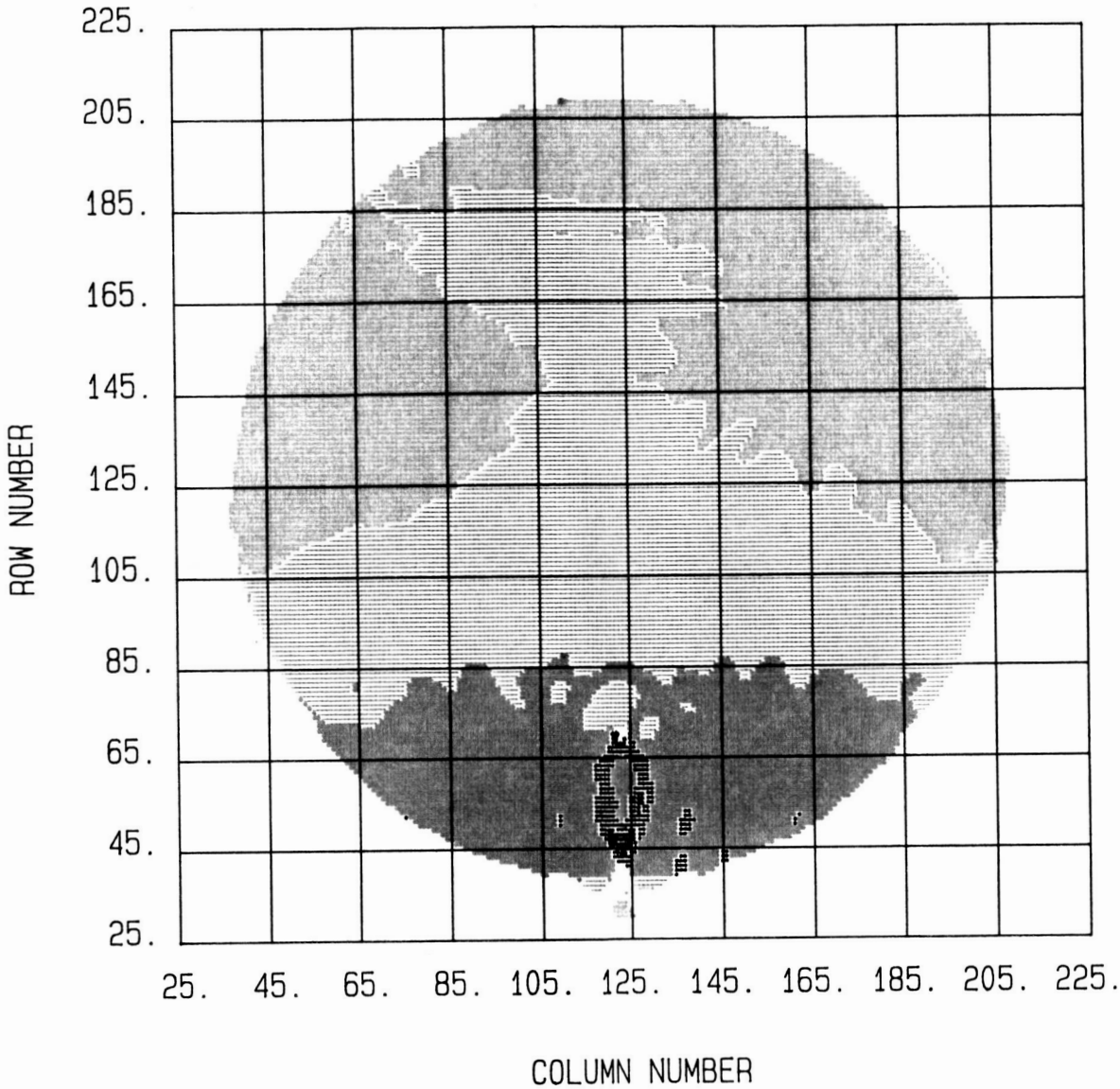


**Color Scale:**

| | | | | | | | | |
|---|---|---|---|---|---|---|---|---|
| -180° | < | Black | < | -135° | 0° | < | Lime | < 45° |
| -135° | < | Red | < | -90° | 45° | < | Green | < 90° |
| -90° | < | Orange | < | -45° | 90° | < | Blue | < 135° |
| -45° | < | Yellow | < | 0° | 135° | < | Purple | < 180° |

Figure 16: Aperture Phase Change of +Y Half Actuation (Test 5)

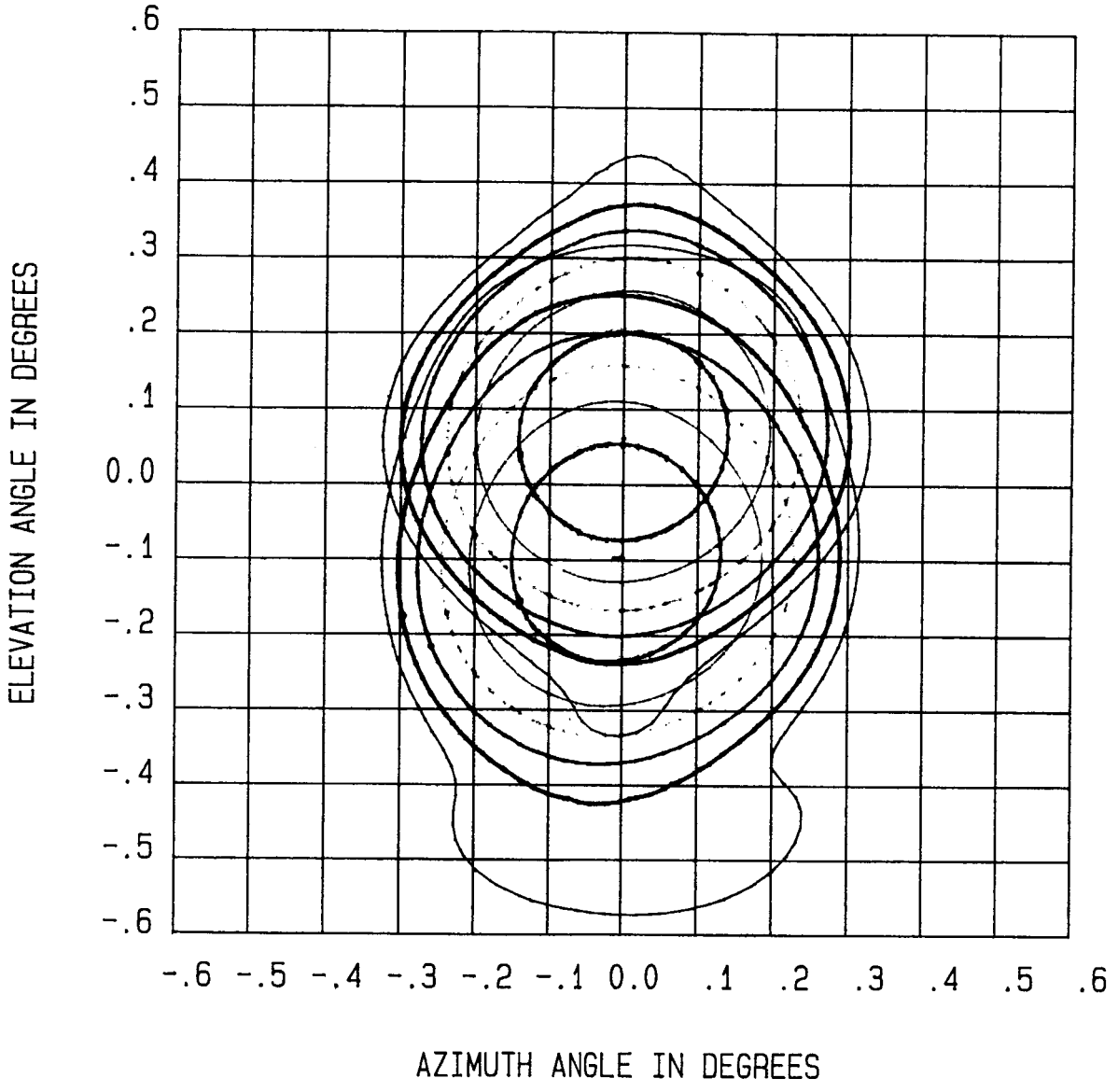


Color Scale (dB):

| | | | | | |
|---|---|---|---|---|---|
| Blue | = | -0.0001 | Orange | = | -12 |
| Green | = | -3 | Red | = | -15 |
| Lime | = | -6 | Black | = | -18 |
| Yellow | = | -9 | | | |

Test 4 = Lower Pattern  Test 5 = Upper Pattern

Figure 17: Overlay of Far-Field Perturbations of Test 4 and 5

During Test 6, all strings on the -X half were actuated (i.e., strings D-J, F-L, G-J, G-K, G-M, I-K, I-L, I-N, J-M, K-M, K-N, K-P, L-N, M-P, N-P). For test 7, all strings on the +X half were actuated (i.e., strings A-B, A-C, A-E, B-D, B-E, B-G, C-E, C-F, C-I, D-G, D-J, E-G, E-I, F-I, F-L). Aperture phase perturbations for Test 6 and 7 are shown in Figures 18 and 19, respectively; a comparison of the far-field perturbations is shown in Figure 20. Both cases resulted in predominantly steering only in elevation. The steering in the desired azimuth direction was minimal, primarily due to the lack of actuators within the area of the aperture beam. The beam distortion and resulting gain reduction was minimal, 0.07 dB for Test 6 and 0.39 dB for Test 7. The fact that gain distortion in Test 6 was less than in Test 7 indicates a possible asymmetry in subreflector stiffness along the X-axis with the -X side being more stiff than the +X. Coupling this information with the previously noted stiffness variation along the Y-axis, one can conclude that -X+Y is probably the most stiff of the four quadrants. Note that results of the theodolite tests also indicated an apparent asymmetry located in the -X+Y quadrant.

Next, three tests (8, 9 & 10) were performed in an attempt to effect a desired change in the subreflector contour. Evaluation of the data obtained in previous tests had indicated that the subreflector surface contour could be improved if the region near hub G were moved in the +Z direction. For Tests 8 & 9, intuitive reasoning (or lack thereof) was used to select the two strings (E-I & E-G for Test 8) and the one string (G-K used in Test 9) thought most likely to produce the desired contour improvement. Unfortunately, these guesses were incorrect because actuation of the selected strings did not improve, instead degraded the subreflector contour. For Test 10, intuitive reason was abandoned and replaced by quantitative assessment using theodolite test data to select all strings that cause +Z motion at hub G. Assuming the effects to be additive, this should produce the maximum possible desired change to the subreflector contour. The following strings were actuated at 20% for Test 10: B-D, C-I, G-J, G-M, I-L, I-N, K-N, K-P, L-N and N-P. (Note that string A-E also causes +Z motion at hub G, see Figure A-3, but was not included in this test -- an oversight.) The aperture phase data for Test 10, shown in Figure 21, indicates that the +Z motion at hub G was obtained as desired. In general, the results from these contour modification tests indicate that although subreflector surface control is feasible, this particular design does not provide for tight control of the image aperture region. This lack of tight control is primarily attributed to the low density spacing of actuators within the region (see Figure 9) and use of an indirect actuation technique that uses actuator motion parallel to the surface (i.e., tension in the shape memory wires) to enact contour changes perpendicular to the surface (i.e., Z-axis displacements). Higher density, direct Z-axis actuation would be preferable.

The final test (Test 11) was conducted to determine the relative amount of antenna pattern variation that could be generated by increasing the subreflector actuation level. For this test, all interior strings were actuated at roughly 50% of their maximum strain capability. Note that use of all interior strings is equivalent to actuating all strings, as proven in Tests 1 & 2. The phase data obtained from this test is presented in Figure 22. Because more than one complete cycle of phase change has occurred across the aperture, the associated deflection is greater than 0.4 inches from nominal. This deflection did introduce an enormous quadratic phase error resulting in a gain loss from nominal of 3.28 dB. The resulting beam, seen in Figure 23, was steered almost a beamwidth and was distorted to roughly double the total beamwidth in the steered plane. Based on these test results it is obvious that with the minimal adjustment capability in this surface, drastic changes can be caused in system pattern performance without using the traditional complex beamforming network.

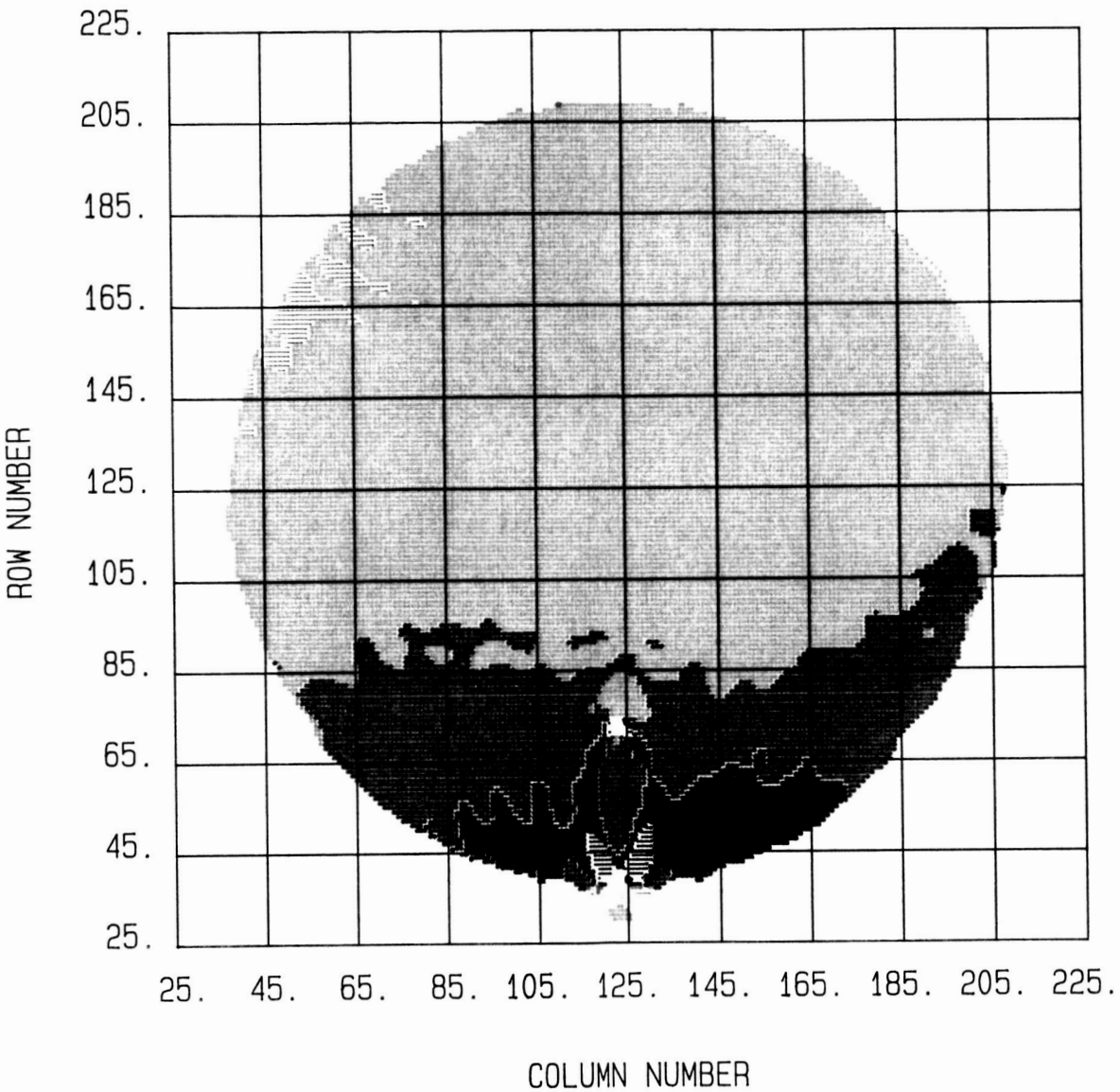


Color Scale:

| | | | | | | | | |
|---|---|---|---|---|---|---|---|---|
| -180° | < | Black | < | -135° | 0° | < | Lime | < 45° |
| -135° | < | Red | < | -90° | 45° | < | Green | < 90° |
| -90° | < | Orange | < | -45° | 90° | < | Blue | < 135° |
| -45° | < | Yellow | < | 0° | 135° | < | Purple | < 180° |

Figure 18: Aperture Phase Change of -X Half Actuation (Test 6)

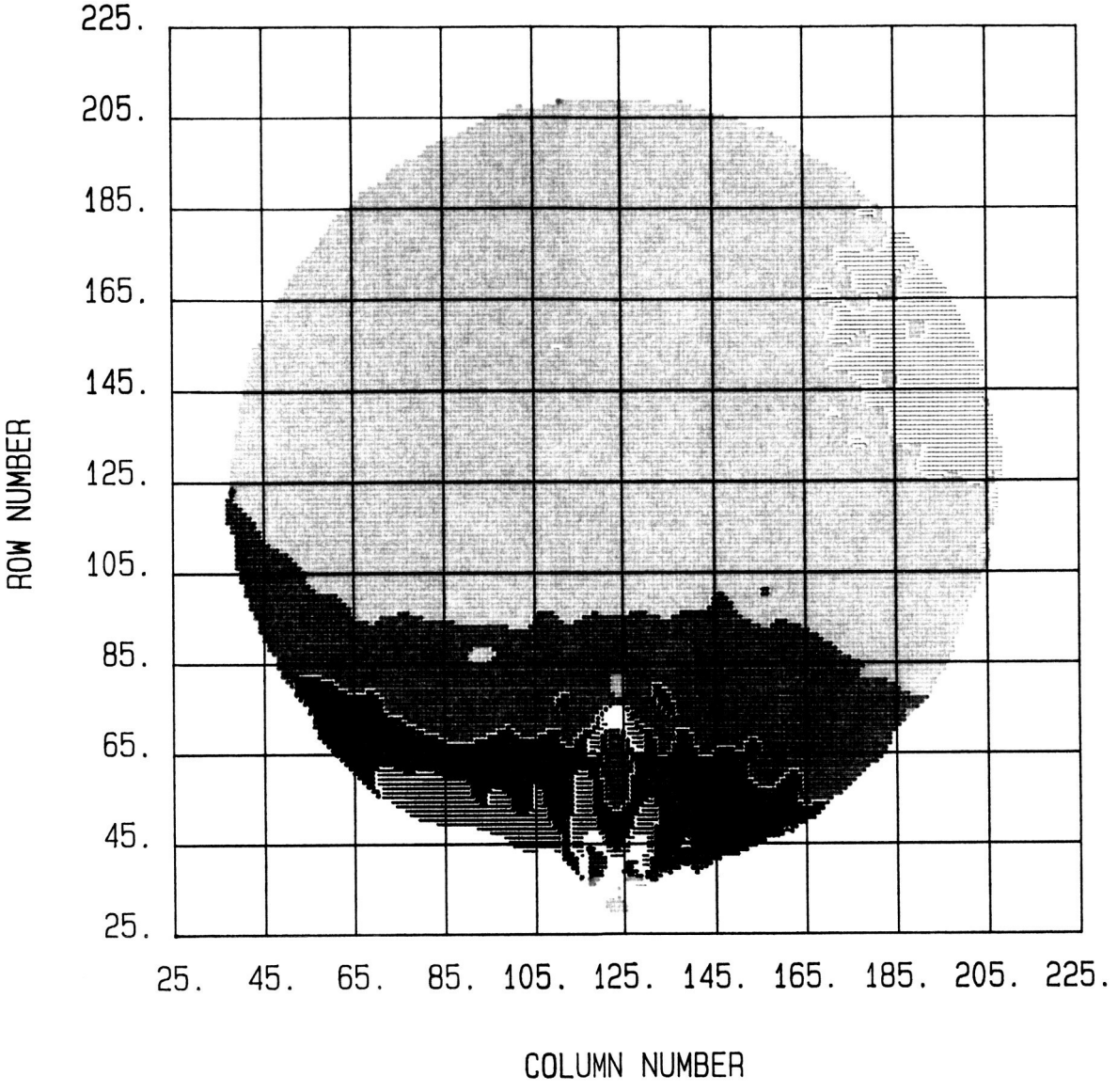


Color Scale:

| | | | | | | | | |
|---|---|---|---|---|---|---|---|---|
| -180° | < | Black | < | -135° | 0° | < | Lime | < 45° |
| -135° | < | Red | < | -90° | 45° | < | Green | < 90° |
| -90° | < | Orange | < | -45° | 90° | < | Blue | < 135° |
| -45° | < | Yellow | < | 0° | 135° | < | Purple | < 180° |

Figure 19: Aperture Phase Change of +X Half Actuation (Test 7)

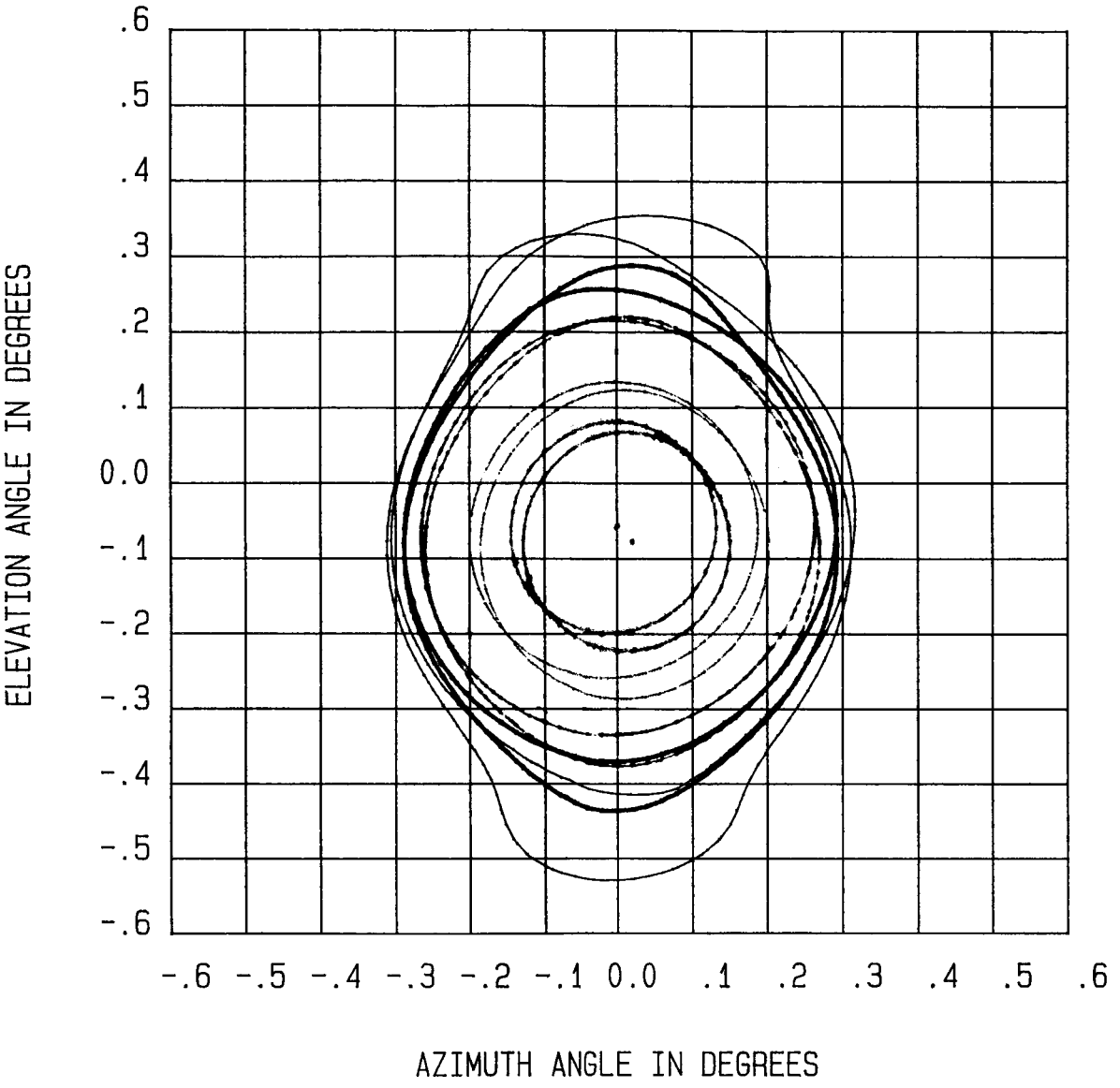


Color Scale (dB):

| | | | | | |
|---|---|---|---|---|---|
| Blue | = | -0.0001 | Orange | = | -12 |
| Green | = | -3 | Red | = | -15 |
| Lime | = | -6 | Black | = | -18 |
| Yellow | = | -9 | | | |

Test 6 = Upper-Left Pattern  Test 7 = Lower-Right Pattern

Figure 20: Overlay of Far-Field Perturbations of Tests 6 and 7

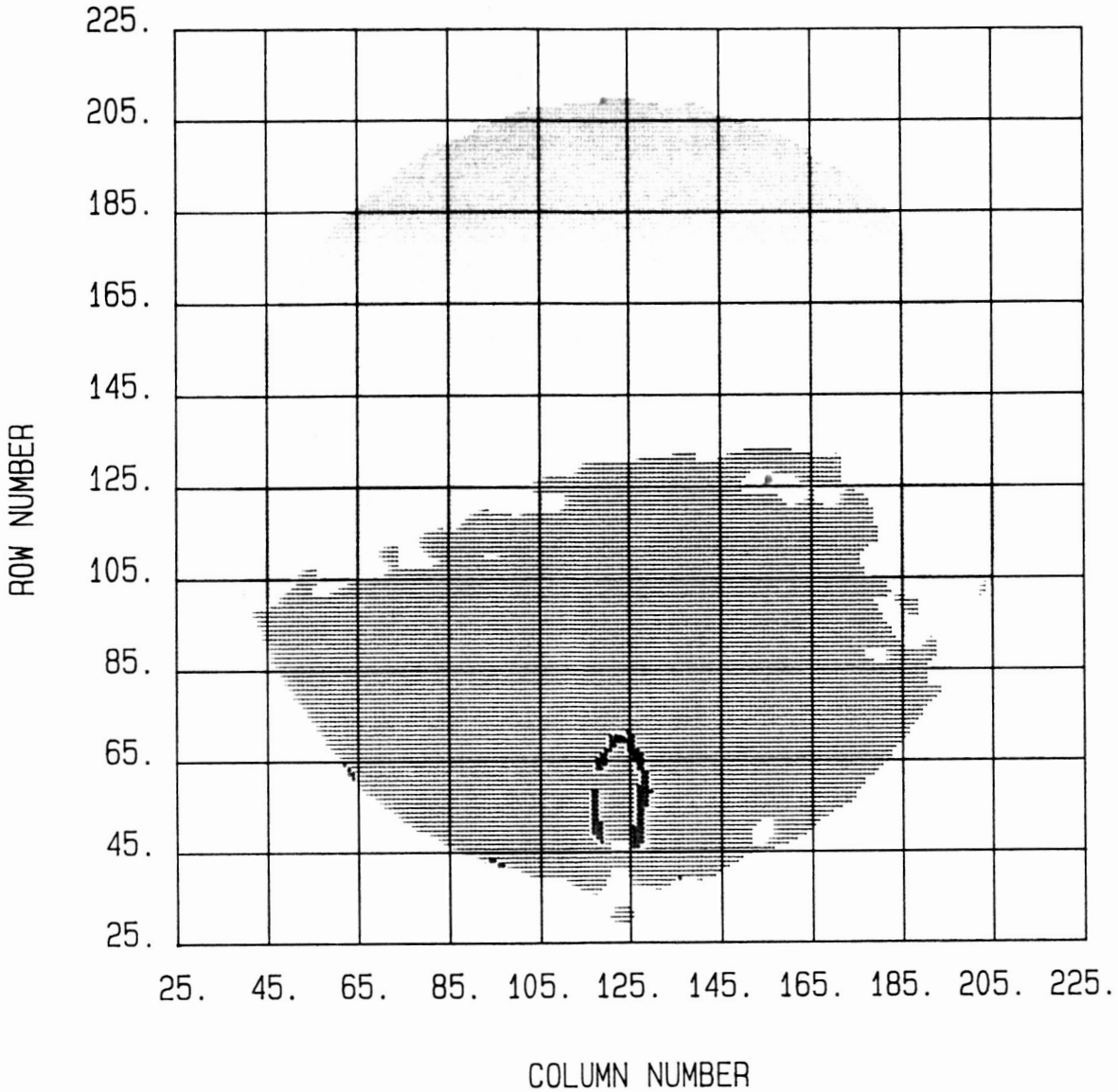


**Color Scale:**

| | | | | | | | | |
|---|---|---|---|---|---|---|---|---|
| -180° | < | Black | < | -135° | 0° | < | Lime | < 45° |
| -135° | < | Red | < | -90° | 45° | < | Green | < 90° |
| -90° | < | Orange | < | -45° | 90° | < | Blue | < 135° |
| -45° | < | Yellow | < | 0° | 135° | < | Purple | < 180° |

Figure 21: Aperture Phase Change in Moving Node G Forward (Test 10)

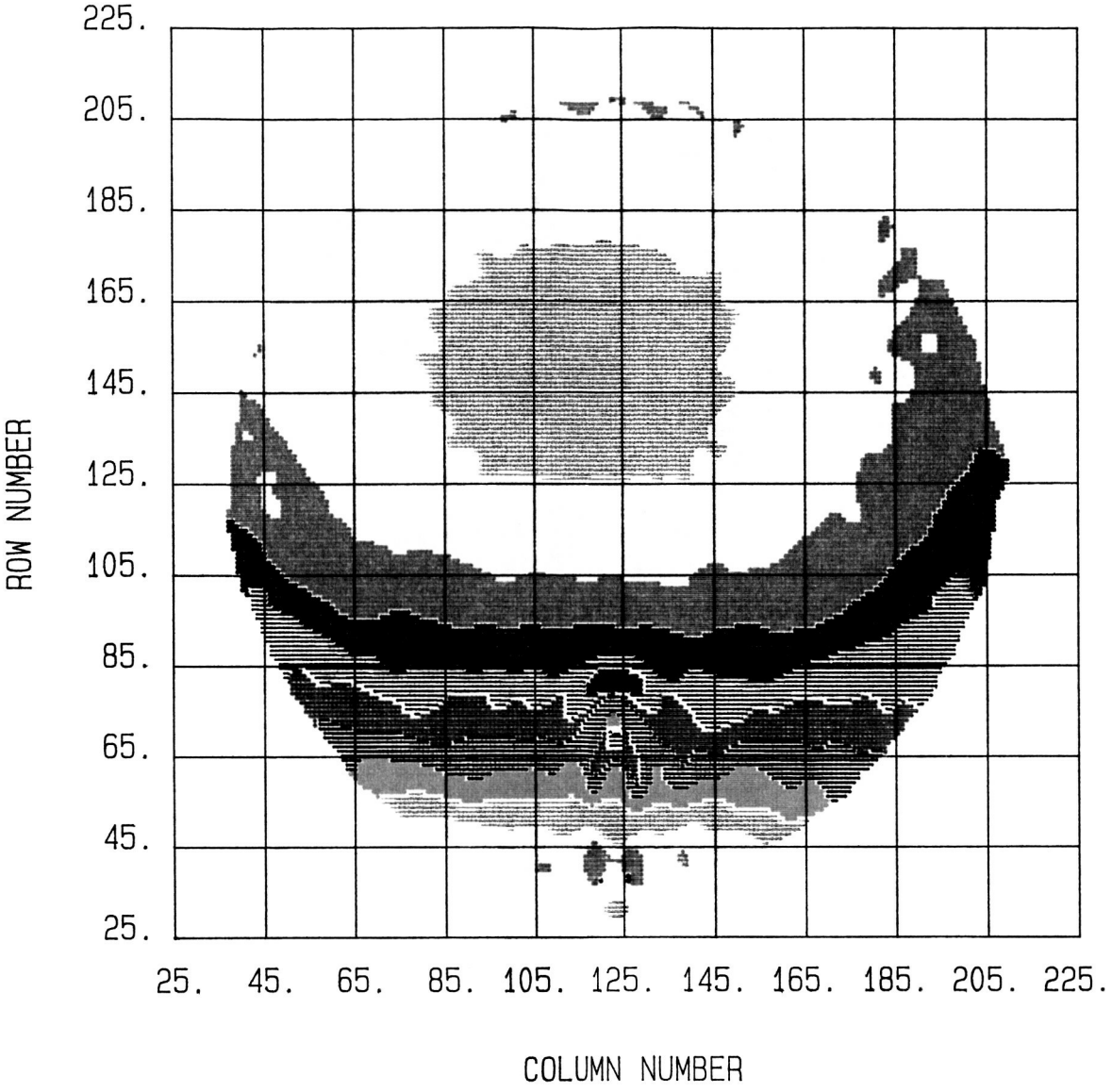


Color Scale:

| | | | | | | | | |
|---|---|---|---|---|---|---|---|---|
| -180° | < | Black | < | -135° | 0° | < | Lime | < 45° |
| -135° | < | Red | < | -90° | 45° | < | Green | < 90° |
| -90° | < | Orange | < | -45° | 90° | < | Blue | < 135° |
| -45° | < | Yellow | < | 0° | 135° | < | Purple | < 180° |

Figure 22: Aperture Phase Change at 40% Actuation (Test 11)

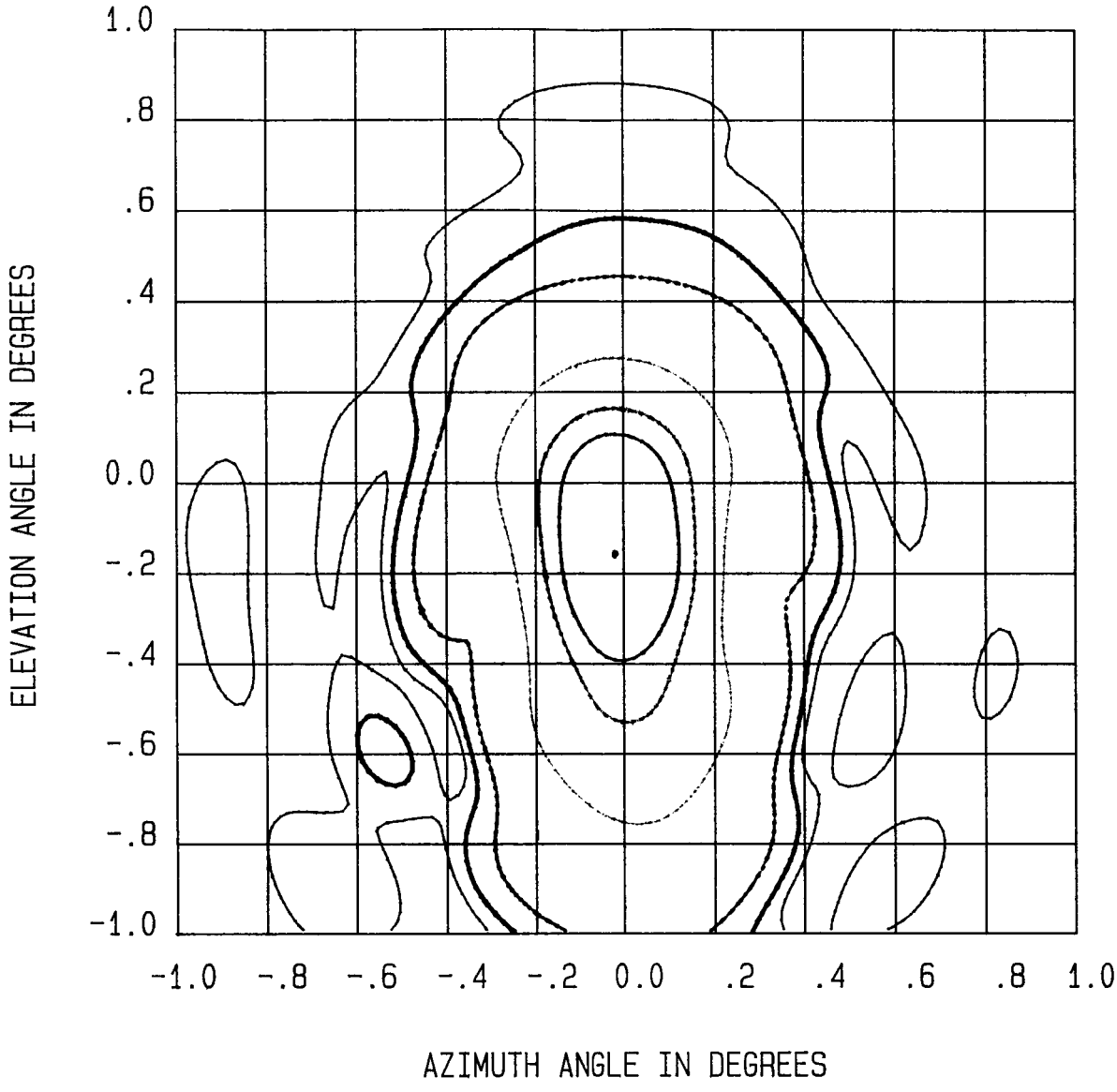


Color Scale (dB):

| | | | | | |
|---|---|---|---|---|---|
| Purple | = | -0.0001 | Yellow | = | -15 |
| Blue | = | -3 | Orange | = | -20 |
| Green | = | -5 | Red | = | -25 |
| Lime | = | -10 | Black | = | -30 |

Figure 23: Far-Field Pattern at 40% Actuation (Test 11)

## Proposed Applications & Recommendations

The subreflector surface control system used for these tests obviously has several iterations to go through before it can be considered a viable technology for satellite use. Important improvements to be implemented in the design include reduction in power consumption, more predictable perpendicularly directed surface distortions and some preloading method to get the actuators in their midrange of travel for nominal condition. This method of surface control could be used on microwave antennas in the same way corrective optics are used on telescopes to compensate for thermal or gravitational loading that introduce a systematic distortion of the main reflector. Also, as the method becomes more refined with more nodes of control on the active surface, the surface could compensate for surface errors in the main reflector and atmospheric distortion. Compensation for the large cubic phase errors seen in beam steering could also be implemented to allow steering with only minor loss for smaller f/d antennas. Currently, the most convenient way to minimize steering losses is with large f/d antennas which can be extremely awkward to deploy. The important feature in whether the shape memory wire actuator technology has an application in the antenna field is whether the technology is cheaper, simpler, and more reliable as a mature technology than the other methods currently in use such as beamformers and mechanical actuator/gimbal systems.

## Conclusions

The adaptive antenna test program demonstrated that noticeable changes to antenna patterns could be caused with minimal actuation of the subreflector, 20% actuation of an actuator string could easily be detected in the near-field measurement. Because the subreflector was shaped for near optimal performance with all actuators turned off, the only variance in gain attained during actuation was negative. Gain loss was accomplished by beam broadening, a similar implementation using a beamforming network would be much more lossy. Beam steering was less than a beamwidth, but this is reasonable for a system designed to produce small deflections. Much larger steering angles could have been achieved using a long shape memory wire actuator pulling perpendicular to the surface like a mechanical actuator. The overall test program described herein is considered to be a success in that the use of shape memory wire actuation to perform adaptive antenna control was proven feasible; however, the technology demonstrated obviously needs to go through several more development iterations to become a useful technology for satellite applications.

Research Support Task for Large Scale Antenna Pattern Measurements in a Near Field Facility - Contract No. NAS1-18455

# Appendix A

## Theodolite Test Data

Contents:

**Figure A-1. Theodolite Test - String A-B Actuated**

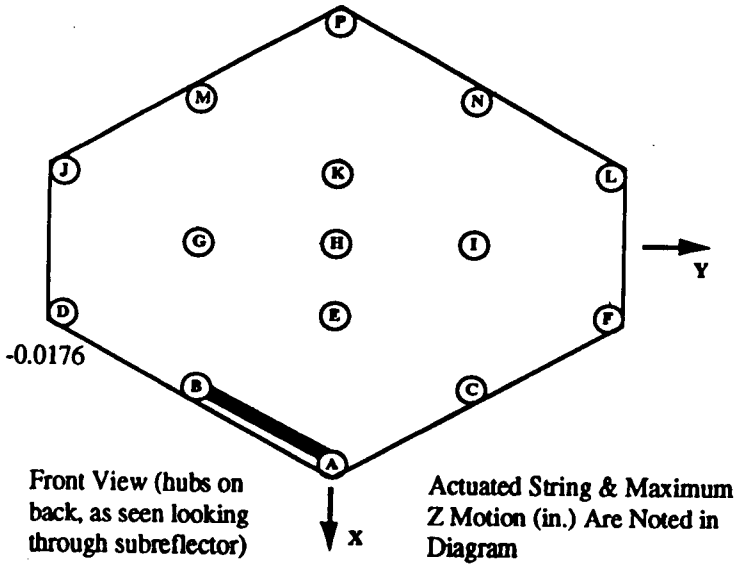


Front View (hubs on back, as seen looking through subreflector)

Actuated String & Maximum Z Motion (in.) Are Noted in Diagram

Power & Strain Data

(nm = not measured)

| String | Power (relative) | Strain (microstrain) |
|---|---|---|
| A-B | 20% | -266 |
| A-C | 0% | 0 |
| A-E | 0% | -44 |
| B-D | 0% | 17 |
| B-E | 0% | -23 |
| B-G | 0% | 22 |
| C-E | 0% | -13 |
| C-F | 0% | -2 |
| C-I | 0% | -11 |
| D-G | 0% | -7 |
| D-J | 0% | -3 |
| E-G | 0% | -29 |
| E-I | 0% | 11 |
| E-K | 0% | nm |
| F-I | 0% | -1 |

| String | Power (relative) | Strain (microstrain) |
|---|---|---|
| F-L | 0% | -6 |
| G-J | 0% | 1 |
| G-K | 0% | -5 |
| G-M | 0% | 7 |
| I-K | 0% | -10 |
| I-L | 0% | 7 |
| I-N | 0% | nm |
| J-M | 0% | nm |
| K-M | 0% | nm |
| K-N | 0% | nm |
| K-P | 0% | nm |
| L-N | 0% | nm |
| M-P | 0% | nm |
| N-P | 0% | nm |

Surface Contour Data

| Hub | Baseline Position | | | Position During Actuation | | | Relative Motion (Actuation - Baseline) | | |
|---|---|---|---|---|---|---|---|---|---|
| | X (in.) | Y (in.) | Z (in.) | X (in.) | Y (in.) | Z (in.) | X (in.) | Y (in.) | Z (in.) |
| A | 18.2866 | -0.3272 | -1.5365 | 18.2846 | -0.3237 | -1.5421 | -0.002 | 0.0035 | -0.0056 |
| B | 12.0141 | -11.1556 | -2.0648 | 12.0138 | -11.1584 | -2.0732 | -0.0003 | -0.0028 | -0.0084 |
| C | 12.2747 | 10.339 | -0.079 | 12.2765 | 10.3377 | -0.0902 | 0.0018 | -0.0013 | -0.0112 |
| D | 6.0355 | -21.2909 | -3.4817 | 6.0377 | -21.2872 | -3.4993 | 0.0022 | 0.0037 | -0.0176 |
| E | 6.3135 | -0.0334 | -0.158 | 6.3152 | -0.0344 | -0.1609 | 0.0017 | -0.001 | -0.0029 |
| F | 6.3108 | 20.8871 | -0.0338 | 6.3109 | 20.8867 | -0.0338 | 1E-04 | -0.0004 | 0 |
| G | -0.1204 | -10.8167 | -1.4397 | -0.1168 | -10.8169 | -1.4462 | 0.0036 | -0.0002 | -0.0065 |
| H | -0.0011 | 0.0001 | -0.0026 | -0.0011 | 0.0015 | -0.0025 | 0 | 0.0014 | 1E-04 |
| I | -0.1106 | 10.5501 | 0.6189 | -0.1094 | 10.5486 | 0.6214 | 0.0012 | -0.0015 | 0.0025 |
| J | -6.3811 | -21.1417 | -3.434 | -6.3844 | -21.1385 | -3.4273 | -0.0033 | 0.0032 | 0.0067 |
| K | -6.2461 | -0.0025 | -0.2017 | -6.246 | -0.0035 | -0.2018 | 1E-04 | -0.001 | -0.0001 |
| L | -5.9982 | 21.0235 | -0.1264 | -5.9999 | 21.024 | -0.123 | -0.0017 | 0.0005 | 0.0034 |
| M | -12.319 | -10.7232 | -2.0158 | -12.3194 | -10.723 | -2.0098 | -0.0004 | 0.0002 | 0.006 |
| N | -12.134 | 10.4924 | -0.2174 | -12.1343 | 10.4924 | -0.2116 | -0.0003 | 0 | 0.0058 |
| P | -18.1703 | -0.1385 | -1.541 | -18.1693 | -0.1389 | -1.5267 | 0.001 | -0.0004 | 0.0143 |

## Figure A-2. Theodolite Test - String A-C Actuated

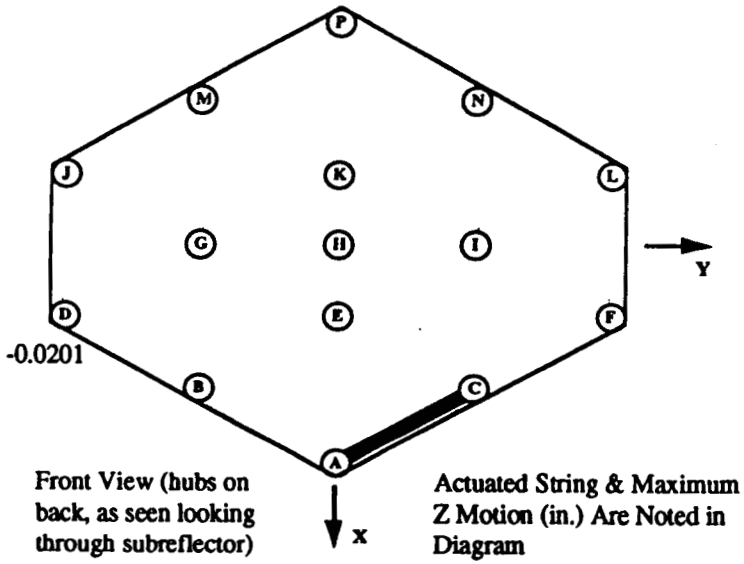


Front View (hubs on back, as seen looking through subreflector)

Actuated String & Maximum Z Motion (in.) Are Noted in Diagram

Power & Strain Data

(nm = not measured)

| String | Power (relative) | Strain (microstrain) |
|---|---|---|
| A-B | 0% | 57 |
| A-C | 20% | -167 |
| A-E | 0% | -25 |
| B-D | 0% | 1 |
| B-E | 0% | -10 |
| B-G | 0% | -6 |
| C-E | 0% | -12 |
| C-F | 0% | 10 |
| C-I | 0% | 14 |
| D-G | 0% | -4 |
| D-J | 0% | -6 |
| E-G | 0% | 7 |
| E-I | 0% | -14 |
| E-K | 0% | nm |
| F-I | 0% | -3 |

| String | Power (relative) | Strain (microstrain) |
|---|---|---|
| F-L | 0% | -2 |
| G-J | 0% | 3 |
| G-K | 0% | -11 |
| G-M | 0% | 7 |
| I-K | 0% | -5 |
| I-L | 0% | 0 |
| I-N | 0% | nm |
| J-M | 0% | nm |
| K-M | 0% | nm |
| K-N | 0% | nm |
| K-P | 0% | nm |
| L-N | 0% | nm |
| M-P | 0% | nm |
| N-P | 0% | nm |

Surface Contour Data

| Hub | Baseline Position | | | Position During Actuation | | | Relative Motion (Actuation - Baseline) | | |
|---|---|---|---|---|---|---|---|---|---|
| | X (in.) | Y (in.) | Z (in.) | X (in.) | Y (in.) | Z (in.) | X (in.) | Y (in.) | Z (in.) |
| A | 18.2876 | -0.3256 | -1.5347 | 18.2846 | -0.3242 | -1.5431 | -0.003 | 0.0014 | -0.0084 |
| B | 12.0139 | -11.1547 | -2.0666 | 12.0146 | -11.1525 | -2.0808 | 0.0007 | 0.0022 | -0.0142 |
| C | 12.276 | 10.3367 | -0.0915 | 12.2762 | 10.3373 | -0.0833 | 0.0002 | 0.0006 | 0.0082 |
| D | 6.0396 | -21.2892 | -3.4877 | 6.0381 | -21.287 | -3.5078 | -0.0015 | 0.0022 | -0.0201 |
| E | 6.3136 | -0.0361 | -0.1571 | 6.3155 | -0.0372 | -0.1603 | 0.0019 | -0.0011 | -0.0032 |
| F | 6.3087 | 20.8901 | -0.0381 | 6.314 | 20.886 | -0.0555 | 0.0053 | -0.0041 | -0.0174 |
| G | -0.1166 | -10.8194 | -1.4375 | -0.1176 | -10.8174 | -1.4403 | -0.001 | 0.002 | -0.0028 |
| H | -0.0012 | -0.0007 | -0.0025 | 0 | -0.0006 | 0 | 0.0012 | 0.0001 | 0.0025 |
| I | -0.1085 | 10.5475 | 0.6241 | -0.1085 | 10.5501 | 0.6241 | 0 | 0.0026 | 0 |
| J | -6.3817 | -21.1401 | -3.4347 | -6.3831 | -21.1406 | -3.4315 | -0.0014 | -0.0005 | 0.0032 |
| K | -6.2437 | -0.0055 | -0.2032 | -6.2442 | -0.0068 | -0.1974 | -0.0005 | -0.0013 | 0.0058 |
| L | -6.0015 | 21.0236 | -0.1119 | -6.0006 | 21.0216 | -0.1234 | 0.0009 | -0.002 | -0.0115 |
| M | -12.3186 | -10.7258 | -2.0148 | -12.3186 | -10.7269 | -2.0147 | 0 | -0.0011 | 0.0001 |
| N | -12.1344 | 10.491 | -0.2045 | -12.1353 | 10.492 | -0.2127 | -0.0009 | 0.001 | -0.0082 |
| P | -18.1703 | -0.1399 | -1.5408 | -18.1704 | -0.1395 | -1.5347 | -1E-04 | 0.0004 | 0.0061 |

**Figure A-3. Theodolite Test - String A-E Actuated**

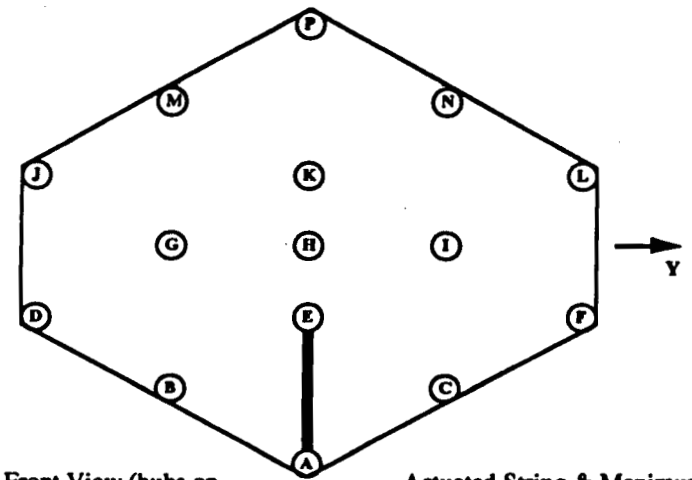


Front View (hubs on back, as seen looking through subreflector)

Actuated String & Maximum Z Motion (in.) Are Noted in Diagram

Power & Strain Data

(nm = not measured)

| String | Power (relative) | Strain (microstrain) |
|---|---|---|
| A-B | 0% | 0 |
| A-C | 0% | -99 |
| A-E | 20% | -161 |
| B-D | 0% | -12 |
| B-E | 0% | 9 |
| B-G | 0% | -23 |
| C-E | 0% | 12 |
| C-F | 0% | -14 |
| C-I | 0% | -25 |
| D-G | 0% | 3 |
| D-J | 0% | 0 |
| E-G | 0% | 17 |
| E-I | 0% | 16 |
| E-K | 0% | nm |
| F-I | 0% | 2 |

| String | Power (relative) | Strain (microstrain) |
|---|---|---|
| F-L | 0% | -5 |
| G-J | 0% | 0 |
| G-K | 0% | 8 |
| G-M | 0% | -1 |
| I-K | 0% | 8 |
| I-L | 0% | 0 |
| I-N | 0% | nm |
| J-M | 0% | nm |
| K-M | 0% | nm |
| K-N | 0% | nm |
| K-P | 0% | nm |
| L-N | 0% | nm |
| M-P | 0% | nm |
| N-P | 0% | nm |

Surface Contour Data

| Hub | Baseline Position | | | Position During Actuation | | | Relative Motion (Actuation - Baseline) | | |
|---|---|---|---|---|---|---|---|---|---|
| | X (in.) | Y (in.) | Z (in.) | X (in.) | Y (in.) | Z (in.) | X (in.) | Y (in.) | Z (in.) |
| A | 18.2845 | -0.3315 | -1.5346 | 18.2825 | -0.3229 | -1.5741 | -0.002 | 0.0086 | -0.0395 |
| B | 12.0145 | -11.159 | -2.0721 | 12.0136 | -11.1583 | -2.0664 | -0.0009 | 0.0007 | 0.0057 |
| C | 12.2781 | 10.3367 | -0.0862 | 12.2762 | 10.3362 | -0.0833 | -0.0019 | -0.0005 | 0.0029 |
| D | 6.0358 | -21.2899 | -3.4901 | 6.04 | -21.2939 | -3.4792 | 0.0042 | -0.004 | 0.0109 |
| E | 6.3137 | -0.037 | -0.1572 | 6.3155 | -0.0351 | -0.1602 | 0.0018 | 0.0019 | -0.003 |
| F | 6.3118 | 20.8835 | -0.0387 | 6.3081 | 20.8858 | -0.0325 | -0.0037 | 0.0023 | 0.0062 |
| G | -0.1163 | -10.816 | -1.4378 | -0.1194 | -10.8197 | -1.4371 | -0.0031 | -0.0037 | 0.0007 |
| H | -0.0002 | -0.0013 | 0.0002 | 0.0011 | 0.0011 | 0.0026 | 0.0013 | 0.0024 | 0.0024 |
| I | -0.1085 | 10.5479 | 0.6241 | -0.1121 | 10.5491 | 0.6305 | -0.0036 | 0.0012 | 0.0064 |
| J | -6.3803 | -21.1419 | -3.4323 | -6.383 | -21.1403 | -3.4168 | -0.0027 | 0.0016 | 0.0155 |
| K | -6.2466 | -0.0034 | -0.2023 | -6.2466 | -0.0034 | -0.2023 | 0 | 0 | 0 |
| L | -5.9998 | 21.0238 | -0.1152 | -6.0032 | 21.0246 | -0.1086 | -0.0034 | 0.0008 | 0.0066 |
| M | -12.317 | -10.7262 | -2.0183 | -12.317 | -10.7262 | -2.0183 | 0 | 0 | 0 |
| N | -12.1356 | 10.4915 | -0.2068 | -12.1344 | 10.4905 | -0.2045 | 0.0012 | -0.001 | 0.0023 |
| P | -18.1689 | -0.1403 | -1.5383 | -18.1688 | -0.1391 | -1.5443 | 1E-04 | 0.0012 | -0.006 |

**Figure A-4. Theodolite Test - String B-D Actuated**

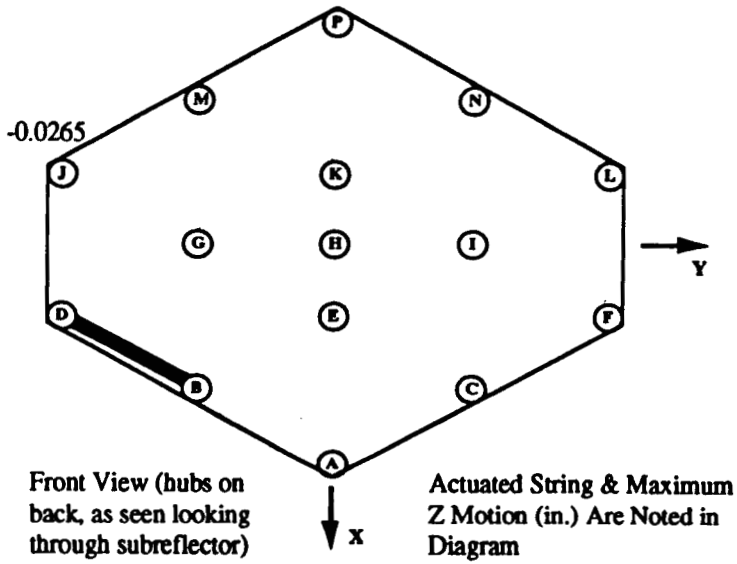


Front View (hubs on back, as seen looking through subreflector)

Actuated String & Maximum Z Motion (in.) Are Noted in Diagram

Power & Strain Data

(nm = not measured)

| String | Power (relative) | Strain (microstrain) |
|---|---|---|
| A-B | 0% | nm |
| A-C | 0% | nm |
| A-E | 0% | nm |
| B-D | 20% | nm |
| B-E | 0% | nm |
| B-G | 0% | nm |
| C-E | 0% | nm |
| C-F | 0% | nm |
| C-I | 0% | nm |
| D-G | 0% | nm |
| D-J | 0% | nm |
| E-G | 0% | nm |
| E-I | 0% | nm |
| E-K | 0% | nm |
| F-I | 0% | nm |

| String | Power (relative) | Strain (microstrain) |
|---|---|---|
| F-L | 0% | nm |
| G-J | 0% | nm |
| G-K | 0% | nm |
| G-M | 0% | nm |
| I-K | 0% | nm |
| I-L | 0% | nm |
| I-N | 0% | nm |
| J-M | 0% | nm |
| K-M | 0% | nm |
| K-N | 0% | nm |
| K-P | 0% | nm |
| L-N | 0% | nm |
| M-P | 0% | nm |
| N-P | 0% | nm |

Surface Contour Data

| Hub | Baseline Position | | | Position During Actuation | | | Relative Motion (Actuation - Baseline) | | |
|---|---|---|---|---|---|---|---|---|---|
| | X (in.) | Y (in.) | Z (in.) | X (in.) | Y (in.) | Z (in.) | X (in.) | Y (in.) | Z (in.) |
| A | 18.2866 | -0.329 | -1.5375 | 18.2854 | -0.3289 | -1.5402 | -0.0012 | 1E-04 | -0.0027 |
| B | 12.0146 | -11.1572 | -2.0722 | 12.0148 | -11.1601 | -2.0637 | 0.0002 | -0.0029 | 0.0085 |
| C | 12.2751 | 10.3361 | -0.0859 | 12.2781 | 10.3361 | -0.0862 | 0.003 | 0 | -0.0003 |
| D | 6.0397 | -21.2914 | -3.4878 | 6.0385 | -21.289 | -3.4992 | -0.0012 | 0.0024 | -0.0114 |
| E | 6.3155 | -0.0345 | -0.1603 | 6.3125 | -0.0356 | -0.1597 | -0.003 | -0.0011 | 0.0006 |
| F | 6.3106 | 20.8859 | -0.0412 | 6.3106 | 20.8848 | -0.0412 | 0 | -0.0011 | 0 |
| G | -0.1164 | -10.8198 | -1.4378 | -0.1194 | -10.817 | -1.4371 | -0.003 | 0.0028 | 0.0007 |
| H | -0.0001 | -0.0028 | 0.0001 | 0.001 | -0.0012 | 0.0027 | 0.0011 | 0.0016 | 0.0026 |
| I | -0.1103 | 10.5464 | 0.6273 | -0.1102 | 10.5476 | 0.6273 | 1E-04 | 0.0012 | 0 |
| J | -6.3833 | -21.1417 | -3.4314 | -6.3826 | -21.1413 | -3.4579 | 0.0007 | 0.0004 | -0.0265 |
| K | -6.2441 | -0.0057 | -0.1975 | -6.2479 | -0.0046 | -0.2047 | -0.0038 | 0.0011 | -0.0072 |
| L | -6.0001 | 21.0202 | -0.1096 | -6.0003 | 21.0246 | -0.1094 | -0.0002 | 0.0044 | 0.0002 |
| M | -12.3199 | -10.7261 | -2.0172 | -12.3209 | -10.7244 | -2.0255 | -0.001 | 0.0017 | -0.0083 |
| N | -12.1843 | 10.4916 | -0.2045 | -12.1373 | 10.4905 | -0.2033 | 0.047 | -0.0011 | 0.0012 |
| P | -18.1718 | -0.1402 | -1.537 | -18.1703 | -0.1405 | -1.5407 | 0.0015 | -0.0003 | -0.0037 |

**Figure A-5. Theodolite Test - String B-E Actuated**

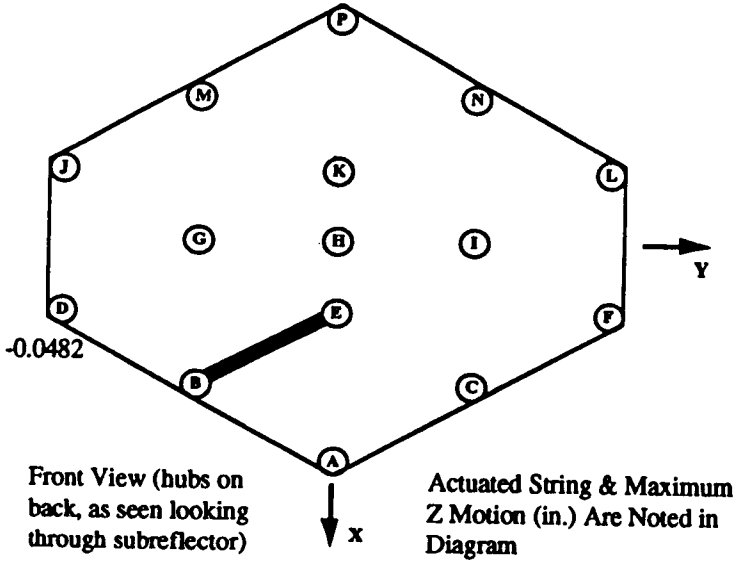


Front View (hubs on back, as seen looking through subreflector)

Actuated String & Maximum Z Motion (in.) Are Noted in Diagram

Power & Strain Data

(nm = not measured)

| String | Power (relative) | Strain (microstrain) |
|---|---|---|
| A-B | 0% | 10 |
| A-C | 0% | -53 |
| A-E | 0% | 21 |
| B-D | 0% | -1 |
| B-E | 20% | -186 |
| B-G | 0% | -66 |
| C-E | 0% | 10 |
| C-F | 0% | 1 |
| C-I | 0% | 7 |
| D-G | 0% | -21 |
| D-J | 0% | -17 |
| E-G | 0% | -6 |
| E-I | 0% | 16 |
| E-K | 0% | nm |
| F-I | 0% | -5 |

| String | Power (relative) | Strain (microstrain) |
|---|---|---|
| F-L | 0% | 9 |
| G-J | 0% | 16 |
| G-K | 0% | -34 |
| G-M | 0% | -4 |
| I-K | 0% | 3 |
| I-L | 0% | -5 |
| I-N | 0% | nm |
| J-M | 0% | nm |
| K-M | 0% | nm |
| K-N | 0% | nm |
| K-P | 0% | nm |
| L-N | 0% | nm |
| M-P | 0% | nm |
| N-P | 0% | nm |

Surface Contour Data

| Hub | Baseline Position | | | Position During Actuation | | | Relative Motion (Actuation - Baseline) | | |
|---|---|---|---|---|---|---|---|---|---|
| | X (in.) | Y (in.) | Z (in.) | X (in.) | Y (in.) | Z (in.) | X (in.) | Y (in.) | Z (in.) |
| A | 18.2845 | -0.3256 | -1.5346 | 18.2865 | -0.326 | -1.5206 | 0.002 | -0.0004 | 0.014 |
| B | 12.0138 | -11.1565 | -2.0665 | 12.0137 | -11.1498 | -2.1059 | -1E-04 | 0.0067 | -0.0394 |
| C | 12.2762 | 10.3362 | -0.0833 | 12.2774 | 10.3368 | -0.0723 | 0.0012 | 0.0006 | 0.011 |
| D | 6.0376 | -21.2911 | -3.4932 | 6.036 | -21.2794 | -3.5414 | -0.0016 | 0.0117 | -0.0482 |
| E | 6.3148 | -0.0348 | -0.1546 | 6.3129 | -0.0345 | -0.1515 | -0.0019 | 0.0003 | 0.0031 |
| F | 6.3106 | 20.8853 | -0.0412 | 6.3099 | 20.885 | -0.0356 | -0.0007 | -0.0003 | 0.0056 |
| G | -0.1163 | -10.8187 | -1.4379 | -0.1156 | -10.8149 | -1.4437 | 0.0007 | 0.0038 | -0.0058 |
| H | 0.001 | -0.0012 | 0.0027 | -0.0001 | -0.0017 | 0.0001 | -0.0011 | -0.0005 | -0.0026 |
| I | -0.1103 | 10.5491 | 0.6273 | -0.1102 | 10.5476 | 0.6273 | 1E-04 | -0.0015 | 0 |
| J | -6.3832 | -21.1412 | -3.4315 | -6.3815 | -21.1387 | -3.4553 | 0.0017 | 0.0025 | -0.0238 |
| K | -6.2454 | -0.0043 | -0.1998 | -6.2454 | -0.0053 | -0.1999 | 0 | -0.001 | -1E-04 |
| L | -6.0003 | 21.024 | -0.1095 | -6.0003 | 21.024 | -0.1095 | 0 | 0 | 0 |
| M | -12.3185 | -10.7252 | -2.0149 | -12.3186 | -10.7236 | -2.0147 | -1E-04 | 0.0016 | 0.0002 |
| N | -12.1344 | 10.491 | -0.2045 | -12.136 | 10.4921 | -0.201 | -0.0016 | 0.0011 | 0.0035 |
| P | -18.1705 | -0.1379 | -1.5346 | -18.1721 | -0.1373 | -1.5249 | -0.0016 | 0.0006 | 0.0097 |

**Figure A-6. Theodolite Test - String B-G Actuated**

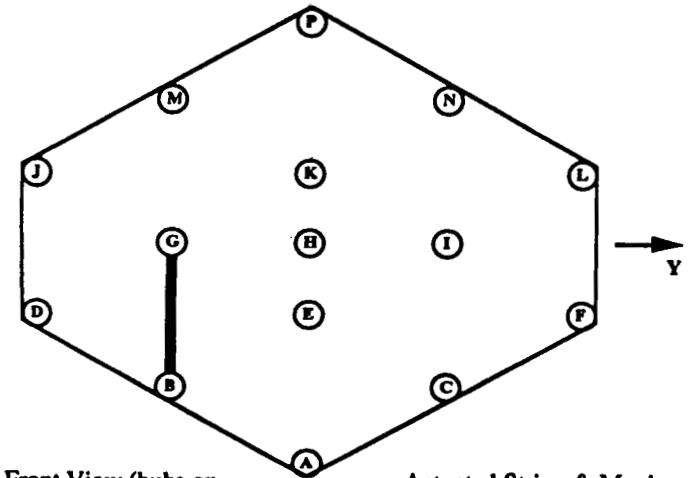


Front View (hubs on back, as seen looking through subreflector)

Actuated String & Maximum Z Motion (in.) Are Noted in Diagram

Power & Strain Data

(nm = not measured)

| String | Power (relative) | Strain (microstrain) |
|---|---|---|
| A-B | 0% | -14 |
| A-C | 0% | -19 |
| A-E | 0% | -17 |
| B-D | 0% | -94 |
| B-E | 0% | -74 |
| B-G | 20% | -199 |
| C-E | 0% | 17 |
| C-F | 0% | -13 |
| C-I | 0% | -19 |
| D-G | 0% | 10 |
| D-J | 0% | -27 |
| E-G | 0% | -12 |
| E-I | 0% | 7 |
| E-K | 0% | nm |
| F-I | 0% | 8 |

| String | Power (relative) | Strain (microstrain) |
|---|---|---|
| F-L | 0% | -12 |
| G-J | 0% | 11 |
| G-K | 0% | 34 |
| G-M | 0% | 3 |
| I-K | 0% | -1 |
| I-L | 0% | 7 |
| I-N | 0% | nm |
| J-M | 0% | nm |
| K-M | 0% | nm |
| K-N | 0% | nm |
| K-P | 0% | nm |
| L-N | 0% | nm |
| M-P | 0% | nm |
| N-P | 0% | nm |

Surface Contour Data

| Hub | Baseline Position | | | Position During Actuation | | | Relative Motion (Actuation - Baseline) | | |
|---|---|---|---|---|---|---|---|---|---|
| | X (in.) | Y (in.) | Z (in.) | X (in.) | Y (in.) | Z (in.) | X (in.) | Y (in.) | Z (in.) |
| A | 18.286 | -0.3245 | -1.5394 | 18.2808 | -0.3193 | -1.5787 | -0.0052 | 0.0052 | -0.0393 |
| B | 12.0152 | -11.1551 | -2.0707 | 12.0094 | -11.15 | -2.1012 | -0.0058 | 0.0051 | -0.0305 |
| C | 12.2759 | 10.3377 | -0.0846 | 12.2755 | 10.3377 | -0.1011 | -0.0004 | 0 | -0.0165 |
| D | 6.0371 | -21.2861 | -3.4937 | 6.036 | -21.29 | -3.4734 | -0.0011 | -0.0039 | 0.0203 |
| E | 6.3136 | -0.0324 | -0.158 | 6.3138 | -0.0341 | -0.1717 | 0.0002 | -0.0017 | -0.0137 |
| F | 6.3104 | 20.8864 | -0.0419 | 6.3099 | 20.8881 | -0.0363 | -0.0005 | 0.0017 | 0.0056 |
| G | -0.1192 | -10.8153 | -1.4373 | -0.1165 | -10.8183 | -1.4377 | 0.0027 | -0.003 | -0.0004 |
| H | -0.0001 | 0.0009 | 0.0001 | 0 | 0.0012 | 0 | 0.0001 | 0.0003 | -0.0001 |
| I | -0.1083 | 10.5506 | 0.624 | -0.1131 | 10.5501 | 0.6279 | -0.0048 | -0.0005 | 0.0039 |
| J | -6.3844 | -21.1368 | -3.4334 | -6.3845 | -21.1379 | -3.4332 | -1E-04 | -0.0011 | 0.0002 |
| K | -6.2468 | -0.0014 | -0.196 | -6.2476 | -0.0027 | -0.2042 | -0.0008 | -0.0013 | -0.0082 |
| L | -6.0012 | 21.0245 | -0.1114 | -6.0034 | 21.0285 | -0.1023 | -0.0022 | 0.004 | 0.0091 |
| M | -12.3181 | -10.7227 | -2.0136 | -12.3189 | -10.7231 | -2.0279 | -0.0008 | -0.0004 | -0.0143 |
| N | -12.1319 | 10.4927 | -0.2126 | -12.1339 | 10.4926 | -0.2033 | -0.002 | -1E-04 | 0.0093 |
| P | -18.1697 | -0.1362 | -1.5388 | -18.1695 | -0.1363 | -1.5449 | 0.0002 | -0.0001 | -0.0061 |

**Figure A-7. Theodolite Test - String C-E Actuated**

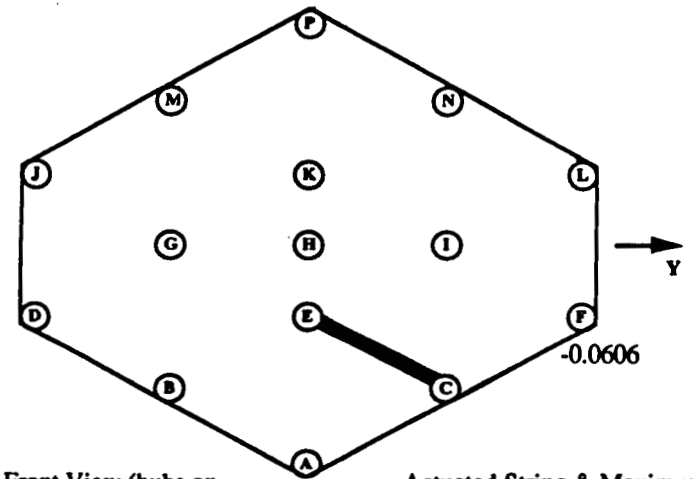


Front View (hubs on back, as seen looking through subreflector)

Actuated String & Maximum Z Motion (in.) Are Noted in Diagram

Power & Strain Data

(nm = not measured)

| String | Power (relative) | Strain (microstrain) |
|---|---|---|
| A-B | 0% | nm |
| A-C | 0% | nm |
| A-E | 0% | nm |
| B-D | 0% | nm |
| B-E | 0% | nm |
| B-G | 0% | nm |
| C-E | 20% | nm |
| C-F | 0% | nm |
| C-I | 0% | nm |
| D-G | 0% | nm |
| D-J | 0% | nm |
| E-G | 0% | nm |
| E-I | 0% | nm |
| E-K | 0% | nm |
| F-I | 0% | nm |

| String | Power (relative) | Strain (microstrain) |
|---|---|---|
| F-L | 0% | nm |
| G-J | 0% | nm |
| G-K | 0% | nm |
| G-M | 0% | nm |
| I-K | 0% | nm |
| I-L | 0% | nm |
| I-N | 0% | nm |
| J-M | 0% | nm |
| K-M | 0% | nm |
| K-N | 0% | nm |
| K-P | 0% | nm |
| L-N | 0% | nm |
| M-P | 0% | nm |
| N-P | 0% | nm |

Surface Contour Data

| Hub | Baseline Position | | | Position During Actuation | | | Relative Motion (Actuation - Baseline) | | |
|---|---|---|---|---|---|---|---|---|---|
| | X (in.) | Y (in.) | Z (in.) | X (in.) | Y (in.) | Z (in.) | X (in.) | Y (in.) | Z (in.) |
| A | 18.286 | -0.3245 | -1.5394 | 18.288 | -0.3302 | -1.5169 | 0.002 | -0.0057 | 0.0225 |
| B | 12.0152 | -11.1551 | -2.0707 | 12.0137 | -11.1573 | -2.0508 | -0.0015 | -0.0022 | 0.0199 |
| C | 12.2759 | 10.3377 | -0.0846 | 12.277 | 10.3395 | -0.1206 | 0.0011 | 0.0018 | -0.036 |
| D | 6.0371 | -21.2861 | -3.4937 | 6.0376 | -21.286 | -3.4853 | 0.0005 | 1E-04 | 0.0084 |
| E | 6.3136 | -0.0324 | -0.158 | 6.3135 | -0.0341 | -0.1579 | -1E-04 | -0.0017 | 1E-04 |
| F | 6.3104 | 20.8864 | -0.0419 | 6.3097 | 20.886 | -0.1025 | -0.0007 | -0.0004 | -0.0606 |
| G | -0.1192 | -10.8153 | -1.4373 | -0.1177 | -10.8159 | -1.4402 | 0.0015 | -0.0006 | -0.0029 |
| H | -0.0001 | 0.0009 | 0.0001 | 0.0011 | 0.0002 | 0.0026 | 0.0012 | -0.0007 | 0.0025 |
| I | -0.1083 | 10.5506 | 0.624 | -0.1107 | 10.5515 | 0.6191 | -0.0024 | 0.0009 | -0.0049 |
| J | -6.3844 | -21.1368 | -3.4334 | -6.3842 | -21.1407 | -3.4389 | 0.0002 | -0.0039 | -0.0055 |
| K | -6.2468 | -0.0014 | -0.196 | -6.244 | -0.0061 | -0.1967 | 0.0028 | -0.0047 | -0.0007 |
| L | -6.0012 | 21.0245 | -0.1114 | -6 | 21.0251 | -0.1426 | 0.0012 | 0.0006 | -0.0312 |
| M | -12.3181 | -10.7227 | -2.0136 | -12.3184 | -10.7247 | -2.0132 | -0.0003 | -0.002 | 0.0004 |
| N | -12.1319 | 10.4927 | -0.2126 | -12.1339 | 10.4915 | -0.2033 | -0.002 | -0.0012 | 0.0093 |
| P | -18.1697 | -0.1362 | -1.5388 | -18.17 | -0.1378 | -1.5267 | -0.0003 | -0.0016 | 0.0121 |

## Figure A-8. Theodolite Test - String C-F Actuated

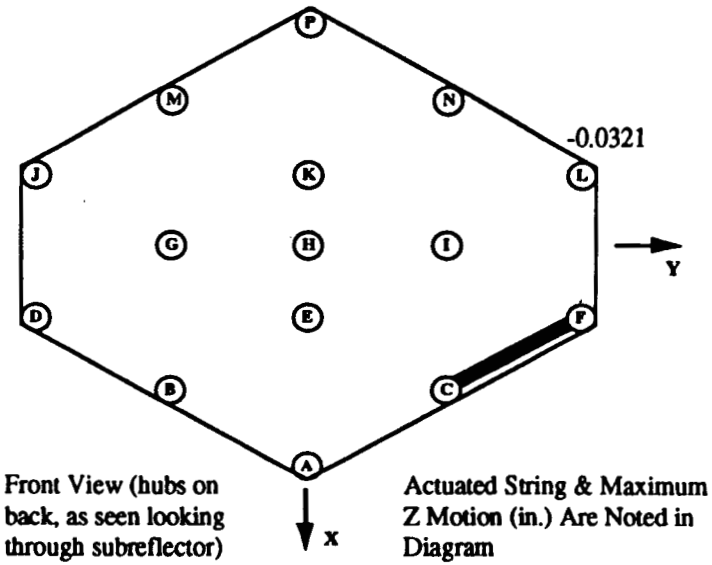


Front View (hubs on back, as seen looking through subreflector)

Actuated String & Maximum Z Motion (in.) Are Noted in Diagram

### Power & Strain Data

(nm = not measured)

| String | Power (relative) | Strain (microstrain) |
|---|---|---|
| A-B | 0% | -18 |
| A-C | 0% | 11 |
| A-E | 0% | -2 |
| B-D | 0% | 10 |
| B-E | 0% | 13 |
| B-G | 0% | 29 |
| C-E | 0% | 7 |
| C-F | 20% | -210 |
| C-I | 0% | -19 |
| D-G | 0% | -2 |
| D-J | 0% | 0 |
| E-G | 0% | 7 |
| E-I | 0% | -25 |
| E-K | 0% | nm |
| F-I | 0% | -32 |

| String | Power (relative) | Strain (microstrain) |
|---|---|---|
| F-L | 0% | 32 |
| G-J | 0% | 1 |
| G-K | 0% | -10 |
| G-M | 0% | -11 |
| I-K | 0% | 8 |
| I-L | 0% | -16 |
| I-N | 0% | nm |
| J-M | 0% | nm |
| K-M | 0% | nm |
| K-N | 0% | nm |
| K-P | 0% | nm |
| L-N | 0% | nm |
| M-P | 0% | nm |
| N-P | 0% | nm |

### Surface Contour Data

| Hub | Baseline Position | | | Position During Actuation | | | Relative Motion (Actuation - Baseline) | | |
|---|---|---|---|---|---|---|---|---|---|
| | X (in.) | Y (in.) | Z (in.) | X (in.) | Y (in.) | Z (in.) | X (in.) | Y (in.) | Z (in.) |
| A | 18.286 | -0.3245 | -1.5394 | 18.284 | -0.3221 | -1.5365 | -0.002 | 0.0024 | 0.0029 |
| B | 12.0152 | -11.1551 | -2.0707 | 12.0129 | -11.1555 | -2.076 | -0.0023 | -0.0004 | -0.0053 |
| C | 12.2759 | 10.3377 | -0.0846 | 12.278 | 10.3372 | -0.0793 | 0.0021 | -0.0005 | 0.0053 |
| D | 6.0371 | -21.2861 | -3.4937 | 6.0378 | -21.2886 | -3.4996 | 0.0007 | -0.0025 | -0.0059 |
| E | 6.3136 | -0.0324 | -0.158 | 6.3154 | -0.0317 | -0.161 | 0.0018 | 0.0007 | -0.003 |
| F | 6.3104 | 20.8864 | -0.0419 | 6.3139 | 20.8849 | -0.0563 | 0.0035 | -0.0015 | -0.0144 |
| G | -0.1192 | -10.8153 | -1.4373 | -0.1189 | -10.8171 | -1.4428 | 0.0003 | -0.0018 | -0.0055 |
| H | -0.0001 | 0.0009 | 0.0001 | -0.0013 | 0.0014 | -0.0024 | -0.0012 | 0.0005 | -0.0025 |
| I | -0.1083 | 10.5506 | 0.624 | -0.1077 | 10.5515 | 0.6184 | 0.0006 | 0.0009 | -0.0056 |
| J | -6.3844 | -21.1368 | -3.4334 | -6.3831 | -21.1369 | -3.4308 | 0.0013 | -1E-04 | 0.0026 |
| K | -6.2468 | -0.0014 | -0.196 | -6.2452 | -0.0014 | -0.1992 | 0.0016 | 0 | -0.0032 |
| L | -6.0012 | 21.0245 | -0.1114 | -5.9971 | 21.0236 | -0.1435 | 0.0041 | -0.0009 | -0.0321 |
| M | -12.3181 | -10.7227 | -2.0136 | -12.3169 | -10.7249 | -2.0111 | 0.0012 | -0.0022 | 0.0025 |
| N | -12.1319 | 10.4927 | -0.2126 | -12.1345 | 10.494 | -0.2173 | -0.0026 | 0.0013 | -0.0047 |
| P | -18.1697 | -0.1362 | -1.5388 | -18.1683 | -0.1368 | -1.5365 | 0.0014 | -0.0006 | 0.0023 |

## Figure A-9. Theodolite Test - String C-I Actuated

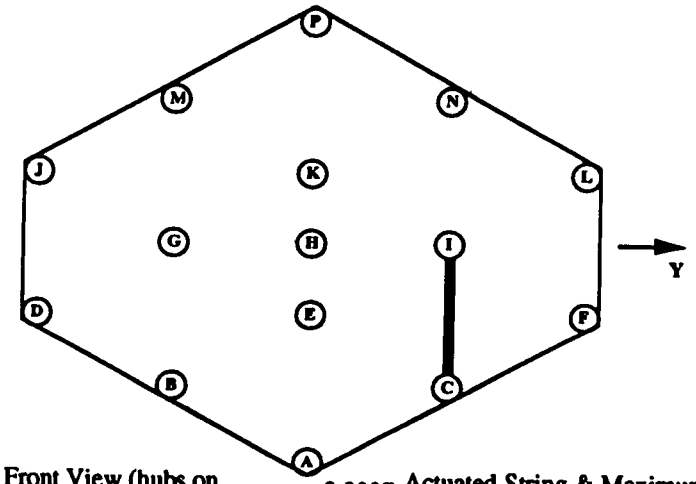


Front View (hubs on back, as seen looking through subreflector)

Actuated String & Maximum Z Motion (in.) Are Noted in Diagram

### Power & Strain Data

(nm = not measured)

| String | Power (relative) | Strain (microstrain) |
|---|---|---|
| A-B | 0% | -28 |
| A-C | 0% | 5 |
| A-E | 0% | -11 |
| B-D | 0% | 2 |
| B-E | 0% | 34 |
| B-G | 0% | 14 |
| C-E | 0% | -75 |
| C-F | 0% | -137 |
| C-I | 20% | -214 |
| D-G | 0% | 5 |
| D-J | 0% | -4 |
| E-G | 0% | 10 |
| E-I | 0% | -13 |
| E-K | 0% | nm |
| F-I | 0% | 24 |

| String | Power (relative) | Strain (microstrain) |
|---|---|---|
| F-L | 0% | -38 |
| G-J | 0% | 5 |
| G-K | 0% | -8 |
| G-M | 0% | -16 |
| I-K | 0% | 38 |
| I-L | 0% | 17 |
| I-N | 0% | nm |
| J-M | 0% | nm |
| K-M | 0% | nm |
| K-N | 0% | nm |
| K-P | 0% | nm |
| L-N | 0% | nm |
| M-P | 0% | nm |
| N-P | 0% | nm |

### Surface Contour Data

| Hub | Baseline Position | | | Position During Actuation | | | Relative Motion (Actuation - Baseline) | | |
|---|---|---|---|---|---|---|---|---|---|
| | X (in.) | Y (in.) | Z (in.) | X (in.) | Y (in.) | Z (in.) | X (in.) | Y (in.) | Z (in.) |
| A | 18.286 | -0.3245 | -1.5394 | 18.2828 | -0.319 | -1.5731 | -0.0032 | 0.0055 | -0.0337 |
| B | 12.0152 | -11.1551 | -2.0707 | 12.0132 | -11.1525 | -2.0762 | -0.002 | 0.0026 | -0.0055 |
| C | 12.2759 | 10.3377 | -0.0846 | 12.2733 | 10.3408 | -0.1064 | -0.0026 | 0.0031 | -0.0218 |
| D | 6.0371 | -21.2861 | -3.4937 | 6.0364 | -21.2865 | -3.4879 | -0.0007 | -0.0004 | 0.0058 |
| E | 6.3136 | -0.0324 | -0.158 | 6.3131 | -0.0314 | -0.1661 | -0.0005 | 0.001 | -0.0081 |
| F | 6.3104 | 20.8864 | -0.0419 | 6.3083 | 20.8904 | -0.025 | -0.0021 | 0.004 | 0.0169 |
| G | -0.1192 | -10.8153 | -1.4373 | -0.1152 | -10.8157 | -1.4353 | 0.004 | -0.0004 | 0.002 |
| H | -0.0001 | 0.0009 | 0.0001 | 0 | 0.0012 | 0 | 0.0001 | 0.0003 | -0.0001 |
| I | -0.1083 | 10.5506 | 0.624 | -0.1101 | 10.5506 | 0.6272 | -0.0018 | 0 | 0.0032 |
| J | -6.3844 | -21.1368 | -3.4334 | -6.3852 | -21.1414 | -3.4215 | -0.0008 | -0.0046 | 0.0119 |
| K | -6.2468 | -0.0014 | -0.196 | -6.2464 | -0.0042 | -0.2017 | 0.0004 | -0.0028 | -0.0057 |
| L | -6.0012 | 21.0245 | -0.1114 | -6 | 21.0273 | -0.1089 | 0.0012 | 0.0028 | 0.0025 |
| M | -12.3181 | -10.7227 | -2.0136 | -12.3182 | -10.7219 | -2.0136 | -1E-04 | 0.0008 | 0 |
| N | -12.1319 | 10.4927 | -0.2126 | -12.1345 | 10.4945 | -0.2173 | -0.0026 | 0.0018 | -0.0047 |
| P | -18.1697 | -0.1362 | -1.5388 | -18.1681 | -0.1361 | -1.5426 | 0.0016 | 1E-04 | -0.0038 |

## Figure A-10. Theodolite Test - String D-G Actuated

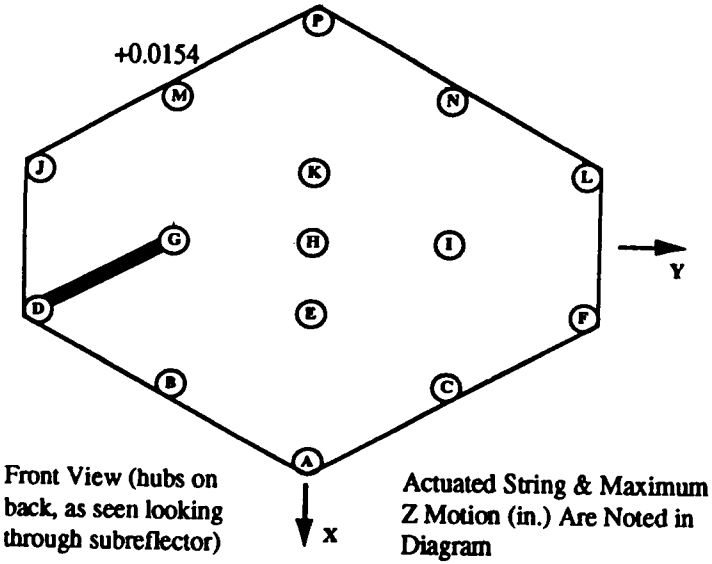


Front View (hubs on back, as seen looking through subreflector)

Actuated String & Maximum Z Motion (in.) Are Noted in Diagram

### Power & Strain Data

(nm = not measured)

| String | Power (relative) | Strain (microstrain) |
|---|---|---|
| A-B | 0% | -49 |
| A-C | 0% | -9 |
| A-E | 0% | 15 |
| B-D | 0% | -108 |
| B-E | 0% | -16 |
| B-G | 0% | 54 |
| C-E | 0% | -5 |
| C-F | 0% | -16 |
| C-I | 0% | 6 |
| D-G | 20% | -217 |
| D-J | 0% | -132 |
| E-G | 0% | 30 |
| E-I | 0% | -4 |
| E-K | 0% | nm |
| F-I | 0% | 0 |

| String | Power (relative) | Strain (microstrain) |
|---|---|---|
| F-L | 0% | 12 |
| G-J | 0% | 23 |
| G-K | 0% | 9 |
| G-M | 0% | -6 |
| I-K | 0% | 4 |
| I-L | 0% | 2 |
| I-N | 0% | nm |
| J-M | 0% | nm |
| K-M | 0% | nm |
| K-N | 0% | nm |
| K-P | 0% | nm |
| L-N | 0% | nm |
| M-P | 0% | nm |
| N-P | 0% | nm |

### Surface Contour Data

| Hub | Baseline Position | | | Position During Actuation | | | Relative Motion (Actuation - Baseline) | | |
|---|---|---|---|---|---|---|---|---|---|
| | X (in.) | Y (in.) | Z (in.) | X (in.) | Y (in.) | Z (in.) | X (in.) | Y (in.) | Z (in.) |
| A | 18.286 | -0.3245 | -1.5394 | 18.286 | -0.3259 | -1.531 | 0 | -0.0014 | 0.0084 |
| B | 12.0152 | -11.1551 | -2.0707 | 12.0153 | -11.1558 | -2.0707 | 1E-04 | -0.0007 | 0 |
| C | 12.2759 | 10.3377 | -0.0846 | 12.2759 | 10.3374 | -0.0846 | 0 | -0.0003 | 0 |
| D | 6.0371 | -21.2861 | -3.4937 | 6.0327 | -21.2759 | -3.5557 | -0.0044 | 0.0102 | -0.062 |
| E | 6.3136 | -0.0324 | -0.158 | 6.3153 | -0.034 | -0.1609 | 0.0017 | -0.0016 | -0.0029 |
| F | 6.3104 | 20.8864 | -0.0419 | 6.3132 | 20.8873 | -0.0506 | 0.0028 | 0.0009 | -0.0087 |
| G | -0.1192 | -10.8153 | -1.4373 | -0.1164 | -10.8154 | -1.4379 | 0.0028 | -1E-04 | -0.0006 |
| H | -0.0001 | 0.0009 | 0.0001 | -0.0001 | 0.001 | 0.0002 | 0 | 0.0001 | 0.0001 |
| I | -0.1083 | 10.5506 | 0.624 | -0.1095 | 10.5506 | 0.6215 | -0.0012 | 0 | -0.0025 |
| J | -6.3844 | -21.1368 | -3.4334 | -6.3837 | -21.137 | -3.4247 | 0.0007 | -0.0002 | 0.0087 |
| K | -6.2468 | -0.0014 | -0.196 | -6.2451 | -0.0029 | -0.1993 | 0.0017 | -0.0015 | -0.0033 |
| L | -6.0012 | 21.0245 | -0.1114 | -6.0002 | 21.0252 | -0.1229 | 0.001 | 0.0007 | -0.0115 |
| M | -12.3181 | -10.7227 | -2.0136 | -12.3204 | -10.7232 | -1.9982 | -0.0023 | -0.0005 | 0.0154 |
| N | -12.1319 | 10.4927 | -0.2126 | -12.1361 | 10.4936 | -0.2139 | -0.0042 | 0.0009 | -0.0013 |
| P | -18.1697 | -0.1362 | -1.5388 | -18.1727 | -0.137 | -1.5315 | -0.003 | -0.0008 | 0.0073 |

## Figure A-11. Theodolite Test - String D-J Actuated

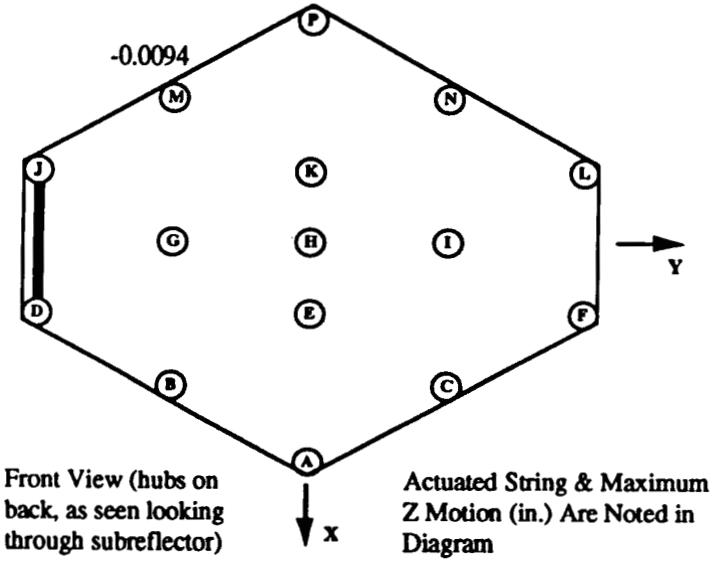


Front View (hubs on back, as seen looking through subreflector)

Actuated String & Maximum Z Motion (in.) Are Noted in Diagram

### Power & Strain Data

(nm = not measured)

| String | Power (relative) | Strain (microstrain) |
|---|---|---|
| A-B | 0% | -63 |
| A-C | 0% | -5 |
| A-E | 0% | 8 |
| B-D | 0% | 56 |
| B-E | 0% | 14 |
| B-G | 0% | 18 |
| C-E | 0% | -3 |
| C-F | 0% | -20 |
| C-I | 0% | 1 |
| D-G | 0% | -3 |
| D-J | 20% | -209 |
| E-G | 0% | 4 |
| E-I | 0% | 0 |
| E-K | 0% | nm |
| F-I | 0% | 2 |

| String | Power (relative) | Strain (microstrain) |
|---|---|---|
| F-L | 0% | 5 |
| G-J | 0% | -39 |
| G-K | 0% | -2 |
| G-M | 0% | -18 |
| I-K | 0% | 4 |
| I-L | 0% | 6 |
| I-N | 0% | nm |
| J-M | 0% | nm |
| K-M | 0% | nm |
| K-N | 0% | nm |
| K-P | 0% | nm |
| L-N | 0% | nm |
| M-P | 0% | nm |
| N-P | 0% | nm |

### Surface Contour Data

| Hub | Baseline Position | | | Position During Actuation | | | Relative Motion (Actuation - Baseline) | | |
|---|---|---|---|---|---|---|---|---|---|
| | X (in.) | Y (in.) | Z (in.) | X (in.) | Y (in.) | Z (in.) | X (in.) | Y (in.) | Z (in.) |
| A | 18.286 | -0.3245 | -1.5394 | 18.284 | -0.3235 | -1.5366 | -0.002 | 0.001 | 0.0028 |
| B | 12.0152 | -11.1551 | -2.0707 | 12.0144 | -11.1543 | -2.0736 | -0.0008 | 0.0008 | -0.0029 |
| C | 12.2759 | 10.3377 | -0.0846 | 12.2759 | 10.341 | -0.0846 | 0 | 0.0033 | 0 |
| D | 6.0371 | -21.2861 | -3.4937 | 6.036 | -21.288 | -3.4964 | -0.0011 | -0.0019 | -0.0027 |
| E | 6.3136 | -0.0324 | -0.158 | 6.3135 | -0.0341 | -0.1579 | -1E-04 | -0.0017 | 1E-04 |
| F | 6.3104 | 20.8864 | -0.0419 | 6.3124 | 20.8897 | -0.045 | 0.002 | 0.0033 | -0.0031 |
| G | -0.1192 | -10.8153 | -1.4373 | -0.1164 | -10.816 | -1.4378 | 0.0028 | -0.0007 | -0.0005 |
| H | -0.0001 | 0.0009 | 0.0001 | 0.0012 | 0.0008 | 0.0025 | 0.0013 | -1E-04 | 0.0024 |
| I | -0.1083 | 10.5506 | 0.624 | -0.1095 | 10.5494 | 0.6215 | -0.0012 | -0.0012 | -0.0025 |
| J | -6.3844 | -21.1368 | -3.4334 | -6.3842 | -21.1367 | -3.439 | 0.0002 | 1E-04 | -0.0056 |
| K | -6.2468 | -0.0014 | -0.196 | -6.2463 | -0.0025 | -0.2018 | 0.0005 | -0.0011 | -0.0058 |
| L | -6.0012 | 21.0245 | -0.1114 | -5.9995 | 21.0254 | -0.1147 | 0.0017 | 0.0009 | -0.0033 |
| M | -12.3181 | -10.7227 | -2.0136 | -12.3163 | -10.7231 | -2.023 | 0.0018 | -0.0004 | -0.0094 |
| N | -12.1319 | 10.4927 | -0.2126 | -12.1352 | 10.4952 | -0.2057 | -0.0033 | 0.0025 | 0.0069 |
| P | -18.1697 | -0.1362 | -1.5388 | -18.1697 | -0.1364 | -1.5389 | 0 | -0.0002 | -1E-04 |

## Figure A-12. Theodolite Test - String E-G Actuated

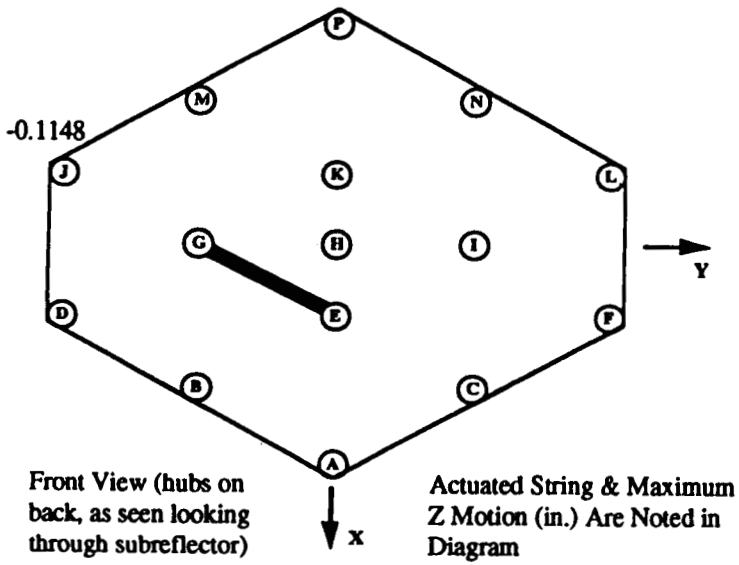


Front View (hubs on back, as seen looking through subreflector)

Actuated String & Maximum Z Motion (in.) Are Noted in Diagram

Power & Strain Data

(nm = not measured)

| String | Power (relative) | Strain (microstrain) |
|---|---|---|
| A-B | 0% | -62 |
| A-C | 0% | -3 |
| A-E | 0% | 42 |
| B-D | 0% | -82 |
| B-E | 0% | 1 |
| B-G | 0% | 11 |
| C-E | 0% | 19 |
| C-F | 0% | -13 |
| C-I | 0% | -2 |
| D-G | 0% | 88 |
| D-J | 0% | 54 |
| E-G | 20% | -234 |
| E-I | 0% | 46 |
| E-K | 0% | nm |
| F-I | 0% | 2 |

| String | Power (relative) | Strain (microstrain) |
|---|---|---|
| F-L | 0% | 4 |
| G-J | 0% | 21 |
| G-K | 0% | -24 |
| G-M | 0% | 19 |
| I-K | 0% | -33 |
| I-L | 0% | 14 |
| I-N | 0% | nm |
| J-M | 0% | nm |
| K-M | 0% | nm |
| K-N | 0% | nm |
| K-P | 0% | nm |
| L-N | 0% | nm |
| M-P | 0% | nm |
| N-P | 0% | nm |

Surface Contour Data

| Hub | Baseline Position | | | Position During Actuation | | | Relative Motion (Actuation - Baseline) | | |
|---|---|---|---|---|---|---|---|---|---|
| | X (in.) | Y (in.) | Z (in.) | X (in.) | Y (in.) | Z (in.) | X (in.) | Y (in.) | Z (in.) |
| A | 18.286 | -0.3245 | -1.5394 | 18.2839 | -0.3226 | -1.545 | -0.0021 | 0.0019 | -0.0056 |
| B | 12.0152 | -11.1551 | -2.0707 | 12.0162 | -11.1546 | -2.0679 | 0.001 | 0.0005 | 0.0028 |
| C | 12.2759 | 10.3377 | -0.0846 | 12.2753 | 10.3396 | -0.1093 | -0.0006 | 0.0019 | -0.0247 |
| D | 6.0371 | -21.2861 | -3.4937 | 6.0414 | -21.2786 | -3.5516 | 0.0043 | 0.0075 | -0.0579 |
| E | 6.3136 | -0.0324 | -0.158 | 6.3142 | -0.033 | -0.1635 | 0.0006 | -0.0006 | -0.0055 |
| F | 6.3104 | 20.8864 | -0.0419 | 6.309 | 20.8874 | -0.0527 | -0.0014 | 0.001 | -0.0108 |
| G | -0.1192 | -10.8153 | -1.4373 | -0.1188 | -10.8102 | -1.471 | 0.0004 | 0.0051 | -0.0337 |
| H | -0.0001 | 0.0009 | 0.0001 | -0.0013 | 0.002 | -0.0024 | -0.0012 | 0.0011 | -0.0025 |
| I | -0.1083 | 10.5506 | 0.624 | -0.1101 | 10.5521 | 0.6272 | -0.0018 | 0.0015 | 0.0032 |
| J | -6.3844 | -21.1368 | -3.4334 | -6.3803 | -21.1229 | -3.5482 | 0.0041 | 0.0139 | -0.1148 |
| K | -6.2468 | -0.0014 | -0.196 | -6.2447 | -0.0033 | -0.2051 | 0.0021 | -0.0019 | -0.0091 |
| L | -6.0012 | 21.0245 | -0.1114 | -6.0026 | 21.026 | -0.0941 | -0.0014 | 0.0015 | 0.0173 |
| M | -12.3181 | -10.7227 | -2.0136 | -12.3171 | -10.7177 | -2.0636 | 0.001 | 0.005 | -0.05 |
| N | -12.1319 | 10.4927 | -0.2126 | -12.1377 | 10.4927 | -0.1847 | -0.0058 | 0 | 0.0279 |
| P | -18.1697 | -0.1362 | -1.5388 | -18.1714 | -0.1342 | -1.5291 | -0.0017 | 0.002 | 0.0097 |

## Figure A-13. Theodolite Test - String E-I Actuated

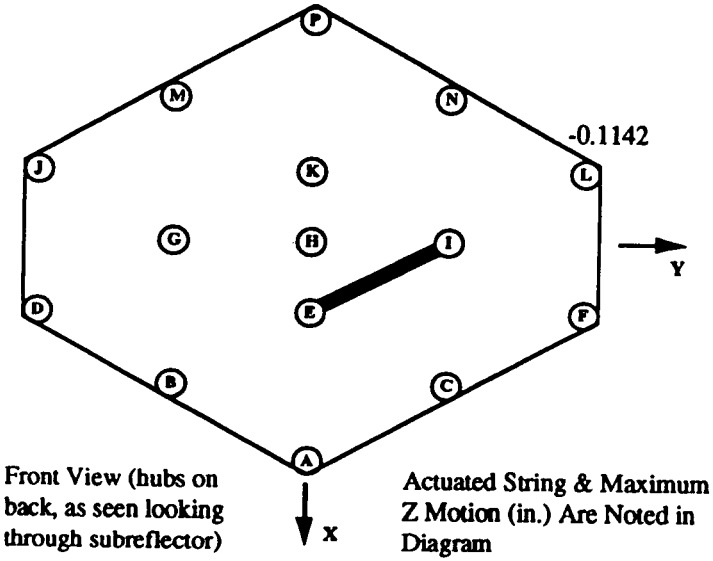


Front View (hubs on back, as seen looking through subreflector)

Actuated String & Maximum Z Motion (in.) Are Noted in Diagram

### Power & Strain Data

(nm = not measured)

| String | Power (relative) | Strain (microstrain) |
|---|---|---|
| A-B | 0% | -67 |
| A-C | 0% | -109 |
| A-E | 0% | 38 |
| B-D | 0% | 49 |
| B-E | 0% | 59 |
| B-G | 0% | 36 |
| C-E | 0% | -28 |
| C-F | 0% | -122 |
| C-I | 0% | -15 |
| D-G | 0% | 41 |
| D-J | 0% | 58 |
| E-G | 0% | 81 |
| E-I | 20% | -234 |
| E-K | 0% | nm |
| F-I | 0% | 39 |

| String | Power (relative) | Strain (microstrain) |
|---|---|---|
| F-L | 0% | 12 |
| G-J | 0% | 8 |
| G-K | 0% | -48 |
| G-M | 0% | -20 |
| I-K | 0% | -23 |
| I-L | 0% | 14 |
| I-N | 0% | nm |
| J-M | 0% | nm |
| K-M | 0% | nm |
| K-N | 0% | nm |
| K-P | 0% | nm |
| L-N | 0% | nm |
| M-P | 0% | nm |
| N-P | 0% | nm |

### Surface Contour Data

| Hub | Baseline Position | | | Position During Actuation | | | Relative Motion (Actuation - Baseline) | | |
|---|---|---|---|---|---|---|---|---|---|
| | X (in.) | Y (in.) | Z (in.) | X (in.) | Y (in.) | Z (in.) | X (in.) | Y (in.) | Z (in.) |
| A | 18.286 | -0.3245 | -1.5394 | 18.2861 | -0.3264 | -1.5395 | 1E-04 | -0.0019 | -1E-04 |
| B | 12.0152 | -11.1551 | -2.0707 | 12.0117 | -11.1529 | -2.0872 | -0.0035 | 0.0022 | -0.0165 |
| C | 12.2759 | 10.3377 | -0.0846 | 12.2789 | 10.3371 | -0.0849 | 0.003 | -0.0006 | -0.0003 |
| D | 6.0371 | -21.2861 | -3.4937 | 6.0335 | -21.2885 | -3.4875 | -0.0036 | -0.0024 | 0.0062 |
| E | 6.3136 | -0.0324 | -0.158 | 6.316 | -0.0338 | -0.1665 | 0.0024 | -0.0014 | -0.0085 |
| F | 6.3104 | 20.8864 | -0.0419 | 6.3146 | 20.8868 | -0.106 | 0.0042 | 0.0004 | -0.0641 |
| G | -0.1192 | -10.8153 | -1.4373 | -0.1164 | -10.816 | -1.4378 | 0.0028 | -0.0007 | -0.0005 |
| H | -0.0001 | 0.0009 | 0.0001 | -0.0012 | 0.0016 | -0.0025 | -0.0011 | 0.0007 | -0.0026 |
| I | -0.1083 | 10.5506 | 0.624 | -0.1101 | 10.5518 | 0.5859 | -0.0018 | 0.0012 | -0.0381 |
| J | -6.3844 | -21.1368 | -3.4334 | -6.3851 | -21.1445 | -3.4067 | -0.0007 | -0.0077 | 0.0267 |
| K | -6.2468 | -0.0014 | -0.196 | -6.2464 | -0.0021 | -0.2016 | 0.0004 | -0.0007 | -0.0056 |
| L | -6.0012 | 21.0245 | -0.1114 | -5.9948 | 21.0246 | -0.2256 | 0.0064 | 1E-04 | -0.1142 |
| M | -12.3181 | -10.7227 | -2.0136 | -12.3198 | -10.727 | -1.9836 | -0.0017 | -0.0043 | 0.03 |
| N | -12.1319 | 10.4927 | -0.2126 | -12.132 | 10.4942 | -0.264 | -1E-04 | 0.0015 | -0.0514 |
| P | -18.1697 | -0.1362 | -1.5388 | -18.1713 | -0.14 | -1.5294 | -0.0016 | -0.0038 | 0.0094 |

## Figure A-14. Theodolite Test - String F-I Actuated

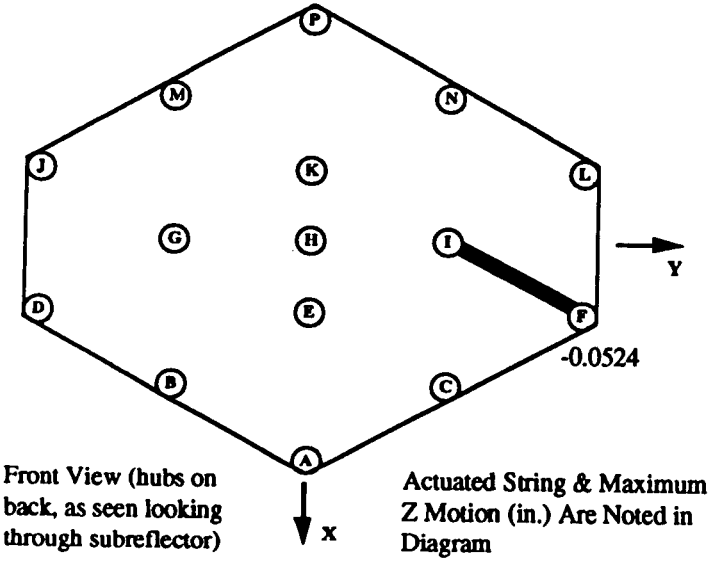


Front View (hubs on back, as seen looking through subreflector)

Actuated String & Maximum Z Motion (in.) Are Noted in Diagram

### Power & Strain Data

(nm = not measured)

| String | Power (relative) | Strain (microstrain) |
|---|---|---|
| A-B | 0% | -97 |
| A-C | 0% | -8 |
| A-E | 0% | 7 |
| B-D | 0% | 41 |
| B-E | 0% | 26 |
| B-G | 0% | 44 |
| C-E | 0% | -34 |
| C-F | 0% | -129 |
| C-I | 0% | 25 |
| D-G | 0% | 43 |
| D-J | 0% | 65 |
| E-G | 0% | 24 |
| E-I | 0% | 26 |
| E-K | 0% | nm |
| F-I | 20% | -205 |

| String | Power (relative) | Strain (microstrain) |
|---|---|---|
| F-L | 0% | -106 |
| G-J | 0% | -2 |
| G-K | 0% | 1 |
| G-M | 0% | -4 |
| I-K | 0% | 13 |
| I-L | 0% | 22 |
| I-N | 0% | nm |
| J-M | 0% | nm |
| K-M | 0% | nm |
| K-N | 0% | nm |
| K-P | 0% | nm |
| L-N | 0% | nm |
| M-P | 0% | nm |
| N-P | 0% | nm |

### Surface Contour Data

| Hub | Baseline Position | | | Position During Actuation | | | Relative Motion (Actuation - Baseline) | | |
|---|---|---|---|---|---|---|---|---|---|
| | X (in.) | Y (in.) | Z (in.) | X (in.) | Y (in.) | Z (in.) | X (in.) | Y (in.) | Z (in.) |
| A | 18.286 | -0.3245 | -1.5394 | 18.2851 | -0.3255 | -1.5253 | -0.0009 | -0.001 | 0.0141 |
| B | 12.0152 | -11.1551 | -2.0707 | 12.0144 | -11.1557 | -2.065 | -0.0008 | -0.0006 | 0.0057 |
| C | 12.2759 | 10.3377 | -0.0846 | 12.2778 | 10.3398 | -0.0875 | 0.0019 | 0.0021 | -0.0029 |
| D | 6.0371 | -21.2861 | -3.4937 | 6.0366 | -21.2868 | -3.4792 | -0.0005 | -0.0007 | 0.0145 |
| E | 6.3136 | -0.0324 | -0.158 | 6.3146 | -0.0346 | -0.1553 | 0.001 | -0.0022 | 0.0027 |
| F | 6.3104 | 20.8864 | -0.0419 | 6.3101 | 20.8856 | -0.0943 | -0.0003 | -0.0008 | -0.0524 |
| G | -0.1192 | -10.8153 | -1.4373 | -0.1164 | -10.816 | -1.4378 | 0.0028 | -0.0007 | -0.0005 |
| H | -0.0001 | 0.0009 | 0.0001 | -0.003 | 0.0018 | 0.0007 | -0.0029 | 0.0009 | 0.0006 |
| I | -0.1083 | 10.5506 | 0.624 | -0.1101 | 10.5495 | 0.6272 | -0.0018 | -0.0011 | 0.0032 |
| J | -6.3844 | -21.1368 | -3.4334 | -6.3847 | -21.1402 | -3.4329 | -0.0003 | -0.0034 | 0.0005 |
| K | -6.2468 | -0.0014 | -0.196 | -6.2451 | -0.0035 | -0.1993 | 0.0017 | -0.0021 | -0.0033 |
| L | -6.0012 | 21.0245 | -0.1114 | -6.0016 | 21.025 | -0.1057 | -0.0004 | 0.0005 | 0.0057 |
| M | -12.3181 | -10.7227 | -2.0136 | -12.3183 | -10.723 | -2.0134 | -0.0002 | -0.0003 | 0.0002 |
| N | -12.1319 | 10.4927 | -0.2126 | -12.1358 | 10.4921 | -0.194 | -0.0039 | -0.0006 | 0.0186 |
| P | -18.1697 | -0.1362 | -1.5388 | -18.1685 | -0.1369 | -1.5304 | 0.0012 | -0.0007 | 0.0084 |

## Figure A-15. Theodolite Test - String F-L Actuated

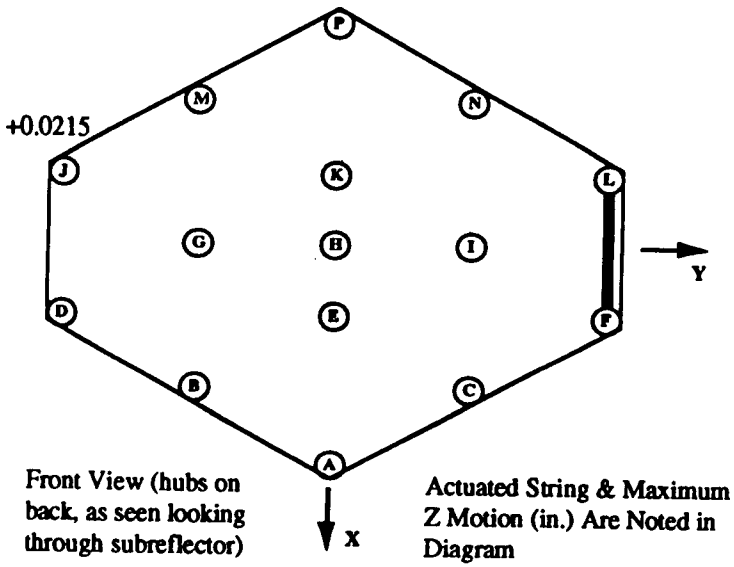


Front View (hubs on back, as seen looking through subreflector)

Actuated String & Maximum Z Motion (in.) Are Noted in Diagram

### Power & Strain Data

(nm = not measured)

| String | Power (relative) | Strain (microstrain) |
|---|---|---|
| A-B | 0% | -81 |
| A-C | 0% | 10 |
| A-E | 0% | -6 |
| B-D | 0% | 29 |
| B-E | 0% | -1 |
| B-G | 0% | -12 |
| C-E | 0% | -2 |
| C-F | 0% | 22 |
| C-I | 0% | -10 |
| D-G | 0% | -14 |
| D-J | 0% | 35 |
| E-G | 0% | -12 |
| E-I | 0% | 11 |
| E-K | 0% | nm |
| F-I | 0% | -22 |

| String | Power (relative) | Strain (microstrain) |
|---|---|---|
| F-L | 20% | -166 |
| G-J | 0% | 2 |
| G-K | 0% | -6 |
| G-M | 0% | 0 |
| I-K | 0% | 32 |
| I-L | 0% | -24 |
| I-N | 0% | nm |
| J-M | 0% | nm |
| K-M | 0% | nm |
| K-N | 0% | nm |
| K-P | 0% | nm |
| L-N | 0% | nm |
| M-P | 0% | nm |
| N-P | 0% | nm |

### Surface Contour Data

| Hub | Baseline Position | | | Position During Actuation | | | Relative Motion (Actuation - Baseline) | | |
|---|---|---|---|---|---|---|---|---|---|
| | X (in.) | Y (in.) | Z (in.) | X (in.) | Y (in.) | Z (in.) | X (in.) | Y (in.) | Z (in.) |
| A | 18.2866 | -0.3272 | -1.5365 | 18.2845 | -0.3268 | -1.542 | -0.0021 | 0.0004 | -0.0055 |
| B | 12.0141 | -11.1556 | -2.0648 | 12.0131 | -11.1559 | -2.0675 | -0.001 | -0.0003 | -0.0027 |
| C | 12.2747 | 10.339 | -0.079 | 12.2754 | 10.3363 | -0.0929 | 0.0007 | -0.0027 | -0.0139 |
| D | 6.0355 | -21.2909 | -3.4817 | 6.0356 | -21.2903 | -3.4818 | 1E-04 | 0.0006 | -1E-04 |
| E | 6.3135 | -0.0334 | -0.158 | 6.3112 | -0.0322 | -0.1631 | -0.0023 | 0.0012 | -0.0051 |
| F | 6.3108 | 20.8871 | -0.0338 | 6.3105 | 20.8889 | -0.02 | -0.0003 | 0.0018 | 0.0138 |
| G | -0.1204 | -10.8167 | -1.4397 | -0.1187 | -10.8188 | -1.4428 | 0.0017 | -0.0021 | -0.0031 |
| H | -0.0011 | 0.0001 | -0.0026 | -0.0012 | 0.0016 | -0.0025 | -1E-04 | 0.0015 | 1E-04 |
| I | -0.1106 | 10.5501 | 0.6189 | -0.1124 | 10.5497 | 0.6221 | -0.0018 | -0.0004 | 0.0032 |
| J | -6.3811 | -21.1417 | -3.434 | -6.3843 | -21.1416 | -3.4125 | -0.0032 | 1E-04 | 0.0215 |
| K | -6.2461 | -0.0025 | -0.2017 | -6.2461 | -0.0025 | -0.2017 | 0 | 0 | 0 |
| L | -5.9982 | 21.0235 | -0.1264 | -6.0016 | 21.0243 | -0.1197 | -0.0034 | 0.0008 | 0.0067 |
| M | -12.319 | -10.7232 | -2.0158 | -12.3193 | -10.7251 | -2.0099 | -0.0003 | -0.0019 | 0.0059 |
| N | -12.134 | 10.4924 | -0.2174 | -12.134 | 10.4937 | -0.2174 | 0 | 0.0013 | 0 |
| P | -18.1703 | -0.1385 | -1.541 | -18.1689 | -0.1373 | -1.5388 | 0.0014 | 0.0012 | 0.0022 |

## Figure A-16. Theodolite Test - String G-J Actuated

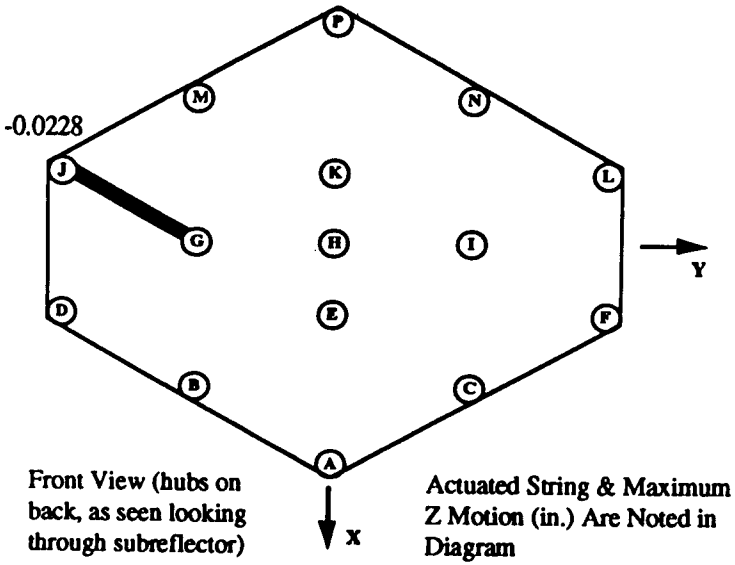


Front View (hubs on back, as seen looking through subreflector)

Actuated String & Maximum Z Motion (in.) Are Noted in Diagram

### Power & Strain Data

(nm = not measured)

| String | Power (relative) | Strain (microstrain) |
|---|---|---|
| A-B | 0% | -91 |
| A-C | 0% | 17 |
| A-E | 0% | -6 |
| B-D | 0% | -12 |
| B-E | 0% | 3 |
| B-G | 0% | 4 |
| C-E | 0% | 3 |
| C-F | 0% | 19 |
| C-I | 0% | 1 |
| D-G | 0% | 7 |
| D-J | 0% | -44 |
| E-G | 0% | 4 |
| E-I | 0% | 8 |
| E-K | 0% | nm |
| F-I | 0% | 2 |

| String | Power (relative) | Strain (microstrain) |
|---|---|---|
| F-L | 0% | 3 |
| G-J | 20% | -165 |
| G-K | 0% | 17 |
| G-M | 0% | 10 |
| I-K | 0% | 29 |
| I-L | 0% | -2 |
| I-N | 0% | nm |
| J-M | 0% | nm |
| K-M | 0% | nm |
| K-N | 0% | nm |
| K-P | 0% | nm |
| L-N | 0% | nm |
| M-P | 0% | nm |
| N-P | 0% | nm |

### Surface Contour Data

| Hub | Baseline Position | | | Position During Actuation | | | Relative Motion (Actuation - Baseline) | | |
|---|---|---|---|---|---|---|---|---|---|
| | X (in.) | Y (in.) | Z (in.) | X (in.) | Y (in.) | Z (in.) | X (in.) | Y (in.) | Z (in.) |
| A | 18.2866 | -0.3272 | -1.5365 | 18.2845 | -0.3256 | -1.5335 | -0.0021 | 0.0016 | 0.003 |
| B | 12.0141 | -11.1556 | -2.0648 | 12.0131 | -11.1594 | -2.059 | -0.001 | -0.0038 | 0.0058 |
| C | 12.2747 | 10.339 | -0.079 | 12.2756 | 10.3357 | -0.0846 | 0.0009 | -0.0033 | -0.0056 |
| D | 6.0355 | -21.2909 | -3.4817 | 6.0379 | -21.2894 | -3.4764 | 0.0024 | 0.0015 | 0.0053 |
| E | 6.3135 | -0.0334 | -0.158 | 6.3122 | -0.0332 | -0.1605 | -0.0013 | 0.0002 | -0.0025 |
| F | 6.3108 | 20.8871 | -0.0338 | 6.3106 | 20.886 | -0.02 | -0.0002 | -0.0011 | 0.0138 |
| G | -0.1204 | -10.8167 | -1.4397 | -0.1195 | -10.8186 | -1.4369 | 0.0009 | -0.0019 | 0.0028 |
| H | -0.0011 | 0.0001 | -0.0026 | 0.0001 | 0.0008 | -0.0001 | 0.0012 | 0.0007 | 0.0025 |
| I | -0.1106 | 10.5501 | 0.6189 | -0.1112 | 10.5492 | 0.6246 | -0.0006 | -0.0009 | 0.0057 |
| J | -6.3811 | -21.1417 | -3.434 | -6.3824 | -21.1382 | -3.4568 | -0.0013 | 0.0035 | -0.0228 |
| K | -6.2461 | -0.0025 | -0.2017 | -6.2461 | -0.0046 | -0.2018 | 0 | -0.0021 | -0.0001 |
| L | -5.9982 | 21.0235 | -0.1264 | -5.9986 | 21.0227 | -0.1206 | -0.0004 | -0.0008 | 0.0058 |
| M | -12.319 | -10.7232 | -2.0158 | -12.3194 | -10.723 | -2.0098 | -0.0004 | 0.0002 | 0.006 |
| N | -12.134 | 10.4924 | -0.2174 | -12.136 | 10.4932 | -0.2081 | -0.002 | 0.0008 | 0.0093 |
| P | -18.1703 | -0.1385 | -1.541 | -18.1693 | -0.1381 | -1.5266 | 0.001 | 0.0004 | 0.0144 |

## Figure A-17. Theodolite Test - String G-K Actuated

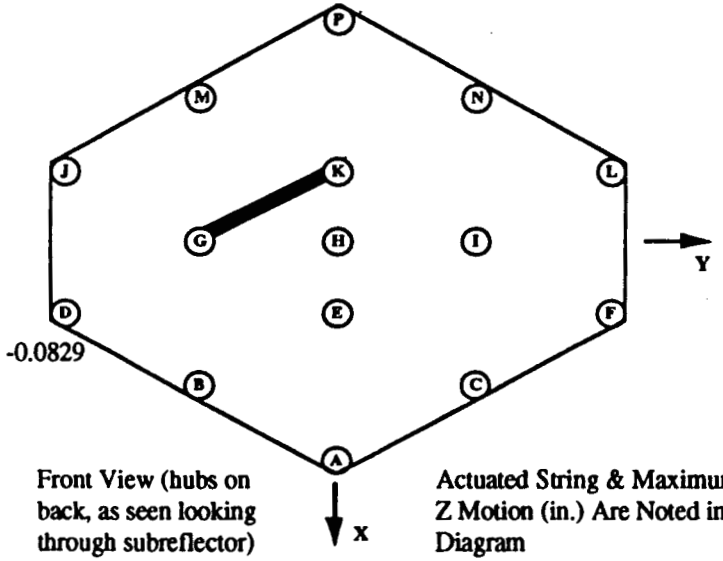


Front View (hubs on back, as seen looking through subreflector)

Actuated String & Maximum Z Motion (in.) Are Noted in Diagram

Power & Strain Data

(nm = not measured)

| String | Power (relative) | Strain (microstrain) |
|---|---|---|
| A-B | 0% | -94 |
| A-C | 0% | -40 |
| A-E | 0% | 27 |
| B-D | 0% | 14 |
| B-E | 0% | -47 |
| B-G | 0% | 31 |
| C-E | 0% | 24 |
| C-F | 0% | -1 |
| C-I | 0% | -12 |
| D-G | 0% | 1 |
| D-J | 0% | 22 |
| E-G | 0% | -32 |
| E-I | 0% | -26 |
| E-K | 0% | nm |
| F-I | 0% | 13 |

| String | Power (relative) | Strain (microstrain) |
|---|---|---|
| F-L | 0% | 0 |
| G-J | 0% | 31 |
| G-K | 20% | -180 |
| G-M | 0% | -8 |
| I-K | 0% | 68 |
| I-L | 0% | -2 |
| I-N | 0% | nm |
| J-M | 0% | nm |
| K-M | 0% | nm |
| K-N | 0% | nm |
| K-P | 0% | nm |
| L-N | 0% | nm |
| M-P | 0% | nm |
| N-P | 0% | nm |

Surface Contour Data

| Hub | Baseline Position | | | Position During Actuation | | | Relative Motion (Actuation - Baseline) | | |
|---|---|---|---|---|---|---|---|---|---|
| | X (in.) | Y (in.) | Z (in.) | X (in.) | Y (in.) | Z (in.) | X (in.) | Y (in.) | Z (in.) |
| A | 18.2866 | -0.3272 | -1.5365 | 18.2877 | -0.3232 | -1.5337 | 0.0011 | 0.004 | 0.0028 |
| B | 12.0141 | -11.1556 | -2.0648 | 12.009 | -11.1509 | -2.1094 | -0.0051 | 0.0047 | -0.0446 |
| C | 12.2747 | 10.339 | -0.079 | 12.2771 | 10.3365 | -0.0654 | 0.0024 | -0.0025 | 0.0136 |
| D | 6.0355 | -21.2909 | -3.4817 | 6.0353 | -21.2778 | -3.5646 | -0.0002 | 0.0131 | -0.0829 |
| E | 6.3135 | -0.0334 | -0.158 | 6.3123 | -0.0341 | -0.1606 | -0.0012 | -0.0007 | -0.0026 |
| F | 6.3108 | 20.8871 | -0.0338 | 6.3124 | 20.8868 | -0.001 | 0.0016 | -0.0003 | 0.0328 |
| G | -0.1204 | -10.8167 | -1.4397 | -0.1211 | -10.8146 | -1.4619 | -0.0007 | 0.0021 | -0.0222 |
| H | -0.0011 | 0.0001 | -0.0026 | -0.0023 | 0.0005 | -0.0051 | -0.0012 | 0.0004 | -0.0025 |
| I | -0.1106 | 10.5501 | 0.6189 | -0.1118 | 10.5502 | 0.6302 | -0.0012 | 1E-04 | 0.0113 |
| J | -6.3811 | -21.1417 | -3.434 | -6.3861 | -21.1355 | -3.4645 | -0.005 | 0.0062 | -0.0305 |
| K | -6.2461 | -0.0025 | -0.2017 | -6.2487 | -0.0045 | -0.2065 | -0.0026 | -0.002 | -0.0048 |
| L | -5.9982 | 21.0235 | -0.1264 | -5.997 | 21.0251 | -0.1239 | 0.0012 | 0.0016 | 0.0025 |
| M | -12.319 | -10.7232 | -2.0158 | -12.3205 | -10.7257 | -2.0124 | -0.0015 | -0.0025 | 0.0034 |
| N | -12.134 | 10.4924 | -0.2174 | -12.1331 | 10.4938 | -0.2349 | 0.0009 | 0.0014 | -0.0175 |
| P | -18.1703 | -0.1385 | -1.541 | -18.1702 | -0.1365 | -1.5471 | 1E-04 | 0.002 | -0.0061 |

## Figure A-18. Theodolite Test - String G-M Actuated

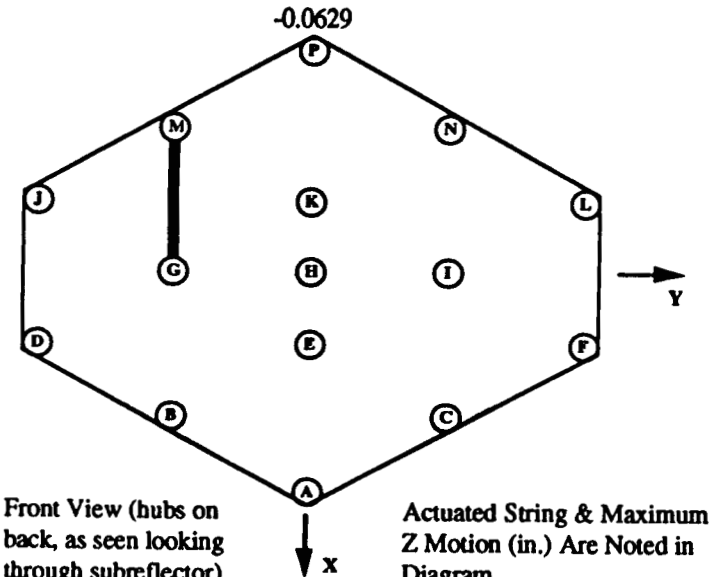


Front View (hubs on back, as seen looking through subreflector)

Actuated String & Maximum Z Motion (in.) Are Noted in Diagram

### Power & Strain Data

(nm = not measured)

| String | Power (relative) | Strain (microstrain) |
|---|---|---|
| A-B | 0% | -153 |
| A-C | 0% | 4 |
| A-E | 0% | -3 |
| B-D | 0% | 55 |
| B-E | 0% | -5 |
| B-G | 0% | 13 |
| C-E | 0% | 24 |
| C-F | 0% | 2 |
| C-I | 0% | -16 |
| D-G | 0% | 8 |
| D-J | 0% | -42 |
| E-G | 0% | 59 |
| E-I | 0% | -4 |
| E-K | 0% | nm |
| F-I | 0% | 20 |

| String | Power (relative) | Strain (microstrain) |
|---|---|---|
| F-L | 0% | -15 |
| G-J | 0% | 23 |
| G-K | 0% | -44 |
| G-M | 20% | -223 |
| I-K | 0% | 51 |
| I-L | 0% | 12 |
| I-N | 0% | nm |
| J-M | 0% | nm |
| K-M | 0% | nm |
| K-N | 0% | nm |
| K-P | 0% | nm |
| L-N | 0% | nm |
| M-P | 0% | nm |
| N-P | 0% | nm |

### Surface Contour Data

| Hub | Baseline Position | | | Position During Actuation | | | Relative Motion (Actuation - Baseline) | | |
|---|---|---|---|---|---|---|---|---|---|
| | X (in.) | Y (in.) | Z (in.) | X (in.) | Y (in.) | Z (in.) | X (in.) | Y (in.) | Z (in.) |
| A | 18.2866 | -0.3272 | -1.5365 | 18.2824 | -0.3223 | -1.5475 | -0.0042 | 0.0049 | -0.011 |
| B | 12.0141 | -11.1556 | -2.0648 | 12.0105 | -11.1552 | -2.0898 | -0.0036 | 0.0004 | -0.025 |
| C | 12.2747 | 10.339 | -0.079 | 12.278 | 10.3358 | -0.071 | 0.0033 | -0.0032 | 0.008 |
| D | 6.0355 | -21.2909 | -3.4817 | 6.038 | -21.2902 | -3.4765 | 0.0025 | 0.0007 | 0.0052 |
| E | 6.3135 | -0.0334 | -0.158 | 6.3142 | -0.0355 | -0.1636 | 0.0007 | -0.0021 | -0.0056 |
| F | 6.3108 | 20.8871 | -0.0338 | 6.3109 | 20.8874 | 0.0103 | 1E-04 | 0.0003 | 0.0441 |
| G | -0.1204 | -10.8167 | -1.4397 | -0.1186 | -10.8175 | -1.4288 | 0.0018 | -0.0008 | 0.0109 |
| H | -0.0011 | 0.0001 | -0.0026 | 0.0001 | -0.0009 | 0 | 0.0012 | -0.001 | 0.0026 |
| I | -0.1106 | 10.5501 | 0.6189 | -0.11 | 10.5498 | 0.627 | 0.0006 | -0.0003 | 0.0081 |
| J | -6.3811 | -21.1417 | -3.434 | -6.3832 | -21.1532 | -3.3841 | -0.0021 | -0.0115 | 0.0499 |
| K | -6.2461 | -0.0025 | -0.2017 | -6.248 | -0.0036 | -0.2125 | -0.0019 | -0.0011 | -0.0108 |
| L | -5.9982 | 21.0235 | -0.1264 | -5.9996 | 21.0264 | -0.1091 | -0.0014 | 0.0029 | 0.0173 |
| M | -12.319 | -10.7232 | -2.0158 | -12.3199 | -10.7211 | -2.0563 | -0.0009 | 0.0021 | -0.0405 |
| N | -12.134 | 10.4924 | -0.2174 | -12.1331 | 10.496 | -0.2349 | 0.0009 | 0.0036 | -0.0175 |
| P | -18.1703 | -0.1385 | -1.541 | -18.1631 | -0.132 | -1.6039 | 0.0072 | 0.0065 | -0.0629 |

## Figure A-19. Theodolite Test - String I-K Actuated

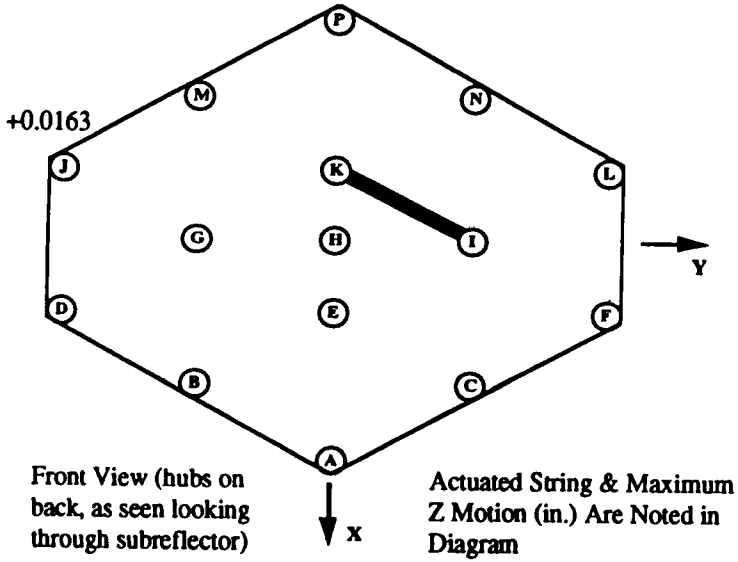


Front View (hubs on back, as seen looking through subreflector)

Actuated String & Maximum Z Motion (in.) Are Noted in Diagram

### Power & Strain Data

(nm = not measured)

| String | Power (relative) | Strain (microstrain) |
|---|---|---|
| A-B | 0% | -174 |
| A-C | 0% | -210 |
| A-E | 0% | 146 |
| B-D | 0% | -70 |
| B-E | 0% | 82 |
| B-G | 0% | -58 |
| C-E | 0% | -228 |
| C-F | 0% | -20 |
| C-I | 0% | 217 |
| D-G | 0% | 33 |
| D-J | 0% | 35 |
| E-G | 0% | -204 |
| E-I | 0% | -88 |
| E-K | 0% | nm |
| F-I | 0% | 50 |

| String | Power (relative) | Strain (microstrain) |
|---|---|---|
| F-L | 0% | 9 |
| G-J | 0% | 2 |
| G-K | 0% | 218 |
| G-M | 0% | -13 |
| I-K | 20% | -23 |
| I-L | 0% | 138 |
| I-N | 0% | nm |
| J-M | 0% | nm |
| K-M | 0% | nm |
| K-N | 0% | nm |
| K-P | 0% | nm |
| L-N | 0% | nm |
| M-P | 0% | nm |
| N-P | 0% | nm |

### Surface Contour Data

| Hub | Baseline Position | | | Position During Actuation | | | Relative Motion (Actuation - Baseline) | | |
|---|---|---|---|---|---|---|---|---|---|
| | X (in.) | Y (in.) | Z (in.) | X (in.) | Y (in.) | Z (in.) | X (in.) | Y (in.) | Z (in.) |
| A | 18.2866 | -0.3272 | -1.5365 | 18.2855 | -0.3265 | -1.5392 | -0.0011 | 0.0007 | -0.0027 |
| B | 12.0141 | -11.1556 | -2.0648 | 12.0139 | -11.1566 | -2.0733 | -0.0002 | -0.001 | -0.0085 |
| C | 12.2747 | 10.339 | -0.079 | 12.2756 | 10.3378 | -0.0846 | 0.0009 | -0.0012 | -0.0056 |
| D | 6.0355 | -21.2909 | -3.4817 | 6.0357 | -21.2897 | -3.4819 | 0.0002 | 0.0012 | -0.0002 |
| E | 6.3135 | -0.0334 | -0.158 | 6.3141 | -0.0334 | -0.1636 | 0.0006 | 0 | -0.0056 |
| F | 6.3108 | 20.8871 | -0.0338 | 6.309 | 20.8877 | -0.0308 | -0.0018 | 0.0006 | 0.003 |
| G | -0.1204 | -10.8167 | -1.4397 | -0.1185 | -10.8192 | -1.443 | 0.0019 | -0.0025 | -0.0033 |
| H | -0.0011 | 0.0001 | -0.0026 | -0.0022 | -0.0001 | -0.0051 | -0.0011 | -0.0002 | -0.0025 |
| I | -0.1106 | 10.5501 | 0.6189 | -0.1088 | 10.5506 | 0.6158 | 0.0018 | 0.0005 | -0.0031 |
| J | -6.3811 | -21.1417 | -3.434 | -6.3867 | -21.1447 | -3.4177 | -0.0056 | -0.003 | 0.0163 |
| K | -6.2461 | -0.0025 | -0.2017 | -6.2473 | -0.0055 | -0.2042 | -0.0012 | -0.003 | -0.0025 |
| L | -5.9982 | 21.0235 | -0.1264 | -5.9999 | 21.024 | -0.123 | -0.0017 | 0.0005 | 0.0034 |
| M | -12.319 | -10.7232 | -2.0158 | -12.3193 | -10.7257 | -2.0098 | -0.0003 | -0.0025 | 0.006 |
| N | -12.134 | 10.4924 | -0.2174 | -12.134 | 10.4913 | -0.2174 | 0 | -0.0011 | 0 |
| P | -18.1703 | -0.1385 | -1.541 | -18.1705 | -0.1376 | -1.5351 | -0.0002 | 0.0009 | 0.0059 |

## Figure A-20. Theodolite Test - String I-L Actuated

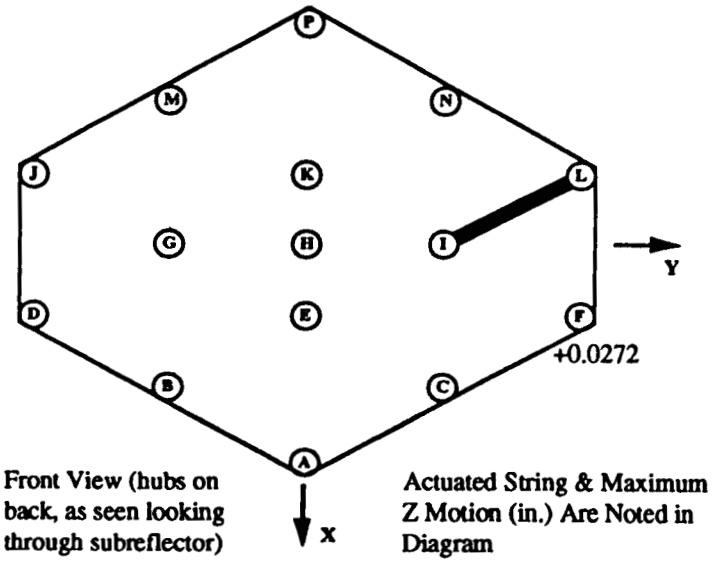


Front View (hubs on back, as seen looking through subreflector)

Actuated String & Maximum Z Motion (in.) Are Noted in Diagram

Power & Strain Data

(nm = not measured)

| String | Power (relative) | Strain (microstrain) |
|---|---|---|
| A-B | 0% | 0 |
| A-C | 0% | 21 |
| A-E | 0% | -9 |
| B-D | 0% | 51 |
| B-E | 0% | -4 |
| B-G | 0% | -6 |
| C-E | 0% | 37 |
| C-F | 0% | -33 |
| C-I | 0% | 18 |
| D-G | 0% | -28 |
| D-J | 0% | 55 |
| E-G | 0% | -9 |
| E-I | 0% | 22 |
| E-K | 0% | nm |
| F-I | 0% | 45 |

| String | Power (relative) | Strain (microstrain) |
|---|---|---|
| F-L | 0% | -93 |
| G-J | 0% | 5 |
| G-K | 0% | -2 |
| G-M | 0% | -32 |
| I-K | 0% | 25 |
| I-L | 20% | -281 |
| I-N | 0% | nm |
| J-M | 0% | nm |
| K-M | 0% | nm |
| K-N | 0% | nm |
| K-P | 0% | nm |
| L-N | 0% | nm |
| M-P | 0% | nm |
| N-P | 0% | nm |

Surface Contour Data

| Hub | Baseline Position | | | Position During Actuation | | | Relative Motion (Actuation - Baseline) | | |
|---|---|---|---|---|---|---|---|---|---|
| | X (in.) | Y (in.) | Z (in.) | X (in.) | Y (in.) | Z (in.) | X (in.) | Y (in.) | Z (in.) |
| A | 18.2866 | -0.3272 | -1.5365 | 18.2846 | -0.327 | -1.5336 | -0.002 | 0.0002 | 0.0029 |
| B | 12.0141 | -11.1556 | -2.0648 | 12.0129 | -11.1563 | -2.076 | -0.0012 | -0.0007 | -0.0112 |
| C | 12.2747 | 10.339 | -0.079 | 12.278 | 10.3364 | -0.071 | 0.0033 | -0.0026 | 0.008 |
| D | 6.0355 | -21.2909 | -3.4817 | 6.0352 | -21.2884 | -3.4903 | -0.0003 | 0.0025 | -0.0086 |
| E | 6.3135 | -0.0334 | -0.158 | 6.3115 | -0.0328 | -0.1549 | -0.002 | 0.0006 | 0.0031 |
| F | 6.3108 | 20.8871 | -0.0338 | 6.3131 | 20.8877 | -0.0066 | 0.0023 | 0.0006 | 0.0272 |
| G | -0.1204 | -10.8167 | -1.4397 | -0.1193 | -10.8163 | -1.437 | 0.0011 | 0.0004 | 0.0027 |
| H | -0.0011 | 0.0001 | -0.0026 | -0.0024 | -0.0018 | -0.005 | -0.0013 | -0.0019 | -0.0024 |
| I | -0.1106 | 10.5501 | 0.6189 | -0.1082 | 10.5507 | 0.6239 | 0.0024 | 0.0006 | 0.005 |
| J | -6.3811 | -21.1417 | -3.434 | -6.3841 | -21.1416 | -3.4181 | -0.003 | 1E-04 | 0.0159 |
| K | -6.2461 | -0.0025 | -0.2017 | -6.2473 | -0.0021 | -0.2042 | -0.0012 | 0.0004 | -0.0025 |
| L | -5.9982 | 21.0235 | -0.1264 | -5.9942 | 21.022 | -0.1584 | 0.004 | -0.0015 | -0.032 |
| M | -12.319 | -10.7232 | -2.0158 | -12.3179 | -10.7243 | -2.0075 | 0.0011 | -0.0011 | 0.0083 |
| N | -12.134 | 10.4924 | -0.2174 | -12.1353 | 10.4935 | -0.2198 | -0.0013 | 0.0011 | -0.0024 |
| P | -18.1703 | -0.1385 | -1.541 | -18.1707 | -0.1383 | -1.529 | -0.0004 | 0.0002 | 0.012 |

## Figure A-21. Theodolite Test - String I-N Actuated

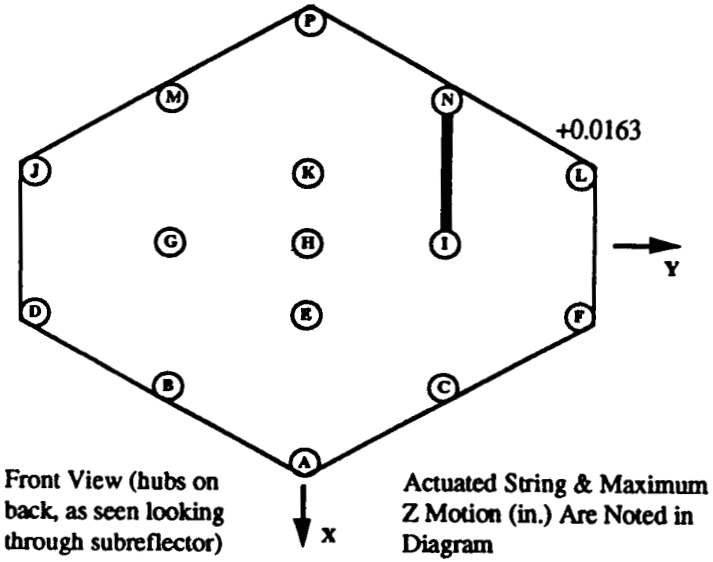


Front View (hubs on back, as seen looking through subreflector)

Actuated String & Maximum Z Motion (in.) Are Noted in Diagram

Power & Strain Data

(nm = not measured)

| String | Power (relative) | Strain (microstrain) |
|---|---|---|
| A-B | 0% | nm |
| A-C | 0% | nm |
| A-E | 0% | nm |
| B-D | 0% | nm |
| B-E | 0% | nm |
| B-G | 0% | nm |
| C-E | 0% | nm |
| C-F | 0% | nm |
| C-I | 0% | -4 |
| D-G | 0% | -19 |
| D-J | 0% | 5 |
| E-G | 0% | -33 |
| E-I | 0% | 44 |
| E-K | 0% | nm |
| F-I | 0% | 12 |

| String | Power (relative) | Strain (microstrain) |
|---|---|---|
| F-L | 0% | -31 |
| G-J | 0% | -1 |
| G-K | 0% | -3 |
| G-M | 0% | 5 |
| I-K | 0% | -2 |
| I-L | 0% | 23 |
| I-N | 20% | -277 |
| J-M | 0% | -19 |
| K-M | 0% | 23 |
| K-N | 0% | -102 |
| K-P | 0% | -40 |
| L-N | 0% | -173 |
| M-P | 0% | -18 |
| N-P | 0% | 15 |

Surface Contour Data

| Hub | Baseline Position | | | Position During Actuation | | | Relative Motion (Actuation - Baseline) | | |
|---|---|---|---|---|---|---|---|---|---|
| | X (in.) | Y (in.) | Z (in.) | X (in.) | Y (in.) | Z (in.) | X (in.) | Y (in.) | Z (in.) |
| A | 18.2856 | -0.3236 | -1.5393 | 18.2835 | -0.3239 | -1.5448 | -0.0021 | -0.0003 | -0.0055 |
| B | 12.0149 | -11.1579 | -2.0791 | 12.0139 | -11.1576 | -2.0733 | -0.001 | 0.0003 | 0.0058 |
| C | 12.2797 | 10.3364 | -0.0823 | 12.2776 | 10.3377 | -0.0876 | -0.0021 | 0.0013 | -0.0053 |
| D | 6.0383 | -21.2889 | -3.4909 | 6.038 | -21.2926 | -3.4765 | -0.0003 | -0.0037 | 0.0144 |
| E | 6.3161 | -0.0368 | -0.1667 | 6.316 | -0.0346 | -0.1666 | -1E-04 | 0.0022 | 1E-04 |
| F | 6.3115 | 20.8901 | -0.0173 | 6.312 | 20.8869 | -0.0092 | 0.0005 | -0.0032 | 0.0081 |
| G | -0.1156 | -10.817 | -1.4436 | -0.1175 | -10.8156 | -1.4403 | -0.0019 | 0.0014 | 0.0033 |
| H | 0.0019 | -0.0004 | -0.0033 | 0.002 | 0.0002 | -0.0034 | 0.0001 | 0.0006 | -1E-04 |
| I | -0.1094 | 10.5501 | 0.6214 | -0.1112 | 10.5483 | 0.6246 | -0.0018 | -0.0018 | 0.0032 |
| J | -6.3822 | -21.143 | -3.4218 | -6.3838 | -21.1431 | -3.4185 | -0.0016 | -1E-04 | 0.0033 |
| K | -6.2431 | -0.0018 | -0.2027 | -6.2451 | -0.002 | -0.2133 | -0.002 | -0.0002 | -0.0106 |
| L | -5.9974 | 21.0233 | -0.1181 | -5.9959 | 21.0274 | -0.1018 | 0.0015 | 0.0041 | 0.0163 |
| M | -12.3179 | -10.7247 | -2.0076 | -12.3187 | -10.7237 | -2.0218 | -0.0008 | 0.001 | -0.0142 |
| N | -12.134 | 10.4926 | -0.2174 | -12.1314 | 10.4942 | -0.2384 | 0.0026 | 0.0016 | -0.021 |
| P | -18.169 | -0.1399 | -1.5386 | -18.1653 | -0.135 | -1.5703 | 0.0037 | 0.0049 | -0.0317 |

## Figure A-22. Theodolite Test - String J-M Actuated

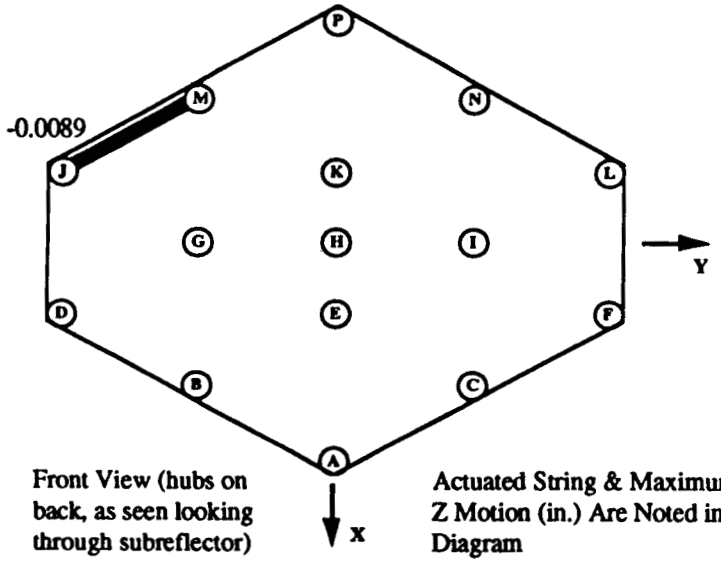


Front View (hubs on back, as seen looking through subreflector)

Actuated String & Maximum Z Motion (in.) Are Noted in Diagram

Power & Strain Data

(nm = not measured)

| String | Power (relative) | Strain (microstrain) |
|---|---|---|
| A-B | 0% | nm |
| A-C | 0% | nm |
| A-E | 0% | nm |
| B-D | 0% | nm |
| B-E | 0% | nm |
| B-G | 0% | nm |
| C-E | 0% | nm |
| C-F | 0% | nm |
| C-I | 0% | -15 |
| D-G | 0% | -46 |
| D-J | 0% | 70 |
| E-G | 0% | -13 |
| E-I | 0% | -9 |
| E-K | 0% | nm |
| F-I | 0% | -2 |

| String | Power (relative) | Strain (microstrain) |
|---|---|---|
| F-L | 0% | 0 |
| G-J | 0% | -25 |
| G-K | 0% | -22 |
| G-M | 0% | 19 |
| I-K | 0% | 15 |
| I-L | 0% | -1 |
| I-N | 0% | -2 |
| J-M | 20% | -303 |
| K-M | 0% | 26 |
| K-N | 0% | -3 |
| K-P | 0% | -17 |
| L-N | 0% | -1 |
| M-P | 0% | 28 |
| N-P | 0% | 9 |

Surface Contour Data

| Hub | Baseline Position | | | Position During Actuation | | | Relative Motion (Actuation - Baseline) | | |
|---|---|---|---|---|---|---|---|---|---|
| | X (in.) | Y (in.) | Z (in.) | X (in.) | Y (in.) | Z (in.) | X (in.) | Y (in.) | Z (in.) |
| A | 18.2856 | -0.3236 | -1.5393 | 18.2856 | -0.3224 | -1.5393 | 0 | 0.0012 | 0 |
| B | 12.0149 | -11.1579 | -2.0791 | 12.0148 | -11.1544 | -2.079 | -0.0001 | 0.0035 | 1E-04 |
| C | 12.2797 | 10.3364 | -0.0823 | 12.2788 | 10.3387 | -0.0767 | -0.0009 | 0.0023 | 0.0056 |
| D | 6.0383 | -21.2889 | -3.4909 | 6.0384 | -21.2843 | -3.5139 | 0.0001 | 0.0046 | -0.023 |
| E | 6.3161 | -0.0368 | -0.1667 | 6.3149 | -0.033 | -0.1693 | -0.0012 | 0.0038 | -0.0026 |
| F | 6.3115 | 20.8901 | -0.0173 | 6.3139 | 20.8882 | -0.0122 | 0.0024 | -0.0019 | 0.0051 |
| G | -0.1156 | -10.817 | -1.4436 | -0.1166 | -10.8156 | -1.4464 | -0.001 | 0.0014 | -0.0028 |
| H | 0.0019 | -0.0004 | -0.0033 | -0.0005 | 0.0014 | -0.0083 | -0.0024 | 0.0018 | -0.005 |
| I | -0.1094 | 10.5501 | 0.6214 | -0.1064 | 10.5488 | 0.6207 | 0.003 | -0.0013 | -0.0007 |
| J | -6.3822 | -21.143 | -3.4218 | -6.3827 | -21.1401 | -3.4307 | -0.0005 | 0.0029 | -0.0089 |
| K | -6.2431 | -0.0018 | -0.2027 | -6.2443 | -0.0035 | -0.2052 | -0.0012 | -0.0017 | -0.0025 |
| L | -5.9974 | 21.0233 | -0.1181 | -5.9975 | 21.0261 | -0.1181 | -1E-04 | 0.0028 | 0 |
| M | -12.3179 | -10.7247 | -2.0076 | -12.3182 | -10.724 | -2.0016 | -0.0003 | 0.0007 | 0.006 |
| N | -12.134 | 10.4926 | -0.2174 | -12.1337 | 10.4936 | -0.2233 | 0.0003 | 0.001 | -0.0059 |
| P | -18.169 | -0.1399 | -1.5386 | -18.1688 | -0.1381 | -1.5448 | 0.0002 | 0.0018 | -0.0062 |

## Figure A-23. Theodolite Test - String K-M Actuated

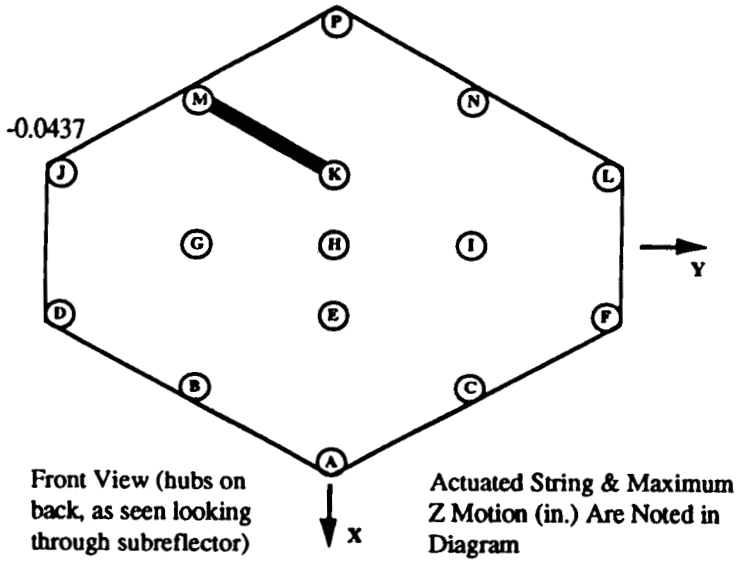


Front View (hubs on back, as seen looking through subreflector)

Actuated String & Maximum Z Motion (in.) Are Noted in Diagram

Power & Strain Data

(nm = not measured)

| String | Power (relative) | Strain (microstrain) |
|---|---|---|
| A-B | 0% | nm |
| A-C | 0% | nm |
| A-E | 0% | nm |
| B-D | 0% | nm |
| B-E | 0% | nm |
| B-G | 0% | nm |
| C-E | 0% | nm |
| C-F | 0% | nm |
| C-I | 0% | -9 |
| D-G | 0% | 9 |
| D-J | 0% | -6 |
| E-G | 0% | -71 |
| E-I | 0% | -1 |
| E-K | 0% | nm |
| F-I | 0% | -11 |

| String | Power (relative) | Strain (microstrain) |
|---|---|---|
| F-L | 0% | 8 |
| G-J | 0% | -18 |
| G-K | 0% | -9 |
| G-M | 0% | -6 |
| I-K | 0% | 26 |
| I-L | 0% | -6 |
| I-N | 0% | 20 |
| J-M | 0% | -6 |
| K-M | 20% | -302 |
| K-N | 0% | 9 |
| K-P | 0% | 18 |
| L-N | 0% | 8 |
| M-P | 0% | -184 |
| N-P | 0% | -63 |

Surface Contour Data

| Hub | Baseline Position | | | Position During Actuation | | | Relative Motion (Actuation - Baseline) | | |
|---|---|---|---|---|---|---|---|---|---|
| | X (in.) | Y (in.) | Z (in.) | X (in.) | Y (in.) | Z (in.) | X (in.) | Y (in.) | Z (in.) |
| A | 18.2856 | -0.3236 | -1.5393 | 18.2845 | -0.3233 | -1.5335 | -0.0011 | 0.0003 | 0.0058 |
| B | 12.0149 | -11.1579 | -2.0791 | 12.0156 | -11.1577 | -2.0761 | 0.0007 | 0.0002 | 0.003 |
| C | 12.2797 | 10.3364 | -0.0823 | 12.2758 | 10.3366 | -0.0763 | -0.0039 | 0.0002 | 0.006 |
| D | 6.0383 | -21.2889 | -3.4909 | 6.0378 | -21.2849 | -3.5082 | -0.0005 | 0.004 | -0.0173 |
| E | 6.3161 | -0.0368 | -0.1667 | 6.3142 | -0.0358 | -0.1636 | -0.0019 | 0.001 | 0.0031 |
| F | 6.3115 | 20.8901 | -0.0173 | 6.3138 | 20.8893 | -0.0122 | 0.0023 | -0.0008 | 0.0051 |
| G | -0.1156 | -10.817 | -1.4436 | -0.1174 | -10.8177 | -1.4544 | -0.0018 | -0.0007 | -0.0108 |
| H | 0.0019 | -0.0004 | -0.0033 | 0.0007 | -0.0011 | -0.0057 | -0.0012 | -0.0007 | -0.0024 |
| I | -0.1094 | 10.5501 | 0.6214 | -0.1088 | 10.5483 | 0.6295 | 0.0006 | -0.0018 | 0.0081 |
| J | -6.3822 | -21.143 | -3.4218 | -6.383 | -21.1356 | -3.4655 | -0.0008 | 0.0074 | -0.0437 |
| K | -6.2431 | -0.0018 | -0.2027 | -6.2447 | -0.0031 | -0.1995 | -0.0016 | -0.0013 | 0.0032 |
| L | -5.9974 | 21.0233 | -0.1181 | -5.998 | 21.0247 | -0.1124 | -0.0006 | 0.0014 | 0.0057 |
| M | -12.3179 | -10.7247 | -2.0076 | -12.3177 | -10.721 | -2.0398 | 0.0002 | 0.0037 | -0.0322 |
| N | -12.134 | 10.4926 | -0.2174 | -12.1333 | 10.494 | -0.2034 | 0.0007 | 0.0014 | 0.014 |
| P | -18.169 | -0.1399 | -1.5386 | -18.1694 | -0.1386 | -1.5208 | -0.0004 | 0.0013 | 0.0178 |

## Figure A-24. Theodolite Test - String K-N Actuated

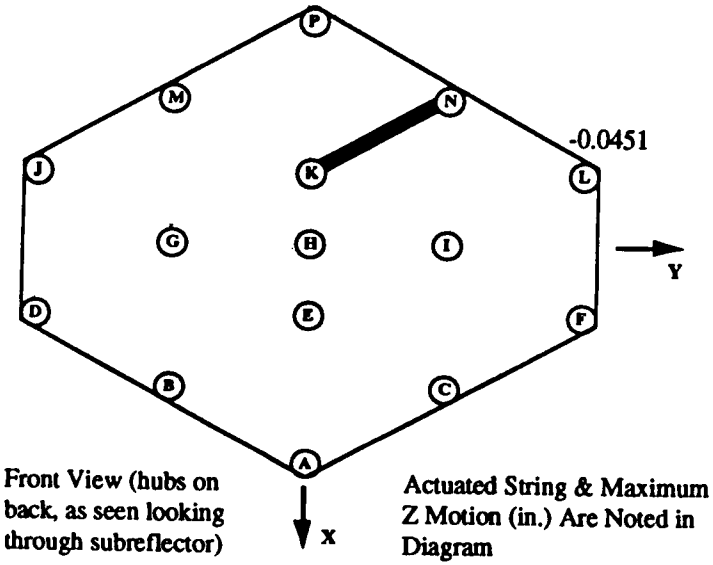


Front View (hubs on back, as seen looking through subreflector)

Actuated String & Maximum Z Motion (in.) Are Noted in Diagram

### Power & Strain Data

(nm = not measured)

| String | Power (relative) | Strain (microstrain) |
|---|---|---|
| A-B | 0% | nm |
| A-C | 0% | nm |
| A-E | 0% | nm |
| B-D | 0% | nm |
| B-E | 0% | nm |
| B-G | 0% | nm |
| C-E | 0% | nm |
| C-F | 0% | nm |
| C-I | 0% | -1 |
| D-G | 0% | -25 |
| D-J | 0% | 29 |
| E-G | 0% | -11 |
| E-I | 0% | -48 |
| E-K | 0% | nm |
| F-I | 0% | 33 |

| String | Power (relative) | Strain (microstrain) |
|---|---|---|
| F-L | 0% | -19 |
| G-J | 0% | -3 |
| G-K | 0% | 9 |
| G-M | 0% | 29 |
| I-K | 0% | 7 |
| I-L | 0% | -22 |
| I-N | 0% | -89 |
| J-M | 0% | -9 |
| K-M | 0% | 15 |
| K-N | 20% | -294 |
| K-P | 0% | 22 |
| L-N | 0% | 4 |
| M-P | 0% | -71 |
| N-P | 0% | -165 |

### Surface Contour Data

| Hub | Baseline Position | | | Position During Actuation | | | Relative Motion (Actuation - Baseline) | | |
|---|---|---|---|---|---|---|---|---|---|
| | X (in.) | Y (in.) | Z (in.) | X (in.) | Y (in.) | Z (in.) | X (in.) | Y (in.) | Z (in.) |
| A | 18.2856 | -0.3236 | -1.5393 | 18.2846 | -0.3247 | -1.5336 | -0.001 | -0.0011 | 0.0057 |
| B | 12.0149 | -11.1579 | -2.0791 | 12.0172 | -11.1567 | -2.0651 | 0.0023 | 0.0012 | 0.014 |
| C | 12.2797 | 10.3364 | -0.0823 | 12.2778 | 10.3366 | -0.0793 | -0.0019 | 0.0002 | 0.003 |
| D | 6.0383 | -21.2889 | -3.4909 | 6.0407 | -21.2882 | -3.4857 | 0.0024 | 0.0007 | 0.0052 |
| E | 6.3161 | -0.0368 | -0.1667 | 6.3142 | -0.0347 | -0.1637 | -0.0019 | 0.0021 | 0.003 |
| F | 6.3115 | 20.8901 | -0.0173 | 6.3127 | 20.8882 | -0.0369 | 0.0012 | -0.0019 | -0.0196 |
| G | -0.1156 | -10.817 | -1.4436 | -0.1161 | -10.8163 | -1.4379 | -0.0005 | 0.0007 | 0.0057 |
| H | 0.0019 | -0.0004 | -0.0033 | 0.0008 | 0.0006 | -0.0058 | -0.0011 | 0.001 | -0.0025 |
| I | -0.1094 | 10.5501 | 0.6214 | -0.107 | 10.5508 | 0.6126 | 0.0024 | 0.0007 | -0.0088 |
| J | -6.3822 | -21.143 | -3.4218 | -6.3829 | -21.1444 | -3.4101 | -0.0007 | -0.0014 | 0.0117 |
| K | -6.2431 | -0.0018 | -0.2027 | -6.2455 | -0.0037 | -0.2076 | -0.0024 | -0.0019 | -0.0049 |
| L | -5.9974 | 21.0233 | -0.1181 | -5.9967 | 21.0235 | -0.1632 | 0.0007 | 0.0002 | -0.0451 |
| M | -12.3179 | -10.7247 | -2.0076 | -12.3172 | -10.7262 | -1.9933 | 0.0007 | -0.0015 | 0.0143 |
| N | -12.134 | 10.4926 | -0.2174 | -12.1321 | 10.4941 | -0.2524 | 0.0019 | 0.0015 | -0.035 |
| P | -18.169 | -0.1399 | -1.5386 | -18.1696 | -0.1409 | -1.5146 | -0.0006 | -0.001 | 0.024 |

## Figure A-25. Theodolite Test - String K-P Actuated

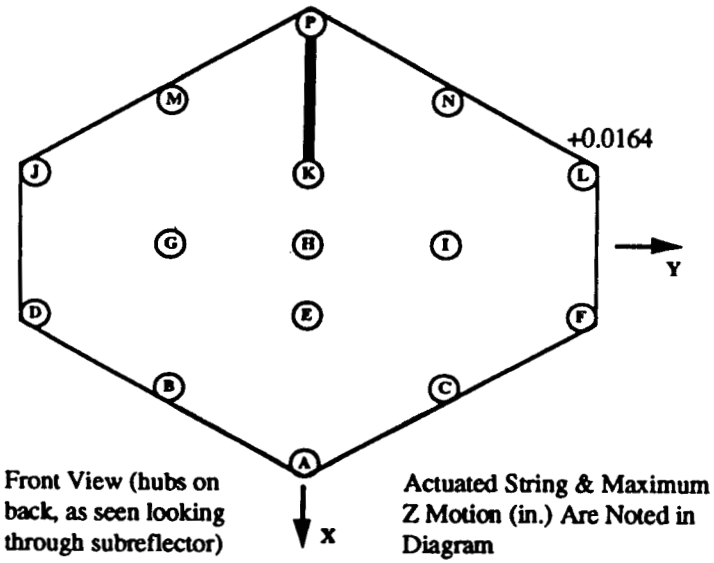


Front View (hubs on back, as seen looking through subreflector)

Actuated String & Maximum Z Motion (in.) Are Noted in Diagram

Power & Strain Data

(nm = not measured)

| String | Power (relative) | Strain (microstrain) |
|---|---|---|
| A-B | 0% | nm |
| A-C | 0% | nm |
| A-E | 0% | nm |
| B-D | 0% | nm |
| B-E | 0% | nm |
| B-G | 0% | nm |
| C-E | 0% | nm |
| C-F | 0% | nm |
| C-I | 0% | -15 |
| D-G | 0% | -20 |
| D-J | 0% | 14 |
| E-G | 0% | -3 |
| E-I | 0% | 10 |
| E-K | 0% | nm |
| F-I | 0% | 1 |

| String | Power (relative) | Strain (microstrain) |
|---|---|---|
| F-L | 0% | -1 |
| G-J | 0% | 1 |
| G-K | 0% | 9 |
| G-M | 0% | -1 |
| I-K | 0% | 32 |
| I-L | 0% | 9 |
| I-N | 0% | -25 |
| J-M | 0% | -33 |
| K-M | 0% | 21 |
| K-N | 0% | 24 |
| K-P | 20% | -286 |
| L-N | 0% | -20 |
| M-P | 0% | -148 |
| N-P | 0% | -142 |

Surface Contour Data

| Hub | Baseline Position | | | Position During Actuation | | | Relative Motion (Actuation - Baseline) | | |
|---|---|---|---|---|---|---|---|---|---|
| | X (in.) | Y (in.) | Z (in.) | X (in.) | Y (in.) | Z (in.) | X (in.) | Y (in.) | Z (in.) |
| A | 18.2856 | -0.3236 | -1.5393 | 18.2865 | -0.3252 | -1.5448 | 0.0009 | -0.0016 | -0.0055 |
| B | 12.0149 | -11.1579 | -2.0791 | 12.0169 | -11.155 | -2.0735 | 0.002 | 0.0029 | 0.0056 |
| C | 12.2797 | 10.3364 | -0.0823 | 12.2788 | 10.3381 | -0.0766 | -0.0009 | 0.0017 | 0.0057 |
| D | 6.0383 | -21.2889 | -3.4909 | 6.0403 | -21.2896 | -3.4801 | 0.002 | -0.0007 | 0.0108 |
| E | 6.3161 | -0.0368 | -0.1667 | 6.316 | -0.034 | -0.1666 | -1E-04 | 0.0028 | 1E-04 |
| F | 6.3115 | 20.8901 | -0.0173 | 6.3143 | 20.8872 | -0.0041 | 0.0028 | -0.0029 | 0.0132 |
| G | -0.1156 | -10.817 | -1.4436 | -0.1182 | -10.8176 | -1.4345 | -0.0026 | -0.0006 | 0.0091 |
| H | 0.0019 | -0.0004 | -0.0033 | 0.0007 | -0.0011 | -0.0057 | -0.0012 | -0.0007 | -0.0024 |
| I | -0.1094 | 10.5501 | 0.6214 | -0.1082 | 10.5494 | 0.6238 | 0.0012 | -0.0007 | 0.0024 |
| J | -6.3822 | -21.143 | -3.4218 | -6.3847 | -21.1443 | -3.4066 | -0.0025 | -0.0013 | 0.0152 |
| K | -6.2431 | -0.0018 | -0.2027 | -6.246 | -0.0033 | -0.2019 | -0.0029 | -0.0015 | 0.0008 |
| L | -5.9974 | 21.0233 | -0.1181 | -5.9959 | 21.0248 | -0.1017 | 0.0015 | 0.0015 | 0.0164 |
| M | -12.3179 | -10.7247 | -2.0076 | -12.318 | -10.7258 | -2.0075 | -1E-04 | -0.0011 | 0.0001 |
| N | -12.134 | 10.4926 | -0.2174 | -12.1314 | 10.4944 | -0.2127 | 0.0026 | 0.0018 | 0.0047 |
| P | -18.169 | -0.1399 | -1.5386 | -18.1665 | -0.1361 | -1.5786 | 0.0025 | 0.0038 | -0.04 |

## Figure A-26. Theodolite Test - String L-N Actuated

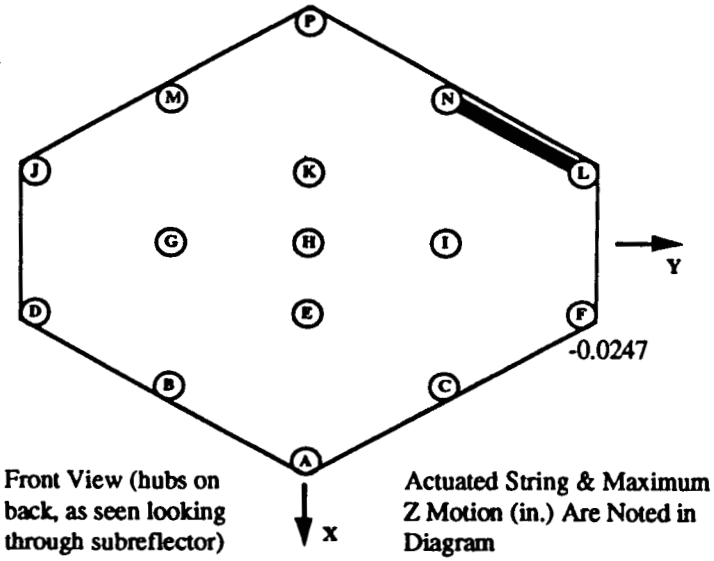


Front View (hubs on back, as seen looking through subreflector)

Actuated String & Maximum Z Motion (in.) Are Noted in Diagram

Power & Strain Data

(nm = not measured)

| String | Power (relative) | Strain (microstrain) |
|---|---|---|
| A-B | 0% | nm |
| A-C | 0% | nm |
| A-E | 0% | nm |
| B-D | 0% | nm |
| B-E | 0% | nm |
| B-G | 0% | nm |
| C-E | 0% | nm |
| C-F | 0% | nm |
| C-I | 0% | 12 |
| D-G | 0% | -17 |
| D-J | 0% | 21 |
| E-G | 0% | -27 |
| E-I | 0% | 5 |
| E-K | 0% | nm |
| F-I | 0% | -28 |

| String | Power (relative) | Strain (microstrain) |
|---|---|---|
| F-L | 0% | 11 |
| G-J | 0% | -2 |
| G-K | 0% | -2 |
| G-M | 0% | 12 |
| I-K | 0% | -9 |
| I-L | 0% | -42 |
| I-N | 0% | -12 |
| J-M | 0% | -10 |
| K-M | 0% | 0 |
| K-N | 0% | 28 |
| K-P | 0% | -6 |
| L-N | 20% | -318 |
| M-P | 0% | 12 |
| N-P | 0% | 27 |

Surface Contour Data

| Hub | Baseline Position | | | Position During Actuation | | | Relative Motion (Actuation - Baseline) | | |
|---|---|---|---|---|---|---|---|---|---|
| | X (in.) | Y (in.) | Z (in.) | X (in.) | Y (in.) | Z (in.) | X (in.) | Y (in.) | Z (in.) |
| A | 18.2856 | -0.3236 | -1.5393 | 18.2855 | -0.3275 | -1.5392 | -1E-04 | -0.0039 | 1E-04 |
| B | 12.0149 | -11.1579 | -2.0791 | 12.012 | -11.1572 | -2.0702 | -0.0029 | 0.0007 | 0.0089 |
| C | 12.2797 | 10.3364 | -0.0823 | 12.2776 | 10.3365 | -0.0875 | -0.0021 | 1E-04 | -0.0052 |
| D | 6.0383 | -21.2889 | -3.4909 | 6.0377 | -21.2881 | -3.4852 | -0.0006 | 0.0008 | 0.0057 |
| E | 6.3161 | -0.0368 | -0.1667 | 6.3172 | -0.0321 | -0.1641 | 0.0011 | 0.0047 | 0.0026 |
| F | 6.3115 | 20.8901 | -0.0173 | 6.3105 | 20.8873 | -0.042 | -0.001 | -0.0028 | -0.0247 |
| G | -0.1156 | -10.817 | -1.4436 | -0.1162 | -10.8163 | -1.4378 | -0.0006 | 0.0007 | 0.0058 |
| H | 0.0019 | -0.0004 | -0.0033 | 0.0007 | -0.0005 | -0.0058 | -0.0012 | -0.0001 | -0.0025 |
| I | -0.1094 | 10.5501 | 0.6214 | -0.1094 | 10.5509 | 0.6214 | 0 | 0.0008 | 0 |
| J | -6.3822 | -21.143 | -3.4218 | -6.3849 | -21.1423 | -3.4212 | -0.0027 | 0.0007 | 0.0006 |
| K | -6.2431 | -0.0018 | -0.2027 | -6.2456 | -0.0042 | -0.2076 | -0.0025 | -0.0024 | -0.0049 |
| L | -5.9974 | 21.0233 | -0.1181 | -5.9983 | 21.0239 | -0.1262 | -0.0009 | 0.0006 | -0.0081 |
| M | -12.3179 | -10.7247 | -2.0076 | -12.3175 | -10.7243 | -2.0136 | 0.0004 | 0.0004 | -0.006 |
| N | -12.134 | 10.4926 | -0.2174 | -12.1346 | 10.4929 | -0.2057 | -0.0006 | 0.0003 | 0.0117 |
| P | -18.169 | -0.1399 | -1.5386 | -18.1659 | -0.1377 | -1.5462 | 0.0031 | 0.0022 | -0.0076 |

## Figure A-27. Theodolite Test - String M-P Actuated

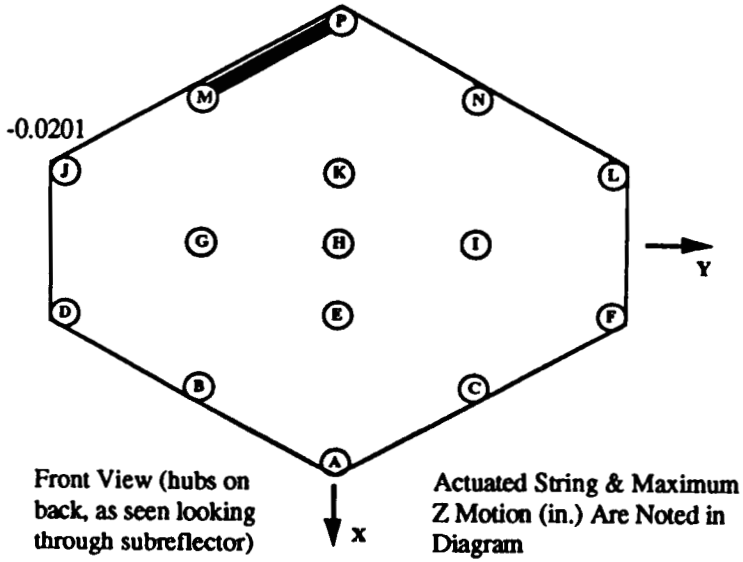


Front View (hubs on back, as seen looking through subreflector)

Actuated String & Maximum Z Motion (in.) Are Noted in Diagram

### Power & Strain Data

(nm = not measured)

| String | Power (relative) | Strain (microstrain) |
|---|---|---|
| A-B | 0% | nm |
| A-C | 0% | nm |
| A-E | 0% | nm |
| B-D | 0% | nm |
| B-E | 0% | nm |
| B-G | 0% | nm |
| C-E | 0% | nm |
| C-F | 0% | nm |
| C-I | 0% | -10 |
| D-G | 0% | -15 |
| D-J | 0% | 26 |
| E-G | 0% | -26 |
| E-I | 0% | -18 |
| E-K | 0% | nm |
| F-I | 0% | 11 |

| String | Power (relative) | Strain (microstrain) |
|---|---|---|
| F-L | 0% | -1 |
| G-J | 0% | -6 |
| G-K | 0% | -26 |
| G-M | 0% | 35 |
| I-K | 0% | 23 |
| I-L | 0% | 5 |
| I-N | 0% | 3 |
| J-M | 0% | 20 |
| K-M | 0% | -47 |
| K-N | 0% | -12 |
| K-P | 0% | -51 |
| L-N | 0% | 18 |
| M-P | 20% | -332 |
| N-P | 0% | 54 |

### Surface Contour Data

| Hub | Baseline Position | | | Position During Actuation | | | Relative Motion (Actuation - Baseline) | | |
|---|---|---|---|---|---|---|---|---|---|
| | X (in.) | Y (in.) | Z (in.) | X (in.) | Y (in.) | Z (in.) | X (in.) | Y (in.) | Z (in.) |
| A | 18.2856 | -0.3236 | -1.5393 | 18.2866 | -0.3243 | -1.5365 | 0.001 | -0.0007 | 0.0028 |
| B | 12.0149 | -11.1579 | -2.0791 | 12.015 | -11.1567 | -2.0706 | 1E-04 | 0.0012 | 0.0085 |
| C | 12.2797 | 10.3364 | -0.0823 | 12.2799 | 10.336 | -0.074 | 0.0002 | -0.0004 | 0.0083 |
| D | 6.0383 | -21.2889 | -3.4909 | 6.0368 | -21.2848 | -3.5021 | -0.0015 | 0.0041 | -0.0112 |
| E | 6.3161 | -0.0368 | -0.1667 | 6.3153 | -0.0325 | -0.161 | -0.0008 | 0.0043 | 0.0057 |
| F | 6.3115 | 20.8901 | -0.0173 | 6.3104 | 20.8891 | -0.0199 | -0.0011 | -0.001 | -0.0026 |
| G | -0.1156 | -10.817 | -1.4436 | -0.1181 | -10.8161 | -1.4486 | -0.0025 | 0.0009 | -0.005 |
| H | 0.0019 | -0.0004 | -0.0033 | 0.0007 | 0 | -0.0058 | -0.0012 | 0.0004 | -0.0025 |
| I | -0.1094 | 10.5501 | 0.6214 | -0.1076 | 10.5476 | 0.6182 | 0.0018 | -0.0025 | -0.0032 |
| J | -6.3822 | -21.143 | -3.4218 | -6.3847 | -21.1403 | -3.4419 | -0.0025 | 0.0027 | -0.0201 |
| K | -6.2431 | -0.0018 | -0.2027 | -6.2461 | -0.005 | -0.2018 | -0.003 | -0.0032 | 0.0009 |
| L | -5.9974 | 21.0233 | -0.1181 | -5.9965 | 21.025 | -0.1296 | 0.0009 | 0.0017 | -0.0115 |
| M | -12.3179 | -10.7247 | -2.0076 | -12.3179 | -10.7247 | -2.0076 | 0 | 0 | 0 |
| N | -12.134 | 10.4926 | -0.2174 | -12.1334 | 10.493 | -0.2291 | 0.0006 | 0.0004 | -0.0117 |
| P | -18.169 | -0.1399 | -1.5386 | -18.166 | -0.138 | -1.5402 | 0.003 | 0.0019 | -0.0016 |

## Figure A-28. Theodolite Test - String N-P Actuated

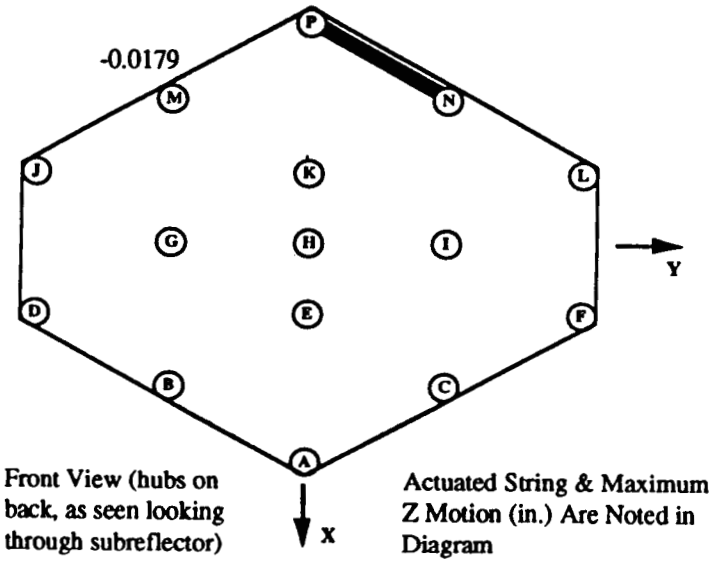


Front View (hubs on back, as seen looking through subreflector)

Actuated String & Maximum Z Motion (in.) Are Noted in Diagram

### Power & Strain Data

(nm = not measured)

| String | Power (relative) | Strain (microstrain) |
|---|---|---|
| A-B | 0% | nm |
| A-C | 0% | nm |
| A-E | 0% | nm |
| B-D | 0% | nm |
| B-E | 0% | nm |
| B-G | 0% | nm |
| C-E | 0% | nm |
| C-F | 0% | nm |
| C-I | 0% | 1 |
| D-G | 0% | -10 |
| D-J | 0% | 15 |
| E-G | 0% | -38 |
| E-I | 0% | -5 |
| E-K | 0% | nm |
| F-I | 0% | 1 |

| String | Power (relative) | Strain (microstrain) |
|---|---|---|
| F-L | 0% | 6 |
| G-J | 0% | -1 |
| G-K | 0% | 6 |
| G-M | 0% | 16 |
| I-K | 0% | -7 |
| I-L | 0% | -4 |
| I-N | 0% | 44 |
| J-M | 0% | -8 |
| K-M | 0% | -13 |
| K-N | 0% | -15 |
| K-P | 0% | -34 |
| L-N | 0% | 38 |
| M-P | 0% | 58 |
| N-P | 20% | -330 |

### Surface Contour Data

| Hub | Baseline Position | | | Position During Actuation | | | Relative Motion (Actuation - Baseline) | | |
|---|---|---|---|---|---|---|---|---|---|
| | X (in.) | Y (in.) | Z (in.) | X (in.) | Y (in.) | Z (in.) | X (in.) | Y (in.) | Z (in.) |
| A | 18.2856 | -0.3236 | -1.5393 | 18.2865 | -0.3267 | -1.5364 | 0.0009 | -0.0031 | 0.0029 |
| B | 12.0149 | -11.1579 | -2.0791 | 12.0142 | -11.156 | -2.0649 | -0.0007 | 0.0019 | 0.0142 |
| C | 12.2797 | 10.3364 | -0.0823 | 12.2797 | 10.3374 | -0.0822 | 0 | 0.001 | 0.0001 |
| D | 6.0383 | -21.2889 | -3.4909 | 6.0364 | -21.2911 | -3.4877 | -0.0019 | -0.0022 | 0.0032 |
| E | 6.3161 | -0.0368 | -0.1667 | 6.3143 | -0.0329 | -0.1637 | -0.0018 | 0.0039 | 0.003 |
| F | 6.3115 | 20.8901 | -0.0173 | 6.3108 | 20.886 | -0.0338 | -0.0007 | -0.0041 | -0.0165 |
| G | -0.1156 | -10.817 | -1.4436 | -0.1174 | -10.8139 | -1.4404 | -0.0018 | 0.0031 | 0.0032 |
| H | 0.0019 | -0.0004 | -0.0033 | 0.0008 | -0.0006 | -0.0058 | -0.0011 | -0.0002 | -0.0025 |
| I | -0.1094 | 10.5501 | 0.6214 | -0.1076 | 10.5488 | 0.6182 | 0.0018 | -0.0013 | -0.0032 |
| J | -6.3822 | -21.143 | -3.4218 | -6.3828 | -21.1435 | -3.4306 | -0.0006 | -0.0005 | -0.0088 |
| K | -6.2431 | -0.0018 | -0.2027 | -6.2431 | -0.0039 | -0.2028 | 0 | -0.0021 | -0.0001 |
| L | -5.9974 | 21.0233 | -0.1181 | -5.9961 | 21.0242 | -0.1354 | 0.0013 | 0.0009 | -0.0173 |
| M | -12.3179 | -10.7247 | -2.0076 | -12.317 | -10.7231 | -2.0255 | 0.0009 | 0.0016 | -0.0179 |
| N | -12.134 | 10.4926 | -0.2174 | -12.1343 | 10.4942 | -0.2116 | -0.0003 | 0.0016 | 0.0058 |
| P | -18.169 | -0.1399 | -1.5386 | -18.1689 | -0.1372 | -1.5388 | 1E-04 | 0.0027 | -0.0002 |

## Figure A-29. Theodolite Test - All Strings Actuated

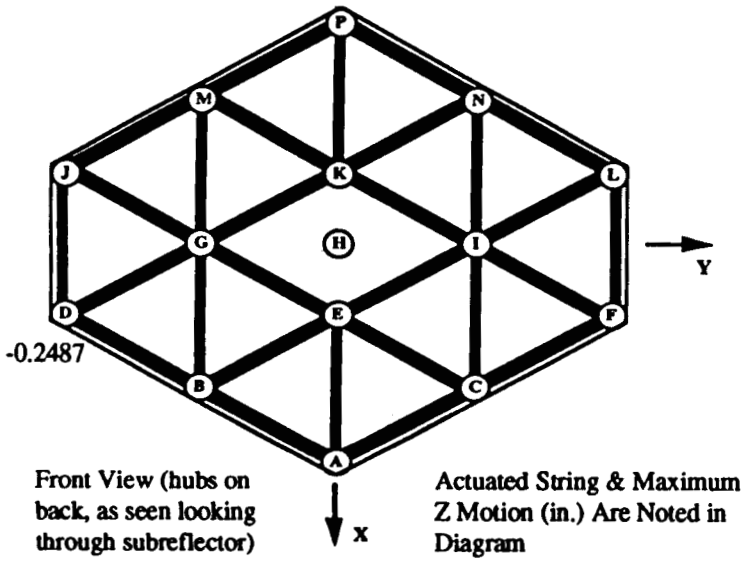


Front View (hubs on back, as seen looking through subreflector)

Actuated String & Maximum Z Motion (in.) Are Noted in Diagram

Power & Strain Data

(nm = not measured)

| String | Power (relative) | Strain (microstrain) |
|---|---|---|
| A-B | 20% | -549 |
| A-C | 20% | -798 |
| A-E | 20% | -176 |
| B-D | 20% | -673 |
| B-E | 20% | -214 |
| B-G | 20% | -213 |
| C-E | 20% | -216 |
| C-F | 20% | -693 |
| C-I | 20% | -228 |
| D-G | 20% | -231 |
| D-J | 20% | -580 |
| E-G | 20% | -231 |
| E-I | 20% | -244 |
| E-K | 0% | nm |
| F-I | 20% | -271 |

| String | Power (relative) | Strain (microstrain) |
|---|---|---|
| F-L | 20% | -619 |
| G-J | 20% | -172 |
| G-K | 20% | -179 |
| G-M | 20% | -204 |
| I-K | 20% | -188 |
| I-L | 20% | -175 |
| I-N | 20% | -171 |
| J-M | 20% | -814 |
| K-M | 20% | -218 |
| K-N | 20% | -180 |
| K-P | 20% | -168 |
| L-N | 20% | -640 |
| M-P | 20% | -529 |
| N-P | 20% | -269 |

Surface Contour Data

| Hub | Baseline Position | | | Position During Actuation | | | Relative Motion (Actuation - Baseline) | | |
|---|---|---|---|---|---|---|---|---|---|
| | X (in.) | Y (in.) | Z (in.) | X (in.) | Y (in.) | Z (in.) | X (in.) | Y (in.) | Z (in.) |
| A | 18.2856 | -0.3236 | -1.5393 | 18.2792 | -0.3118 | -1.666 | -0.0064 | 0.0118 | -0.1267 |
| B | 12.0149 | -11.1579 | -2.0791 | 12.0104 | -11.1437 | -2.1688 | -0.0045 | 0.0142 | -0.0897 |
| C | 12.2797 | 10.3364 | -0.0823 | 12.2798 | 10.3418 | -0.1595 | 1E-04 | 0.0054 | -0.0772 |
| D | 6.0383 | -21.2889 | -3.4909 | 6.0353 | -21.2503 | -3.7396 | -0.003 | 0.0386 | -0.2487 |
| E | 6.3161 | -0.0368 | -0.1667 | 6.3146 | -0.0323 | -0.1775 | -0.0015 | 0.0045 | -0.0108 |
| F | 6.3115 | 20.8901 | -0.0173 | 6.3127 | 20.8862 | -0.2492 | 0.0012 | -0.0039 | -0.2319 |
| G | -0.1156 | -10.817 | -1.4436 | -0.1173 | -10.813 | -1.4968 | -0.0017 | 0.004 | -0.0532 |
| H | 0.0019 | -0.0004 | -0.0033 | -0.0004 | 0.0025 | -0.0083 | -0.0023 | 0.0029 | -0.005 |
| I | -0.1094 | 10.5501 | 0.6214 | -0.1063 | 10.5542 | 0.5657 | 0.0031 | 0.0041 | -0.0557 |
| J | -6.3822 | -21.143 | -3.4218 | -6.3815 | -21.1126 | -3.6411 | 0.0007 | 0.0304 | -0.2193 |
| K | -6.2431 | -0.0018 | -0.2027 | -6.2464 | -0.0021 | -0.2158 | -0.0033 | -0.0003 | -0.0131 |
| L | -5.9974 | 21.0233 | -0.1181 | -5.9924 | 21.0217 | -0.3414 | 0.005 | -0.0016 | -0.2233 |
| M | -12.3179 | -10.7247 | -2.0076 | -12.3141 | -10.713 | -2.1112 | 0.0038 | 0.0117 | -0.1036 |
| N | -12.134 | 10.4926 | -0.2174 | -12.1312 | 10.4988 | -0.2957 | 0.0028 | 0.0062 | -0.0783 |
| P | -18.169 | -0.1399 | -1.5386 | -18.1613 | -0.1264 | -1.6704 | 0.0077 | 0.0135 | -0.1318 |

**Figure A-30. Theodolite Test - Perimeter Strings Actuated**

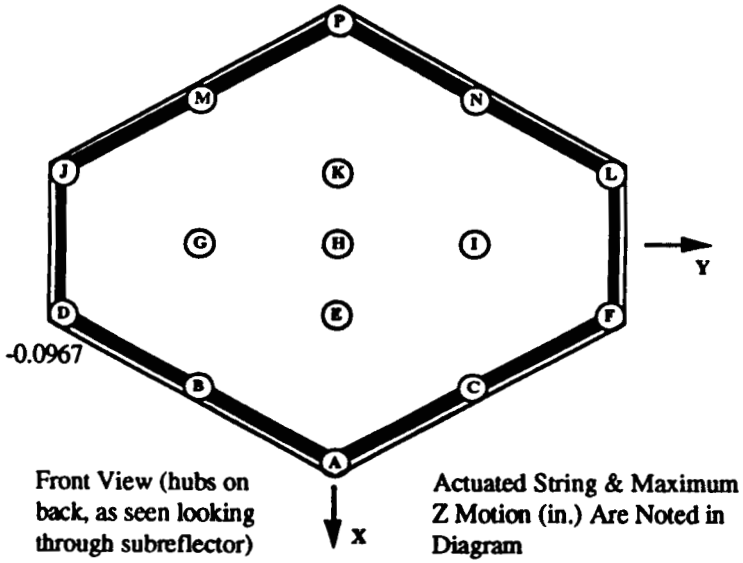


Front View (hubs on back, as seen looking through subreflector)

Actuated String & Maximum Z Motion (in.) Are Noted in Diagram

Power & Strain Data

(nm = not measured)

| String | Power (relative) | Strain (microstrain) |
|---|---|---|
| A-B | 20% | -171 |
| A-C | 20% | -176 |
| A-E | 0% | -19 |
| B-D | 20% | -182 |
| B-E | 0% | 6 |
| B-G | 0% | 9 |
| C-E | 0% | 6 |
| C-F | 20% | -216 |
| C-I | 0% | 3 |
| D-G | 0% | -63 |
| D-J | 20% | -210 |
| E-G | 0% | -17 |
| E-I | 0% | 3 |
| E-K | 0% | nm |
| F-I | 0% | -70 |

| String | Power (relative) | Strain (microstrain) |
|---|---|---|
| F-L | 20% | -168 |
| G-J | 0% | -73 |
| G-K | 0% | -22 |
| G-M | 0% | 18 |
| I-K | 0% | 6 |
| I-L | 0% | -52 |
| I-N | 0% | 30 |
| J-M | 20% | -177 |
| K-M | 0% | -30 |
| K-N | 0% | 1 |
| K-P | 0% | -11 |
| L-N | 20% | -193 |
| M-P | 20% | -205 |
| N-P | 20% | -79 |

Surface Contour Data

| Hub | Baseline Position | | | Position During Actuation | | | Relative Motion (Actuation - Baseline) | | |
|---|---|---|---|---|---|---|---|---|---|
| | X (in.) | Y (in.) | Z (in.) | X (in.) | Y (in.) | Z (in.) | X (in.) | Y (in.) | Z (in.) |
| A | 18.2856 | -0.3236 | -1.5393 | 18.2834 | -0.318 | -1.5871 | -0.0022 | 0.0056 | -0.0478 |
| B | 12.0149 | -11.1579 | -2.0791 | 12.0143 | -11.1529 | -2.1044 | -0.0006 | 0.005 | -0.0253 |
| C | 12.2797 | 10.3364 | -0.0823 | 12.2802 | 10.3411 | -0.1044 | 0.0005 | 0.0047 | -0.0221 |
| D | 6.0383 | -21.2889 | -3.4909 | 6.0355 | -21.277 | -3.5876 | -0.0028 | 0.0119 | -0.0967 |
| E | 6.3161 | -0.0368 | -0.1667 | 6.3165 | -0.0311 | -0.1585 | 0.0004 | 0.0057 | 0.0082 |
| F | 6.3115 | 20.8901 | -0.0173 | 6.3115 | 20.8904 | -0.0835 | 0 | 0.0003 | -0.0662 |
| G | -0.1156 | -10.817 | -1.4436 | -0.1162 | -10.817 | -1.466 | -0.0006 | 0 | -0.0224 |
| H | 0.0019 | -0.0004 | -0.0033 | 0 | -0.0036 | 0 | -0.0019 | -0.0032 | 0.0033 |
| I | -0.1094 | 10.5501 | 0.6214 | -0.1112 | 10.5502 | 0.6108 | -0.0018 | 1E-04 | -0.0106 |
| J | -6.3822 | -21.143 | -3.4218 | -6.3867 | -21.133 | -3.5149 | -0.0045 | 0.01 | -0.0931 |
| K | -6.2431 | -0.0018 | -0.2027 | -6.2456 | -0.0042 | -0.2076 | -0.0025 | -0.0024 | -0.0049 |
| L | -5.9974 | 21.0233 | -0.1181 | -5.9974 | 21.0255 | -0.1911 | 0 | 0.0022 | -0.073 |
| M | -12.3179 | -10.7247 | -2.0076 | -12.3193 | -10.7244 | -2.0362 | -0.0014 | 0.0003 | -0.0286 |
| N | -12.134 | 10.4926 | -0.2174 | -12.1347 | 10.4964 | -0.2314 | -0.0007 | 0.0038 | -0.014 |
| P | -18.169 | -0.1399 | -1.5386 | -18.1683 | -0.1361 | -1.5629 | 0.0007 | 0.0038 | -0.0243 |

# REPORT DOCUMENTATION PAGE

*Form Approved*
*OMB No. 0704-0188*

Public reporting burden for this collection of information is estimated to average 1 hour per response, including the time for reviewing instructions, searching existing data sources, gathering and maintaining the data needed, and completing and reviewing the collection of information. Send comments regarding this burden estimate or any other aspect of this collection of information, including suggestions for reducing this burden, to Washington Headquarters Services, Directorate for Information Operations and Reports, 1215 Jefferson Davis Highway, Suite 1204, Arlington, VA 22202-4302, and to the Office of Management and Budget, Paperwork Reduction Project (0704-0188), Washington, DC 20503.

| 1. AGENCY USE ONLY *(Leave blank)* | 2. REPORT DATE | 3. REPORT TYPE AND DATES COVERED |
|---|---|---|
| | September 1994 | Contractor Report |

**4. TITLE AND SUBTITLE**
Experimental Evaluation of Shape Memory Alloy Actuation Technique in Adaptive Antenna Design Concepts

**5. FUNDING NUMBERS**
C NAS1-18455
WU 233-01-03-22

**6. AUTHOR(S)**
W. Neill Kefauver and Bernie F. Carpenter

**7. PERFORMING ORGANIZATION NAME(S) AND ADDRESS(ES)**
Martin Marietta Corporation
PO Box 179
Denver, CO 80201

**8. PERFORMING ORGANIZATION REPORT NUMBER**

**9. SPONSORING/MONITORING AGENCY NAME(S) AND ADDRESS(ES)**
National Aeronautics and Space Administration
Langley Research Center
Hampton, VA 23681-0001

**10. SPONSORING/MONITORING AGENCY REPORT NUMBER**
NASA CR-194983

**11. SUPPLEMENTARY NOTES**
Langley Technical Monitor: L. C. Schroeder
Final Report

**12a. DISTRIBUTION/AVAILABILITY STATEMENT**
Unclassified-Unlimited

Subject Category ~~15~~ 32

**12b. DISTRIBUTION CODE**

**13. ABSTRACT** *(Maximum 200 words)*

Creation of an antenna system that could autonomously adapt contours of reflecting surfaces to compensate for structural loads induced by a variable environment would maximize performance of space-based communication systems. Design of such a system requires the comprehensive development and integration of advanced actuator, sensor, and control technologies. As an initial step in this process, a test has been performed to assess the use of a shape memory alloy as a potential actuation technique. For this test, an existing, offset, cassegrain antenna system was retrofit with a subreflector equipped with shape memory alloy actuators for surface contour control. The impacts that the actuators had on both the subreflector contour and the antenna system patterns were measured. The results of this study indicate the potential for using shape memory alloy actuation techniques to adaptively control antenna performance; both variations in gain and beam steering capabilities were demonstrated. Future development effort is required to evolve this potential into a useful technology for satellite applications.

| 14. SUBJECT TERMS | 15. NUMBER OF PAGES |
|---|---|
| antenna beam steering, shape memory alloy, adaptive reflector shape control, near-field pattern tests | 65 |
| | 16. PRICE CODE A04 |

| 17. SECURITY CLASSIFICATION OF REPORT | 18. SECURITY CLASSIFICATION OF THIS PAGE | 19. SECURITY CLASSIFICATION OF ABSTRACT | 20. LIMITATION OF ABSTRACT |
|---|---|---|---|
| Unclassified | Unclassified | | |